

Dissertations and Theses

8-2013

Numerical Analysis and Theory of Oblique Alfvénic Solitons Observed in the Interplanetary Magnetic Field

Harry Raphael Wheeler IV
Embry-Riddle Aeronautical University - Daytona Beach

Follow this and additional works at: <https://commons.erau.edu/edt>



Part of the [Engineering Physics Commons](#)

Scholarly Commons Citation

Wheeler, Harry Raphael IV, "Numerical Analysis and Theory of Oblique Alfvénic Solitons Observed in the Interplanetary Magnetic Field" (2013). *Dissertations and Theses*. 147.
<https://commons.erau.edu/edt/147>

This Thesis - Open Access is brought to you for free and open access by Scholarly Commons. It has been accepted for inclusion in Dissertations and Theses by an authorized administrator of Scholarly Commons. For more information, please contact commons@erau.edu.

NUMERICAL ANALYSIS AND THEORY OF OBLIQUE
ALFVÉNIC SOLITONS OBSERVED IN THE INTERPLANETARY
MAGNETIC FIELD

BY
HARRY RAPHAEL WHEELER IV

A Thesis
Submitted to the Department of Physical Sciences
and the Committee on Graduate Studies
In partial fulfillment of the requirements
for the degree of
Master in Science in Engineering Physics

08/2013
Embry-Riddle Aeronautical University
Daytona Beach, Florida

© Copyright by Harry Raphael Wheeler IV 2013

All Rights Reserved

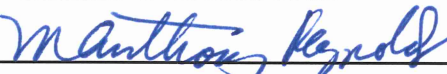
NUMERICAL ANALYSIS AND THEORY OF OBLIQUE
ALFVÉNIC SOLITONS OBSERVED IN THE INTERPLANETARY
MAGNETIC FIELD

by

Harry Raphael Wheeler IV

This thesis was prepared under the direction of the candidate's thesis committee chair, Dr. Anthony Reynolds, Department of Physical Sciences, and has been approved by the members of the thesis committee. It was submitted to the Department of Physical Sciences and was accepted in partial fulfillment of the requirements of the Degree of
Master of Science in Engineering Physics

THESIS COMMITTEE:


Dr. Anthony Reynolds

Dr. Anthony Reynolds, Chair


Dr. Bereket Berhane

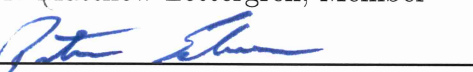
Dr. Bereket Berhane, Member


Dr. Andrei Ludu

Dr. Andrei Ludu, Member


Dr. Matthew Zettergren

Dr. Matthew Zettergren, Member


Dr. Peter Erdman

Dr. Peter Erdman, MSEP Graduate Program Coordinator


Dr. Terry Oswalt

Dr. Terry Oswalt, Department Chair, Physical Sciences


Dr. Robert Oxley

Dr. Robert Oxley, Associate V.P. for Academics

Abstract

Recently, there have been reports of small magnetic pulses or bumps in the interplanetary magnetic field observed by various spacecraft. Most of these reports claim that these localized pulses or bumps are solitons. Solitons are weakly nonlinear localized waves that tend to retain their form as they propagate and can be observed in various media which exhibit nonlinear steepening and dispersive effects. This thesis expands the claim that these pulses or bumps are nonlinear oblique Alfvén waves with soliton components, through the application of analytical techniques used in the inverse scattering transform in a numerical context and numerical integration of nonlinear partial differential equations. One event, which was observed by the Ulysses spacecraft on February 21st, 2001, is extensively scrutinized through comparison with soliton solutions that emerge from the Derivative Nonlinear Schrödinger (DNLS) equation. The direct scattering transform of a wave profile that has corresponding morphology to the selected magnetic bump leads to the implication of a soliton component. Numerical integration of the scaled profile matching the event in the context of the DNLS leads to generation of dispersive waves and a one parameter dark soliton.

Acknowledgments

I am greatly thankful for my advisor and his guidance throughout the endeavor of completing my thesis. Without his direction and keen intuition and intellect, I would have had an intense struggle throughout the process. I would also like to thank my committee members, Dr. Berhane, Dr. Zettegren and Dr. Ludu, in all what they have taught me over the years I have experienced at Embry-Riddle Aeronautical University. Also, I would like to thank Dr. Maronde, Dr. Barjatya and the Physical Sciences department for employment as a graduate teaching assistant, which supported me financially throughout my career as a prospective masters student. I would also like to thank my family for their strong support and encouragement.

Contents

Abstract	iv
Acknowledgments	v
1 INTRODUCTION	1
1.1 Nonlinear Waves	1
1.1.1 Solitons	1
1.2 Solitons in Space Plasmas	7
1.2.1 Nonlinear Oblique Alfvèn Waves	7
1.3 Synopsis of Thesis	9
2 Waves in plasmas	11
2.1 Magnetohydrodynamics	12
2.1.1 Linear waves permitted by the ideal MHD equations	14
2.2 Nonlinear waves in plasmas	19
2.2.1 Weakly Nonlinear waves in Plasmas	19
2.2.2 Derivative Nonlinear Schrödinger (DNLS) Equation	21
2.3 Analytical Solutions of the DNLS	22
2.3.1 One Parameter Soliton	23
2.3.2 Two Parameter Soliton	23
3 Soliton Theory	29
3.1 Fourier-Laplace transform for linear wave theory	29
3.2 Sturm-Liouville Theory	33

3.2.1	The Sturm-Liouville problem	33
3.3	Sturm-Liouville operator in Soliton theory	36
3.3.1	Importance of the Eigenvalues	37
3.3.2	Non-reflectionless Potentials	41
3.4	2x2 eigenvalue problem for the DNLS	42
4	Numerical Solutions of Nonlinear Partial Differential Equations	48
4.1	Convection Equation	48
4.1.1	Von Neumann Stability Analysis	51
4.2	Diffusion Equation	54
4.3	Korteweg-de Vries Equation	58
4.4	Periodic Boundary Conditions	62
4.5	Derivative Nonlinear Schrödinger Equation	64
4.5.1	Stability Analysis of the Lax-Wendroff Two-Step/BTCS scheme	68
5	Preliminary Analysis of Ulysses data	73
5.1	Magnetic bump observed on February 21st, 2001	77
5.1.1	Plasma Characteristics	78
5.2	Minimum Variance Analysis of Observed Solitary Structure	81
5.3	Comparison of observed event with solitons solutions of the DNLS	83
5.3.1	Previous comparison to one parameter bright soliton	83
5.3.2	Two parameter soliton comparison	86
5.4	Application of the Direct scattering transform	86
5.4.1	Calculation of Eigenvalues through the Numerical DST	87
5.5	Numerical Integration of the DNLS equation	89
5.5.1	Analytical two parameter soliton as initial profile	93
5.5.2	Ulysses magnetometer data as initial profile	93
6	Conclusions and Further study	98
A	APPENDIX	100
A.1	Scaling for KdV equation for Shallow water waves	100

A.2 Scaling for the Derivative Nonlinear Schrödinger Equation	102
Bibliography	105

List of Tables

5.1 Ulysses Orbital Elements	75
--	----

List of Figures

1.1	Single soliton wave form.	4
1.2	Two soliton solution.	5
1.3	Contour plot of soliton-soliton interaction.	6
2.1	Low beta phase velocity wave modes	18
2.2	High beta wave modes	18
2.3	One-parameter solution to DNLS: Dark Soliton	24
2.4	One-parameter solution to DNLS: Bright Soliton	25
2.5	Two-Parameter Soliton	28
3.1	Flow of using Fourier-Laplace transform on linear PDE's	31
3.2	Flow of the inverse scattering transform on nonlinear PDE's	37
3.3	Initial wave form with radiation due to reflection	43
3.4	Scattering of One-Paramter solitons	47
4.1	Domain of dependence	51
4.2	Locus plot of G	55
4.3	Grid spacing with periodic boundary conditions	63
4.4	Dependence of dt on Error for DNLS finite difference equation	69
4.5	Root Mean Square Error with increasing time steps	70
4.6	Testing the Lax Wendroff/BTCS method	72
5.1	Ulysses Spacecraft Trajectory	74
5.2	List of solitary magnetic pulses	76
5.3	Radial-Tangential-Normal Coordinates	78

5.4	Event on day 52 of 2001	79
5.5	Number of data points effects on the Minimum Variance	82
5.6	Minimum Variance Transformation of Event on day 52 of 2001	83
5.7	Comparison of Data with One parameter Bright	84
5.8	Comparison of data to a scaled Two Parameter Soliton	85
5.9	Root Finding method for Two parameter analytical solution	89
5.10	Shooting method applied to scaled 2p soliton	90
5.11	Numerical integration of DNLS with a Two parameter soliton	91
5.12	Numerical integration of DNLS with a Two parameter soliton with background oscillations	92
5.13	Numerical integration of DNLS with data	94
5.14	Numerical integration of DNLS with scaled two parameter soliton . .	95
5.15	Dark soliton comparison	96

Chapter 1

INTRODUCTION

A vast majority of linear phenomena observed in mathematics and physics has been thoroughly studied to a large extent. In contrast, nonlinear phenomena still pose interesting, complex, and addling problems. Soliton theory is one branch of nonlinear applied mathematics that has had a great expansion in the knowledge and understanding of the weakly nonlinear phenomena known as solitons. Solitons are nonlinear waves that preserve their shape as they propagate forward in space and time. They are solutions to nonlinear partial differential equations that exhibit both dispersive and nonlinear effects that allow these structures to move with unaltered form. The dynamics of these waves will be introduced in the following sections.

1.1 Nonlinear Waves

1.1.1 Solitons

These curious waveforms, known as solitons, present puzzling and interesting behavior have been observed in various media over the past century. The first observation of a soliton was made in 1834 by Scott Russell, in the Union Canal in Scotland [26]. Scott Russell was observing a boat moving down the canal that had come to a complete stop. When the boat suddenly stopped, the wake in front of the boat continued to travel forward along the channel and he followed it for a few miles until he lost

the wave in the turns of the channel. He reported his observation to the British Association in his ‘Report on Waves’ in 1844, which read

I believe I shall best introduce the phenomenon by describing the circumstances of my own first acquaintance with it. I was observing the motion of a boat which was rapidly drawn along a narrow channel by a pair of horses, when the boat suddenly stopped - not so the mass of water in the channel which it had put in motion; it accumulated round the prow of the vessel in a state of violent agitation, then suddenly leaving it behind, rolled forward with great velocity, assuming the form of a large solitary elevation, a rounded, smooth and well-defined heap of water, which continued its course along the channel apparently without change of form or diminution of speed. I followed it on horseback, and overtook it still rolling on at a rate of some eight or nine miles an hour, preserving its original figure some thirty feet long and a foot to a foot and a half in height. Its height gradually diminished, and after a chase of one or two miles I lost it in the windings of the channel. [26]

He also continued to study these phenomenon in the laboratory setting by dropping a stone at one end of a water channel [8]. Through empirical evidence, Russell was able to deduce that the speed of the wave, c , was determined by

$$c^2 = g(h + a) \quad (1.1)$$

where g is the acceleration of gravity, h is the depth of the undisturbed water, and a is the amplitude of the wave. We can notice immediately by inspection of Eq. (1.1) that the higher amplitudes result in higher wave speeds. Later on, Joseph Bussinesq and Lord Rayleigh both arrived at Russell’s relation of the speed of the solitary wave with the assumption that the wave length was much larger than the depth of the water. They had derived the relation from a set of idealized fluid equations of motion, which will be discussed later.

They also managed to produce an analytical representation of one of these solitary waves with the form

$$u(x, t) = a \operatorname{sech}^2\{\beta(x - ct)\} \quad (1.2)$$

where u is the height of the fluid surface relative to its equilibrium position, $\beta^{-2} = 4h^2(h + a)/3a$ where $a > 0$ with the restriction that $a/h \ll 1$ (see pages 7-9 from Ref. [8]). The next section reveals an equation that will produce such a solution.

Korteweg-de Vries equation

A typical nonlinear equation the solutions of which are solitons is the Korteweg-de Vries (KdV) equation, which was first introduced by Boussinesq in 1877 but then later rediscovered by Diederik Korteweg and Gustav de Vries in 1895 [6]. The KdV equation exhibits both dispersive and nonlinear steepening effects. It has the form

$$U_t + 6UU_x + U_{xxx} = 0, \quad (1.3)$$

where U , x and t have all been scaled and denote dimensionless quantities. The second term in Eq. (1.3) produces the steepening effect, because of its nonlinearity, and the third term induces a dispersive effect. Solutions to the KdV equation along with methods to produce the many forms of this equation are in vast quantity. The simplest solution, which was previewed in the previous section, has the form

$$U(x, t) = 2 \operatorname{sech}^2(x - 4t), \quad (1.4)$$

which is also known as the *single soliton solution*, where $a = 2$ and $c = 4$. Figure 1.1 displays the wave form and time evolution of the single soliton.

As it turns out, the KdV has a peculiar characteristic where it can generate an infinite number of soliton solutions, also known as a train of solitons. Therefore, for example, a two soliton solution exists, and has the form

$$U(x, t) = 12 \frac{3 + 4\cosh(2x - 8t) + \cosh(4x - 64t)}{[3\cosh(x - 28t) + \cosh(3x - 36t)]^2}. \quad (1.5)$$

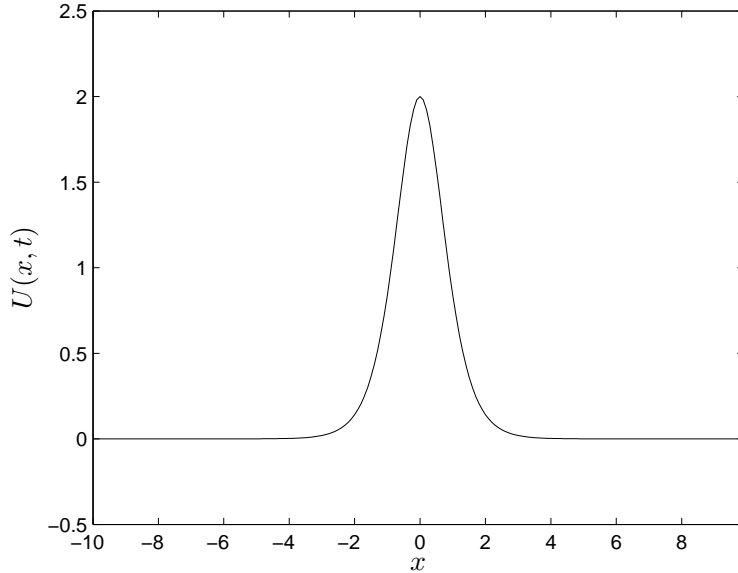


Figure 1.1: Single soliton solution of the KdV equation Eq. (1.4), at $t = 0$. The solution U at anytime other than $t = 0$ can be obtained by a simple linear translation.

Figure 1.2 shows the time evolution of this function. The nature of the two soliton solution is where the odd behavior of these solitons arises. First of all, at $t = 0$ in Figure 1.2 shows the wave as a single displacement, but then splits into two individual solitons as time progresses. They retain the same relationship between speed and amplitude that was deduced from Russell's early experiments.

Another odd trait that this two soliton solution displays is when the two solitons interact with each other. When the soliton with a larger amplitude "catches up" with the soliton with a smaller amplitude, the two will "collide," creating a larger amplitude structure, then split again, unaltered in shape with a shift in phase, which can be seen in Figure 1.3. Essentially, the solitons are dispersionless when it comes to soliton-soliton interactions. Mathematically, in the limit $|t| \rightarrow \infty$, the solution in Eq. (1.5) can be approximated as a sum of two terms, each with the form of (1.4) but with different amplitudes.

In the end, there are three main characteristics that can aide in the process of determining if a nonlinear wave is indeed a soliton. The most striking is that it

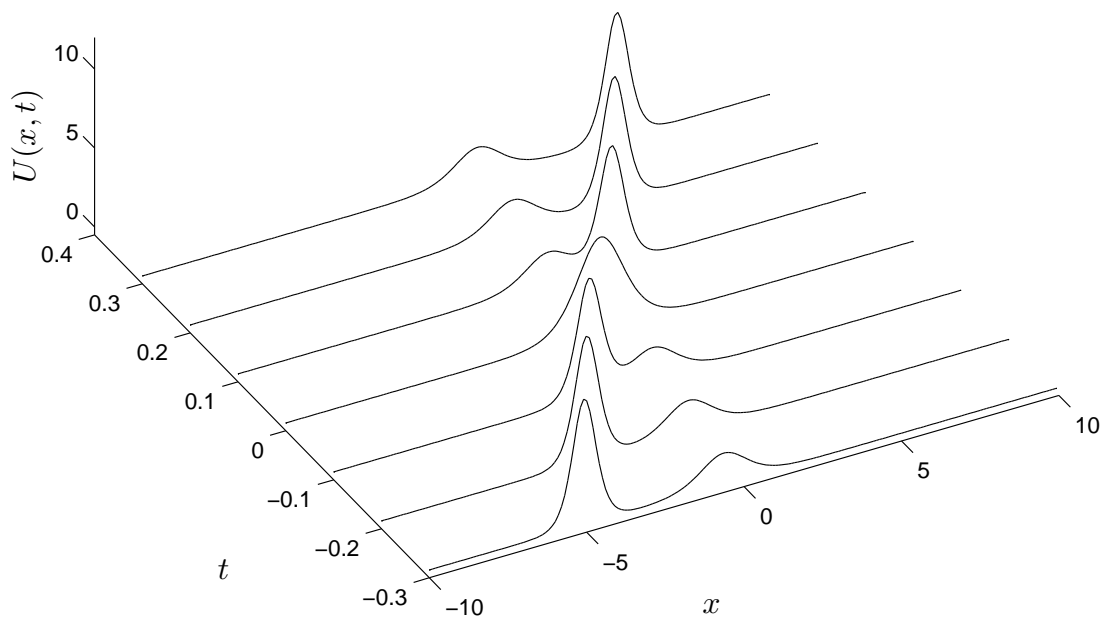


Figure 1.2: Two soliton solution of the KdV equation, Eq (1.5). At $t = 0$ the wave form is similar to the one soliton solution in that it is a single localized displacement. Since it has a different amplitude and width relation, as time progresses, the single localized structure splits into two solitons with different speeds and different amplitudes. As deduced from Eq. (1.1), the larger amplitude soliton has a larger speed.

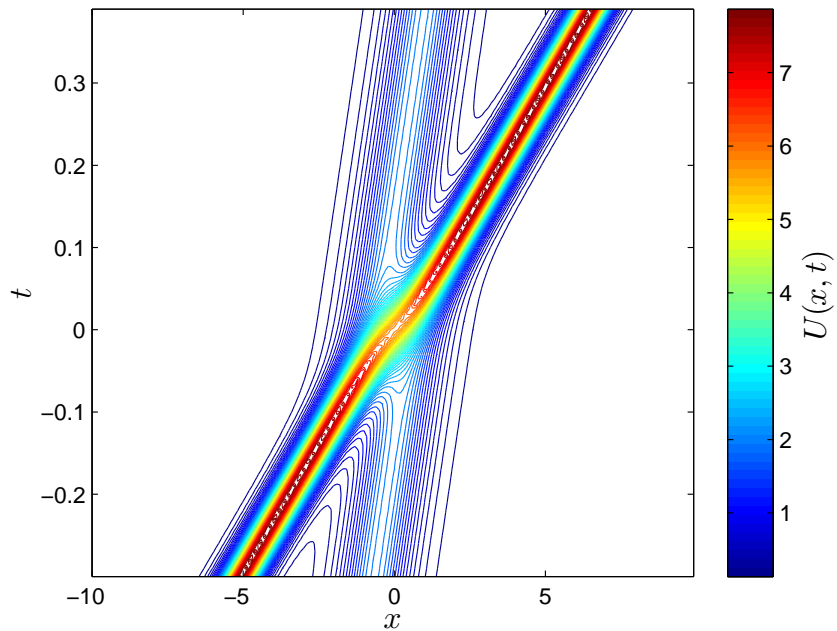


Figure 1.3: This figure shows the same two-soliton solution as in Fig 1.2. However, it is a contour plot where the axes are time and space and the color represents the value of U . The larger soliton starts behind the smaller and eventually passes it. The two waves retain their shape, but the smaller soliton has a larger phase shift than the larger amplitude soliton.

has permanent form, not changing its geometry as it progresses in time. Another important factor is that it is a localized entity. Lastly, solitons are dispersionless, i.e., they can interact and emerge from any “collision” without any change in shape, only suffering a shift in their phase. However, it is important to know that not all of these properties are necessarily true for solitons that are solutions to the DNLS equation or other various nonlinear equations with soliton solutions, this issue will be addressed in Chapter 2 for the DNLS equation.

1.2 Solitons in Space Plasmas

Recently, there has been an increased attraction for soliton based theory and observations [27] for as explanations to localized magnetic bumps occurring in plasmas. There is also an interest in developing methods to control similar phenomena in thermonuclear fusion installation environments [17]. Nonlinear partial differential equations with soliton solutions have been derived for the structure of the magnetic field from Hall [23] and two fluid [14] magnetohydrodynamic equations for various assumptions.

1.2.1 Nonlinear Oblique Alfvèn Waves

In the 1970’s and 1980’s, numerical and computational studies of nonlinear plasma waves were difficult because of the lack of computers that were capable of handling such problems. As a result, many nonlinear processes occurring in plasmas had to be treated analytically. This led to a technique called *reductive perturbation*, which allowed researchers to produce a single nonlinear equation that would describe specific processes under different cases and assumptions. Reductive perturbation is an extension of linear perturbation theory in which the weak nonlinear first order terms were kept selectively.

A vast number of nonlinear equations that described nonlinear plasma wave propagation were derived. Usually they were extensions to the linear wave theory of magnetohydrodynamic waves, where the nonlinear equations described different wave modes (i.e., slow, intermediate and fast waves - which will be discussed later). Many

of these nonlinear equations permitted soliton solutions (which were also defined as *integrable* or *evolution equations*).

One of the most studied of these integrable equations that is used to describe weakly nonlinear dispersive waves is the *Derivative Nonlinear Schrödinger* (DNLS) equation where the name was coined by Kaup and Newell in 1978 [12]. Because of the integrability of the DNLS equation, an analytical soliton solution can be produced through the inverse scattering transformation or IST. The IST for vanishing boundary conditions, or parallel wave propagation, was developed by Kaup and Newell (1978) [12], and for non-vanishing boundary conditions by Kawata and Inoue [13] for oblique and perpendicular wave travel.

The physical importance of the DNLS equation is that it can be used to describe oblique and parallel Alfvèn wave travel for both low and high β plasmas [14]. Here, β is a key plasma parameter used as a convenient way to characterize the general behavior of the plasma, because it relates the gas pressure of the plasma and the magnetic pressure exerted by the restoring force of the field lines (see §2.1.1 for details on β). For low β , the magnetosonic and Alfvènic wave speeds coincide at parallel wave travel and for small angles relative to the background magnetic field. For high β , the slow and intermediate wave speeds are approximately the same for any propagation angle with respect to the background magnetic field. The DNLS is also applicable to these types of waves in the case that they have large amplitudes [23]. Large reductions in the magnetic field strength observed in the solar wind, known as *magnetic holes*, in conditions of high β have been theorized to behave according to the DNLS equation [11]. Magnetic holes have also been observed in low β environments as well [27]. In the presence of dissipation, it was shown that the Derivative Nonlinear Schrödinger Burgers equation (DNLSB) for various initial wave configurations can generate dark solitons, which are the class of solitons as a possible explanation of magnetic holes [11].

1.3 Synopsis of Thesis

This thesis provides an in depth evaluation of the DNLS equation and its significance in the behavior of weakly nonlinear dispersive magnetohydrodynamic (MHD) waves. The second chapter will introduce the regime of MHD waves with a linearization of the ideal MHD equations, illustrating the effect of the plasma β on the relative phase velocities with respect to angle of propagation from the background magnetic field. Each of these phase velocities relate to a different nonlinear partial differential equation, but the focus will be on oblique Alfvén waves which could be described by the DNLS equation. Following the demonstration of the weak nonlinear equations as analogue to the three characteristic speeds for the linear MHD regime, analytical solutions of the DNLS equation will be shown. There are two main classes of soliton solutions for the DNLS, the one-parameter and two-parameter solutions. One parameter solitons come in two varieties, “dark” (rarefractive) and “bright” (compressive). It will be seen later that two parameter solitons have a variety of forms.

Chapter 3 will cover the mathematical theory of the direct scattering transformation in regard to the inverse scattering transformation. An analogy between the linear wave theory of using Fourier analysis to study linear PDE’s and the use of the IST to study nonlinear PDE’s will be discussed. The primary focus will be on Sturm-Liouville theory, or the direct scattering transformation, and the implication and meaning of the scattering data. A derivation using Lax pairs will prove how the eigenvalues, λ , are constant in time for the KdV equation (and can be extended to other nonlinear PDE’s). Details on the effect of the scattering data will be presented, focusing on the meaning of “reflection” in regard to soliton theory and how a nonzero reflection coefficient will lead to dispersive waves. This will lead up to the 2x2 eigenvalue problem onto which the DNLS equation is mapped, and which has been shown to be integrable through solutions produced by the IST [13].

Chapter 4 will begin with a brief demonstration of producing the finite difference equations for the linear convection and diffusion equations. Stability for these linear equations will be determined with von Neumann stability analysis. Building on the methods for the linear convection and diffusion equations will lead up to a numerical

scheme for nonlinear equations that exhibit nonlinear steepening and dispersive properties, such as the KdV and DNLS equations. Implementation of periodic boundary conditions are detailed for both explicit and implicit numerical schemes. Since stability criteria are difficult to obtain with nonlinear equations, comparison with known analytical solutions that have been produced from IST for the DNLS equation will be used to assess the numerical schemes' stability. Inspection of the root mean square error between the analytical solution and the numerical solution (with the initial condition being the analytical solution at $t = 0$) for different time steps will lead to stable solutions for sufficiently small values of the time step.

In the closing chapter, Chapter 5, a specific solitary structure that was observed by the Ulysses spacecraft on February 21st, 2001 is closely analyzed using theory that was developed in Chapters 2-4. Presentation of the spacecraft's orbital parameters and the characteristics of the plasma during the observed event are detailed to establish that the singular wave does fit in the regime of the DNLS equation. A minimum variance transformation is then used to change reference frames to one where one of the components is normal to a boundary, and where the minimal variance direction is the direction of propagation with respect to the background magnetic field.

The morphology of the transformed magnetometer data is then compared to that of a two parameter soliton, which shares the similar "banana-polarization" as the data. Three methods were used to demonstrate if the observed magnetic bump contains a soliton component. First, to obtain a close comparison of the two parameter soliton with the magnetic pulse, the amplitude of the two parameter soliton was scaled. Second, a Runge-Kutta fourth order shooting method coupled with Muller's method for root finding was performed to determine if any solitons were present in the profile, and one was identified. Finally, a DNLS numerical integration scheme was used to confirm that a soliton was present in the scaled profile that resembled the magnetic pulse by using the profile as the initial condition. A dark one parameter soliton formed, along with dispersive waves, which implies that the event does contain a soliton component.

Chapter 2

Waves in plasmas

Since the basis of this thesis is nonlinear waves occurring in plasmas, it is appropriate to discuss the basics of the dynamics of plasmas. A plasma has been popularly defined as a quasi-neutral ionized gas. Technically it is a gas, but the temperatures (or the average kinetic energy of the particles present) range higher than normal. Temperatures are so high that the amount of energy present in the gas is enough to sever the bond between the electron and its atomic nucleus. Essentially, the electrons tend to freely move within the plasma without the restriction of being attached to a single atom. The term “quasi-neutral” arises from the assumption that the number of positive charges in the collection of particles is approximately the same as the freely moving electrons. If this were not the case, strong electric fields would develop in an attempt to neutralize the plasma.

The consequence of freely moving electrons within the plasma means that the dynamics and overall behavior of the gas changes. Since plasma is technically a gas, it still retains its fluid nature, and the general kinetic nature of gases still apply, but now it can be subject to electromagnetic forces; therefore, plasmas exhibit collective behavior that is not seen in neutral gases. The next section will build a foundation of the fluid-like behavior and properties of these magnetized fluids.

2.1 Magnetohydrodynamics

Magnetohydrodynamics, or simply MHD, is the study of fluids that have electromagnetic properties due to currents that flow in the quasi-neutral medium. The equations that describe MHD are essentially the hydrodynamic equations with the Lorentz force included. In the neutral case, these equations are also known as Euler's equations for describing a fluid with no viscosity,

$$\frac{\partial \rho}{\partial t} + \nabla \cdot (\rho \mathbf{u}) = 0 \quad (2.1a)$$

$$\frac{\partial(\rho \mathbf{u})}{\partial t} + \nabla \cdot (\rho \mathbf{u} \mathbf{u}) + \nabla p = 0 \quad (2.1b)$$

$$\frac{\partial E}{\partial t} + \nabla \cdot (\mathbf{u}(E + p)) = 0 \quad (2.1c)$$

which are a set of conservation equations for mass, momentum, and energy, respectively. The quantity ρ is the mass density, \mathbf{v} is the fluid velocity vector, p is the pressure, and E is the total energy density which includes both the thermal and bulk flow energy.

As mentioned earlier, the Lorentz force is necessary to include because it describes the behavior of charged particles under the influence of electromagnetic fields. The fluid effect of the Lorentz force appears on the right hand side of the momentum equation, Eq. (2.1b).

$$\frac{\partial(\rho \mathbf{u})}{\partial t} + \nabla \cdot (\mathbf{u}(\rho \mathbf{u})) + \nabla p = \mathbf{J} \times \mathbf{B}, \quad (2.2)$$

where \mathbf{J} is the current density and \mathbf{B} is the magnetic field. A term describing the electric field is not present because the plasma is assumed to be infinitely conducting (i.e., no free charge distribution). Typically it is important to distinguish between the species of particles contained in the plasma because the level of ionization for the ions could determine different overall behavior of the plasma, but we have treated the magnetized fluid as a single fluid as opposed to two fluids (electrons and ions) because in the ideal case these two species effects are neglected.

In addition to Eqs. (2.1a) and (2.2), an equation is needed to describe the energy

transfer. Equation (2.1c) is correct, but under the ideal description, it is typically assumed that the plasma is adiabatic, and it can be shown that the energy equation (2.1c) reduces to

$$\frac{d}{dt} \left(\frac{p}{\rho^\gamma} \right) = 0 \quad (2.3)$$

where $\gamma = 5/3$ is the ratio of specific heats for an adiabatic equation of state for an ideal monoatomic gas.

There is another set of equations that is needed to complete the picture of MHD, which are Maxwell's equations that describe the nature of \mathbf{J} and \mathbf{B} . Maxwell's equations are

$$\nabla \cdot \mathbf{E} = \frac{\rho_c}{\epsilon_0} = 0 \quad (2.4a)$$

$$\nabla \cdot \mathbf{B} = 0 \quad (2.4b)$$

$$\nabla \times \mathbf{E} = -\frac{\partial \mathbf{B}}{\partial t} \quad (2.4c)$$

$$\nabla \times \mathbf{B} = \mu_0 \mathbf{J} + \frac{1}{c^2} \frac{\partial \mathbf{E}}{\partial t}, \quad (2.4d)$$

which are presented in differential form, where c is the speed of light, μ_0 is the permeability of free space, and ϵ_0 is the permittivity of free space. For the purposes of ideal MHD, the displacement current term is neglected because it is assumed that the electromagnetic waves generated in the plasma are of low frequency which is consistent with $\rho_c = 0$. This is the last term in Ampere's law, Eq. (2.4d). With application of the charge neutrality argument, it can be shown that the first two equations, Eq. (2.4a) and Eq. (2.4b), are redundant (That is, they simply act as initial conditions for Faraday's (2.4c) and Ampere's (2.4d) law, which are time evolution equations for \mathbf{E} and \mathbf{B}).

Another equation is needed to close the system and describe the plasma's ability to conduct electrical currents. In Ideal MHD, the plasma is considered to have a conductivity that is infinitely large, which leads to the ideal Ohms law

$$\mathbf{E} + \mathbf{u} \times \mathbf{B} = \eta \mathbf{J}, \quad (2.5)$$

where $\eta = 1/\sigma$ is the resistivity of the plasma, and σ is the conductivity, which $\sigma \rightarrow \infty$.

2.1.1 Linear waves permitted by the ideal MHD equations

Since there are a vast amount of driving forces in the MHD equations, there is a possibility for different types of waves that would propagate through the plasma. We can inspect what kind of waves that can exist through linearization of the MHD equations in parallel with applying Fourier transforms. As a reminder, the ideal MHD equations are

$$\frac{\partial \rho}{\partial t} + \nabla \cdot (\rho \mathbf{u}) = 0 \quad (2.6a)$$

$$\frac{\partial(\rho \mathbf{u})}{\partial t} + \nabla \cdot (\mathbf{u}(\rho \mathbf{u})) = \mathbf{J} \times \mathbf{B} - \nabla p \quad (2.6b)$$

$$\frac{d}{dt} \left(\frac{p}{\rho^\gamma} \right) = 0, \quad (2.6c)$$

along with Maxwell's equations

$$\nabla \times \mathbf{E} = -\frac{\partial \mathbf{B}}{\partial t} \quad (2.7a)$$

$$\nabla \times \mathbf{B} = \mu_0 \mathbf{J}, \quad (2.7b)$$

and generalized Ohm's Law, which describes electrical conduction in the plasma,

$$\mathbf{E} + \mathbf{u} \times \mathbf{B} = \eta \mathbf{J} = 0 \quad (2.8)$$

where $\eta = 1/\sigma \rightarrow 0$ because $\sigma \rightarrow \infty$ because the plasma is considered infinitely conducting in ideal MHD.

Linearization, or in this case *linear perturbation theory*, is a method for eliminating nonlinear terms through expansion about an assumed equilibrium state. For a plasma, most of the ideal MHD approximations apply here, such as charge neutrality (where the number of ions is the same as electrons) which results in no equilibrium electric field. Also, we assume that there is no initial bulk flow, the particles are distributed

evenly in space, and the plasma is in steady state. This leads to the conditions

$$\frac{\partial \rho_0}{\partial t} = \frac{\partial \mathbf{u}_0}{\partial t} = \frac{\partial \mathbf{E}_0}{\partial t} = 0 \quad (2.9)$$

$$\nabla \rho_0 = \mathbf{u}_0 = \mathbf{E}_0 = 0, \quad (2.10)$$

where the 0 subscript denotes the equilibrium state. The next order in the expansion is the small perturbations, which are taken to be plane waves with small amplitudes (which have the form $e^{i(\mathbf{k}\cdot\mathbf{r}-\omega t)}$, where \mathbf{r} is a position vector and \mathbf{k} is the wave number) where the permitted variables that are allowed to vary are \mathbf{B} , \mathbf{E} , \mathbf{u} , ρ and p . These perturbed quantities have the same effect as a Fourier transformation in space and time (i.e., $\nabla \rightarrow i\mathbf{k}$ and $\partial/\partial t \rightarrow -i\omega$). After some work, the continuity and momentum equations reduce to

$$-\omega \rho_1 + \rho_0 \mathbf{k} \cdot \mathbf{u} = 0 \quad (2.11)$$

$$-\rho_0 \omega \mathbf{u} + c_s^2 \rho_1 \mathbf{k} = -i \mathbf{J} \times \mathbf{B}_0 \quad (2.12)$$

where the 1 subscripts denote the amplitude of the perturbed quantity and

$$c_s^2 = \frac{\gamma p_0}{\rho_0}, \quad (2.13)$$

which is the sound speed. Applying the same technique to Faraday's and Ampere's law yields

$$\mathbf{k} \times \mathbf{E} = \omega \mathbf{B}_1 \quad (2.14)$$

$$\mathbf{k} \times \mathbf{B}_1 = -i \mu_0 \mathbf{J}. \quad (2.15)$$

We can further simplify by restricting of the wave propagation to two cases, propagation of the waves parallel to the background magnetic field (i.e., $\mathbf{k} \times \mathbf{B}_0 = 0$) and perpendicular to the background magnetic field (i.e., $\mathbf{k} \cdot \mathbf{B}_0 = 0$). First, we can look at the transverse component of the momentum equation, Eq. (2.12), for parallel

propagating waves which gives

$$\mathbf{u}_t \left[1 - \frac{k^2}{\omega^2} \frac{B_0^2}{\rho_0 \mu_0} \right] = 0 \quad (2.16)$$

where \mathbf{u}_t is the first order velocity oscillation transverse to \mathbf{B}_0 (i.e., $\mathbf{u}_t \cdot \mathbf{B}_0 = 0$). Since we are looking at the parallel propagating case we know $\mathbf{u}_t \neq 0$, so then the term inside the brackets has to be zero, which gives us the dispersion relation

$$\frac{\omega^2}{k^2} = \frac{B_0^2}{\rho_0 \mu_0} = v_A^2 \quad (2.17)$$

which is the Alfvén velocity. Alfvén waves are low-frequency traveling waves that are caused by the oscillations between the ions and the magnetic field. Essentially, the magnetic tension acts as a restoring force where the ion mass density provides the inertia.

After a further generalization, one can show after manipulation of Eqs. (2.11)-(2.15) that a more general dispersion relation for waves in a magnetized plasma is

$$\mathbf{B}_1 \left[1 - \frac{c_A^2 \cos^2 \theta}{V^2} \right] = \frac{c_A^2 \hat{b} \cdot \mathbf{B}_1 (\hat{b} - \hat{k} \cos \theta)}{V^2 - c_s^2} \quad (2.18)$$

where $V = \omega/k$ which is the phase velocity of the wave, $\hat{b} = \mathbf{B}_0/B_0$, $\hat{k} = \mathbf{k}/k$, $\cos \theta = \hat{k} \cdot \hat{b}$, and θ is the direction of propagation with respect to the background magnetic field. Furthermore, we can inspect two limiting cases where the perturbed magnetic field, \mathbf{B}_1 , is (a) perpendicular to the background magnetic field, B_0 , i.e., $\mathbf{B}_1 \cdot \hat{b} = 0$ and (b) where it is not perpendicular, i.e., $\mathbf{B}_1 \cdot \hat{b} \neq 0$. For the first case, the assumption of $\mathbf{B}_1 \cdot \hat{b} = 0$ means Eq. (2.18) reduces to

$$\mathbf{B}_1 \left[1 - \frac{c_A^2 \cos^2 \theta}{V^2} \right] = 0 \quad (2.19)$$

and since $\mathbf{B}_1 \neq 0$, we arrive at

$$V^2 = c_A^2 \cos^2 \theta \quad (2.20)$$

which is also known as the “shear Alfvén wave”. In general, if $\mathbf{B}_1 \cdot \hat{b} \neq 0$ one can

show, through Eq. (2.18), that

$$\hat{b} \cdot \mathbf{B}_1 [(V^2 - c_A^2 \cos^2 \theta)(V^2 - c_s^2) - V^2 c_A^2 \sin^2 \theta] = 0 , \quad (2.21)$$

which gives

$$V^2 = \frac{1}{2} \left[(c_s^2 + c_A^2) \pm \sqrt{(c_s^2 + c_A^2)^2 - 4c_s^2 c_A^2 \cos^2 \theta} \right] \quad (2.22)$$

where the + sign, will produce the “fast Alfvèn” wave phase velocity, and the – sign will produce the “slow Alfvèn” velocity. Now if we introduce a plasma parameter, known as the “plasma beta”, with the form

$$\beta \equiv \frac{c_s^2}{c_A^2}, \quad (2.23)$$

which allows the simplification of Eq. (2.22) to be written in terms of only β and θ . More importantly, the plasma β expresses which of the two processes are more dominant, the random thermal movement or the magnetic field strength. We can further inspect the effect of the two different cases for Eq. (2.22), low beta ($\beta < 1$) and high beta ($\beta > 1$).

Figures 2.1 and 2.2 display the relative phase velocities for low β and high β , respectively. When the thermal gas pressure is low compared to the pressure exerted by the restoring force of the magnetic field lines, the Alfvèn speed is much higher than the sound speed meaning the response of the field lines occurs much quicker than the inertial forces of the ions in the plasma.

For high beta, the acoustic wave speed and the Alfvèn speed coincide at parallel propagation and separate at high angles of propagation, but the separation is not as vast as what happens in the low beta limit. At small propagation angle with respect to the background magnetic field, the ion inertial forces and the magnetic restoration forces compete, and this will become important in the case of nonlinear waves.

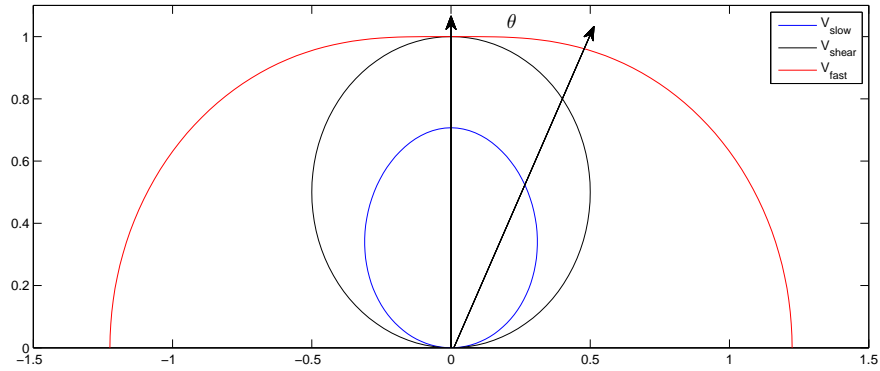


Figure 2.1: Phase velocity wave modes of the ideal MHD equations with low beta ($\beta = 0.5$). This plot represents the phase velocities as functions of the angle, θ , of propagation with respect to the normal, \hat{b} , of the background magnetic field. The three wave modes are the slow, or acoustic wave, the shear or Alfvénic wave, and the fast magnetosonic wave. At angles parallel to the background magnetic field, $\theta = 0$, the magnetosonic (fast) and the Alfvénic (intermediate) wave speeds coincide.

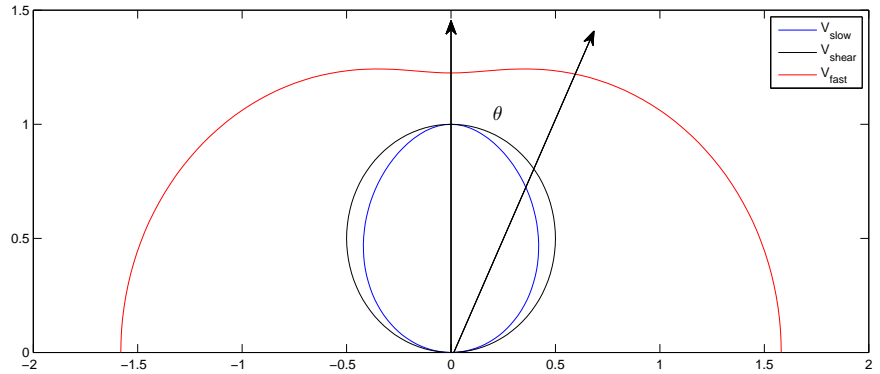


Figure 2.2: Phase velocity wave modes of the ideal MHD equations with high beta ($\beta = 1.5$). At angles parallel to the background magnetic field, the acoustic (slow) and the Alfvénic (intermediate) wave speeds coincide and separate with larger angles.

2.2 Nonlinear waves in plasmas

The inherent nature of plasmas and magnetohydrodynamics is nonlinear, therefore it is reasonable to conclude that nonlinear wave structures can and do exist in the MHD realm. Recent developments in nonlinear waves in plasmas have led to the conclusion that one class of these nonlinear MHD waves are indeed solitons. These solitary waves behave in a peculiar manner where they tend to preserve their waveform as they evolve in time, which was discussed in Chapter 1. The rigorous details of the dynamics and mathematical theory will be provided later in Chapter 3.

There are many partial differential equations that produce soliton solutions, but each evolution equation behaves differently and is applied to a specific governing media or multiple types of media (according to the approximations required to produce the PDE). The purpose of this section is to introduce two evolution equations that can be used to describe nonlinear waves in plasmas, in the perspective of the MHD.

2.2.1 Weakly Nonlinear waves in Plasmas

As mentioned earlier, in the case of a low plasma β , the intermediate and fast wave speeds coincide at parallel propagation. This was a direct result of linearization and assumption of simple plane wave propagation, which meant that the dispersive terms of the MHD equations were not included. In addition, in the case of large amplitude waves, the lowest order nonlinear effects become important. Inclusion of the dispersive terms in the MHD equations and use of the reductive perturbation method with various assumptions can lead to three different nonlinear evolution equations that have soliton solutions.

For a wave that is oblique to the background magnetic field, it was shown by Mjølhus and Hada [18] that the MHD equations, using a two fluid adiabatic model, can lead to the KdV equation for the fast mode waves for low β , i.e., nonlinear magnetosonic waves. Focusing on a nonlinear equation that can be applied to the intermediate wave mode, it was demonstrated that the Modified Korteweg-de Vries (MKdV) equation could be obtained (by Kakutani and Ono in 1969 see Ref. [18]).

The MKdV equation has the general form

$$u_t + u_{xxx} \pm 6u^2u_x = 0 \quad (2.24)$$

although it may, of course, be scaled differently. Reference [18] also outlines how Taniuti and Yajima in 1968 and Hasegawa in 1971 showed that for monochromatic and strongly dispersive waves along with a reduction, the dispersive MHD equations can lead to the nonlinear Schrödinger equation (NLS),

$$i\psi_t = -\frac{1}{2}\psi_{xx} + \kappa|\psi|^2\psi. \quad (2.25)$$

This thesis focuses on another nonlinear evolution equation, the DNLS equation, that actually reduces to the previously mentioned equations as limiting cases (e.g. KdV, MKdV, NLS equations). For quasi-parallel propagating waves, there is a degeneracy between the magnetosonic and Alfvénic modes for a low β and between the acoustic and Alfvénic modes for high β (which can be seen in Figures 2.1 and 2.2). For the low β case, where the two wave modes coincide, the two equations describing weak nonlinear waves, the KdV and the MKdV, become coupled. Writing them in complex form leads to one single equation,

$$\frac{\partial b}{\partial t} + \alpha \frac{\partial}{\partial x}(|b|^2 b) + i\mu \frac{\partial^2 b}{\partial x^2} = 0 \quad (2.26)$$

which is the DNLS equation. But like the other nonlinear evolution equations derived from MHD equations, it is possible to use the same reductive perturbation technique to derive the DNLS equation. The DNLS equation was first derived by Rogister using kinetic theory starting from the Vlasov description [22]. It was also derived by Mjølhus [19] with a two fluid model using a hybrid fluid and kinetic guiding center model [20].

Another derivation of the DNLS equation using the reductive perturbation technique was made by Ruderman [23] by starting with the Hall MHD equations. It was assumed that the pressure was isotropic, and the plasma was adiabatic and infinitely

conducting. The main assumptions that permitted the reductive perturbation technique's effectiveness was that the amplitudes were large and β was high, but the propagation direction was arbitrary.

Finally, Kennel et al. [14] were able to produce the DNLS equation using the two fluid model, with an adiabatic assumption and inclusion of ion dispersion, which comes from inclusion of ion dispersion term in the generalized Ohm's law. It was shown that for a low β plasma, the quasi-parallel propagating waves with intermediate and fast speeds where described by the DNLS equation and for larger angles of propagation the KdV equations describes fast and slow wave solitons and the MKdV describes intermediate speed solitons. They were also able to show that the coefficients of the DNLS equation, Eq. (2.26), for quasi-parallel wave travel are

$$\alpha = \frac{1}{4} \frac{c_A}{B_0^2} \frac{1}{1 - \beta} \quad (2.27)$$

for the nonlinear coefficient and

$$\mu = \frac{1}{2} \frac{c}{\omega_{pi}} \quad (2.28)$$

for the dispersive term.

2.2.2 Derivative Nonlinear Schrödinger (DNLS) Equation

The DNLS has been used recently as a nonlinear equation that produces solitary waves in the form of magnetic field perturbations. This is due to the fact that it has been derived for multiple different approximations utilizing the reductive perturbation method. Reductive perturbation combines the governing equations, in this case the MHD equations, by choosing specific assumptions and keeping low order terms to produce a single evolution equation.

Of course, not all assumptions can yield an evolution equation or a simplified equation at all, but there have been many works that have been able to produce the DNLS equation from MHD equations. The assumptions typically include long

wavelength, small amplitude and slowly evolving waves. The DNLS equation is

$$\frac{\partial b}{\partial t} + \alpha \frac{\partial}{\partial t} (|b|^2 b) + i\mu \frac{\partial^2 b}{\partial x^2} = 0, \quad (2.29)$$

where

$$b(x, t) = b_y + i b_z . \quad (2.30)$$

This equation describes waves propagating in the x -direction, where b_y and b_z are the real of the magnetic field that are transverse to the propagation direction.

Although the DNLS describes one dimensional propagation, there are two different flavors of the DNLS that have two different boundary conditions. The form of Eq. (2.29) represents the nonlinear wave that is propagating parallel to the background magnetic field, b_0 . Its boundary conditions are when $b \rightarrow 0$ as $x \rightarrow \pm\infty$, or it is said to have “vanishing” boundary conditions.

The other case is when the wave is propagating at an oblique angle to the background magnetic field. There is a difference in the scalings, so the DNLS takes on the form

$$\frac{\partial b}{\partial t} + \alpha \frac{\partial}{\partial t} ((|b|^2 - b_0^2)b) + i\mu \frac{\partial^2 b}{\partial x^2} = 0, \quad (2.31)$$

where the boundary conditions are “non-vanishing”, $b \rightarrow b_0 \neq 0$ as $x = \pm\infty$. Analytical solutions to Eq. (2.29) are hard to produce because they require the mathematically intensive inverse scattering transform, which will be explained in depth later.

2.3 Analytical Solutions of the DNLS

The DNLS equation has been investigated thoroughly from a mathematical perspective, and many analytical solutions have been found. Two classes of solutions will be presented here, these so-called one and two parameter solitons. Techniques to arrive at these types of soliton solutions will be discussed in the following chapter, Chapter 3, which revolves around soliton theory.

2.3.1 One Parameter Soliton

When referring to *one parameter* solitons, a single parameter determines the shape of the wave. It turns out, that this parameter is the real component of the eigenvalue (see Chapter 3 for a discussion of the importance of the eigenvalues). These solutions arise in the case when the wave is moving oblique or nearly parallel to the background magnetic field, under nonvanishing boundary conditions.

The analytical form of the one parameter solitons is [13, 18]

$$b_y = b_0 + \frac{2\lambda\eta^2 s}{b_0^2} \frac{(\cosh(2\theta/L) - b_0 s/\lambda)}{\cosh(2\theta/L) - \lambda s/b_0)^2} \quad (2.32)$$

and

$$b_z = -\frac{2\eta^3 s}{b_0^2} \frac{\sinh(2\theta/L)}{\cosh(2\theta/L) - \lambda s/b_0)^2}, \quad (2.33)$$

where $\theta = x - ct$, $\eta = \sqrt{b_0^2 - \lambda^2}$, $L = 1/(\lambda\eta)$, $c = 2\lambda^2$, and $s = \pm 1$. It becomes clear why this solution is coined as a one parameter soliton because the value of λ determines the amplitude and speed of the wave. The sign of s determines the “flavor” of soliton, dark ($s = -1$) or bright ($s = 1$). Bright and dark refer to the fact that the magnitude of b (i.e., $\sqrt{b_y^2 + b_z^2}$) increases or decreases over its equilibrium value. Note that the space and time dependence is encapsulated into one single quantity, $\theta = x - ct$, which means that the shape of these one parameter solitons just translates without any alterations in the form, as with the KdV soliton solution.

Figures 2.3 and 2.4 show the functions $b_y(\theta)$ and $b_z(\theta)$ for the dark and bright soliton analytical solutions, respectively. These solutions to the DNLS equation exhibit the same behavior as the KdV solitons, where they hold their shape as they propagate forward in time.

2.3.2 Two Parameter Soliton

Solutions of the DNLS equation belonging to the *two parameter* class of solitons arise in both classes of wave propagation, oblique or parallel propagation. They can be

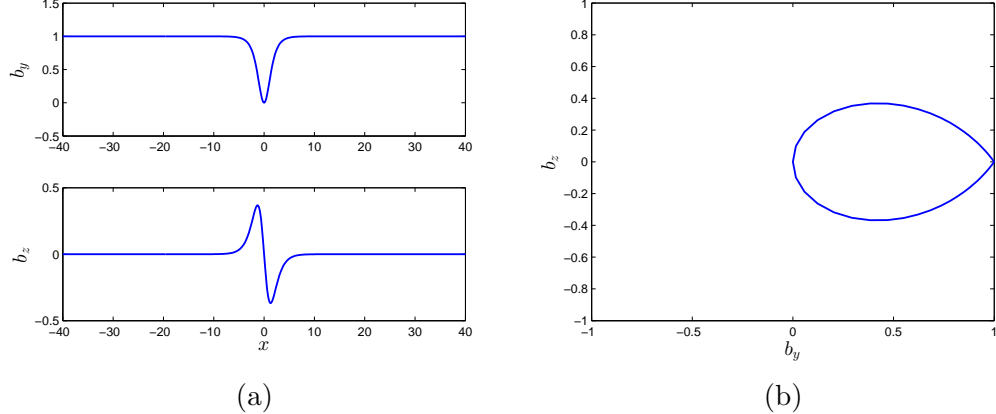


Figure 2.3: Dark soliton with an eigenvalue of $\lambda = 0.5$. The magnitude and the two components of b are plotted. It is clear that the magnitude of b gives the classification of a “dark” soliton because of the localized depression in b .

expressed in analytical form for oblique wave travel [18].

$$b = b_0 - 2\frac{\gamma}{\theta} \left(\frac{\bar{\theta}}{\theta} \right) - b_0 \left(1 - \frac{\bar{\theta}}{\theta} \right)^2, \quad (2.34)$$

where the functional forms of θ and γ are given by

$$\theta = 1 + \theta_1 \phi + \tilde{\theta}_1 \bar{\phi} + \theta_2 |\phi|^2; \quad \gamma = \gamma_1 \phi + \tilde{\gamma}_1 \bar{\phi} + \gamma_2 |\phi|^2. \quad (2.35)$$

where $\bar{\phi}$ and $\bar{\gamma}$ denote complex conjugate of ϕ and γ . The function ϕ has the only dependence on x and t and takes the form

$$\phi = \exp[2i(\Lambda x - \Omega t)]. \quad (2.36)$$

In addition, the variables θ_1 and $\tilde{\theta}_1$ are

$$\theta_1 = \frac{b_0}{2\Lambda} \left(\frac{\lambda}{\zeta} - 1 \right); \quad \tilde{\theta}_1 = \frac{b_0}{2\bar{\Lambda}} \left(\frac{\bar{\lambda}}{\bar{\zeta}} - 1 \right), \quad (2.37)$$

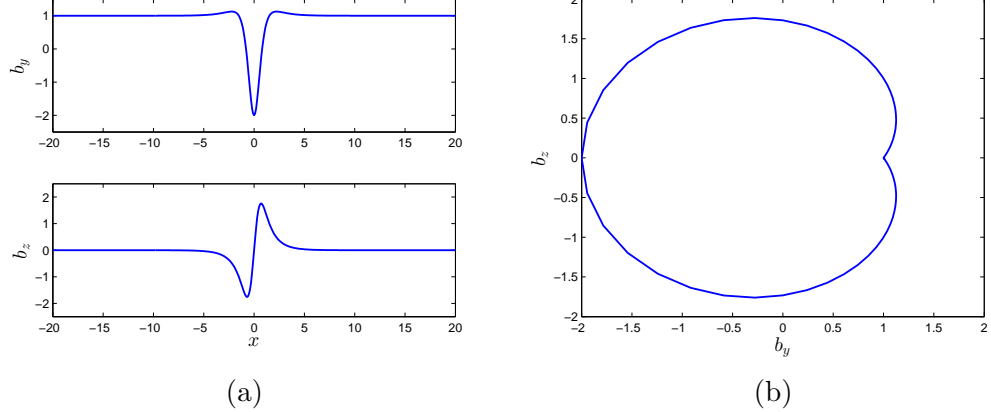


Figure 2.4: Bright soliton with an eigenvalue of $\lambda = 0.5$. The localized enhancement of $|b|$ accounts for the “bright” soliton description.

and the variables γ_1 and $\tilde{\gamma}_1$ are

$$\gamma_1 = \frac{\zeta}{\lambda} - 1 ; \quad \tilde{\gamma}_1 = -\frac{\bar{\zeta}}{\bar{\lambda}} - 1. \quad (2.38)$$

Finally the functional forms of θ_2 and γ_2 are

$$\begin{aligned} \theta_2 = b_0^2 & \left[\left(\frac{1}{|\Lambda - \bar{\Lambda}|^2} - \frac{1}{4|\Lambda|^2} \right) \left(1 - \frac{|\lambda|^2}{|\zeta|^2} \right) - \frac{1}{4|\Lambda|^2} \left(\frac{\bar{\lambda}}{\bar{\zeta}} - \frac{\lambda}{\zeta} \right) \right] \\ & - \left(\frac{1}{|\Lambda - \bar{\Lambda}|^2} \right) \left[(\bar{\Lambda} - \Lambda) \left(\frac{|\lambda|^2}{|\zeta|^2} + 1 \right) + (\bar{\Lambda} + \Lambda) \left(\frac{\bar{\lambda}}{\bar{\zeta}} - \frac{\lambda}{\zeta} \right) \right] \end{aligned}$$

and

$$\begin{aligned} \gamma_2 = b_0 & \left[(\bar{\lambda} + \bar{\zeta})(\zeta - \lambda) \left(\frac{1}{2\bar{\Lambda}} \frac{1}{\bar{\zeta}\lambda} + \frac{1}{2\Lambda} \frac{1}{\zeta\bar{\lambda}} \right) \right. \\ & \left. + \left(\frac{1}{\Lambda - \bar{\Lambda}} \right) \left((\zeta - \lambda) \left(\frac{\lambda}{\bar{\Lambda}} + \frac{1}{\lambda} \right) + (\bar{\lambda} + \bar{\zeta}) \left(\frac{\bar{\lambda}}{\Lambda} - \frac{1}{\bar{\lambda}} \right) \right) \right]. \end{aligned}$$

From inspecting the forms of all the equations presented above, all of them essentially depend on three complex quantities Λ , ζ and Ω . Their definitions are

$$\zeta = \sqrt{\lambda^2 - b_0^2}, \text{ for } (\text{Im } \zeta > 0) \quad (2.41\text{a})$$

$$\Lambda = \zeta \lambda \quad (2.41\text{b})$$

$$\Omega = \Lambda(2\lambda^2 + b_0^2) \quad (2.41\text{c})$$

are the main parameters that dictate the behavior of the wave. Again, λ is the eigenvalue, but in this case it is complex. This means that the two values needed to construct the solution of the two parameter soliton solution are $\text{Re}(\lambda)$ and $\text{Im}(\lambda)$. Another important fact with the two parameter soliton, is that its eigenvalues appear in complex conjugate pairs [11].

Figure 2.5 displays an example of the behavior of a two parameter soliton. It can be seen that the soliton does not retain its shape, but has a periodic behavior where it eventually returns to the initial wave form. This is due to the fact that one way of looking at the two parameter solution is as a combination of a bright soliton and a dark soliton. The bright and dark solitons are superposed and interchange their locations periodically. When the eigenvalue approaches the real axis, while inspecting a specific time (e.g. $t =$), the dark and bright solitons that had been exchanging their position periodically, separate and no longer interact with each other.

Since the solution $b(x, t)$ has a periodic behavior to it, we can attempt to determine when and where the waveform returns to its original state. This can be done by the assumption that at some length, L , and some later time, T , we will have $b(x + L, t + T) = b(x, t)$. Obtaining relations of L and T will give us insight into the periodic behavior of this soliton. Also, since $b(x, t)$ is a rational expression of $\phi(x, t)$ we can rewrite $\phi(x, t)$ to look like

$$\phi(x, t) = \exp[-\kappa(x - c_g t)] \exp[-\kappa(x - c_p h t)] \quad (2.42)$$

where

$$\kappa = 2\Lambda_i, \quad c_g = \Omega_i/\Lambda_i \quad (2.43a)$$

$$k = 2\Lambda_r, \quad c_{ph} = \Omega_r/\Lambda_r \quad (2.43b)$$

where $\Omega = \Omega_r + i\Omega_i$ and $\Lambda = \Lambda_r + i\Lambda_i$ ($\Lambda_{r,i}$ and $\Omega_{r,i}$ are real valued) and is analogous to its “phase velocity” and “group velocity” [18]. Now with the use of $b(x + L, t + T)$, this leads to

$$L = c_g T \quad (2.44a)$$

$$T = \frac{2\pi}{|k(c_{ph} - c_g)|}. \quad (2.44b)$$

Therefore, with Eqs. (2.44a) and (2.44b) it can be seen that if the eigenvalue, λ , has bias towards the real or imaginary axis, it will determine the periodicity of the waveform.

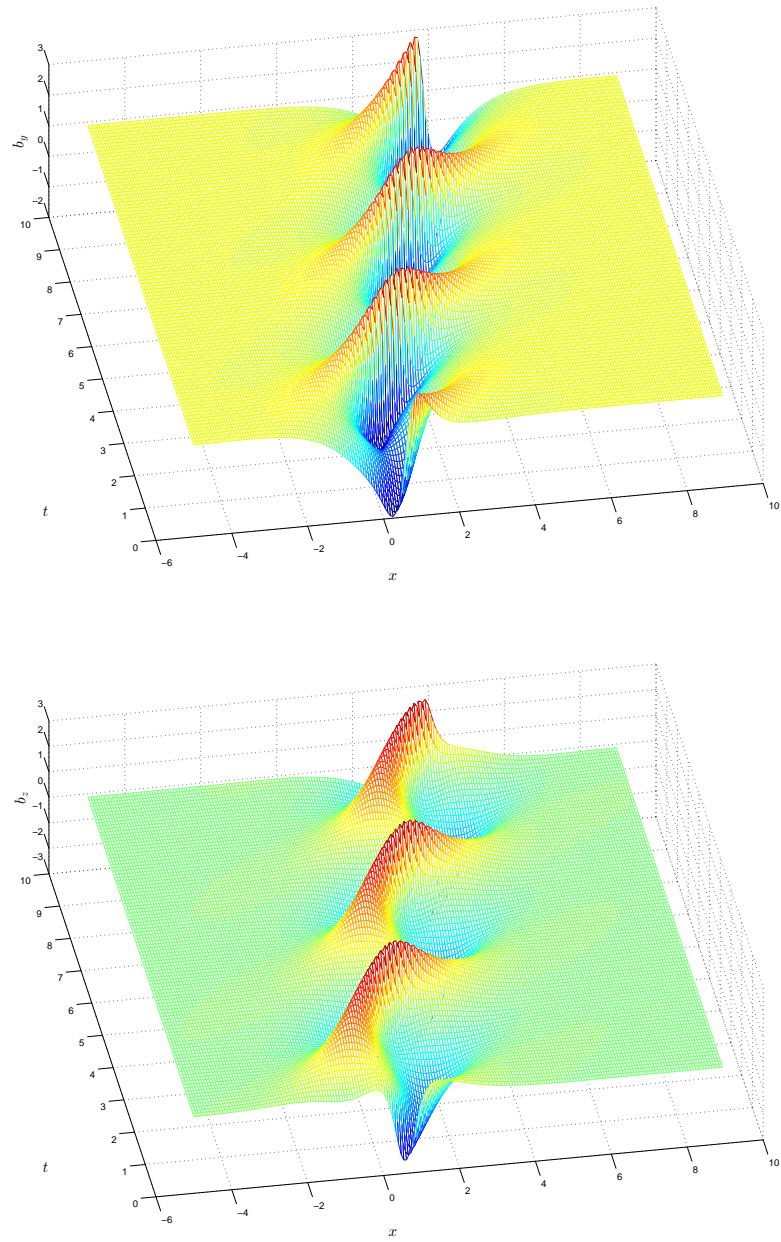


Figure 2.5: The behavior of a two parameter soliton with $\lambda = 0.5 + 0.5i$. Figure (a) shows the time evolution of b_y , and (b) is the time evolution of b_z

Chapter 3

Soliton Theory

The inverse scattering transform (IST) has been one of the most important developments in nonlinear differential equations since its introduction into mathematics in the 1960's. The method of the transform allows for the production of an analytical solution, as well as other relevant quantities, of several different nonlinear partial differential equations. It can be thought of as a nonlinear analogue of the Fourier transform, or a generalization of the Fourier transform, which will be presented in the following sections.

3.1 Fourier-Laplace transform for linear wave theory

Linear waves are thought to be well understood, with a vast amount of techniques used to produce traveling wave solutions. This section will provide a detailed description of constructing a solution with appropriate use of the Fourier and Laplace transformations. Since we will be treating this problem as an initial value problem, the Laplace transform is used to perform the transformation in time instead of a Fourier transform in time. This is a result from the fact that $U(x, t = 0)$ is known, while $U(x, t \rightarrow \infty)$ is unknown and is essentially what is being sought out. During each transition of the process, similarities between the IST and this method will be

discussed slightly, even though details have yet to be provided on the IST. Figure 3.1 attempts to illustrate the process of this section pictorially.

First, we can consider the Korteweg de Vries equation,

$$U_t + 6UU_x + U_{xxx} = 0 . \quad (3.1)$$

Since the Fourier transform is typically used to manipulate linear PDE's, a linearized form of the KdV equation is required if we are to use the Fourier-Laplace transform on Eq. (3.1). The linearized approximation to (3.1) is

$$U_t + U_{xxx} = 0 , \quad (3.2)$$

where the nonlinear term is eliminated. Following the procedure in Figure 3.1, if the initial condition of Eq. (3.2) is known, $U(x, 0)$ can be treated as a one dimensional function and therefore the Fourier transform, $A(k)$, can be represented as

$$U(x, 0) = \frac{1}{2\pi} \int_{-\infty}^{\infty} A(k, 0) e^{ikx} dx, \quad (3.3)$$

and the inverse transform is

$$A(k, 0) = \int_{-\infty}^{\infty} U(x, 0) e^{-ikx} dk. \quad (3.4)$$

Since the goal is to produce a time varying solution $U(x, t)$ for a linear wave, we can apply a Fourier-Laplace transform to the unknown solution $U(x, t)$

$$U(k, \omega) = \int_{-\infty}^{\infty} dx \int_0^{\infty} dt e^{-i(kx - \omega t)} U(x, t) \quad (3.5)$$

where we assume that $|U(x, t)| \rightarrow 0$ as $|x| \rightarrow \infty$, but not necessarily for $t \rightarrow \infty$. It is also important that $\text{Im}(\omega) > 0$ and large enough so the integral converges. Inversion of the Fourier and Laplace transforms produce

$$U(x, t) = \frac{1}{(2\pi)^2} \int_{-\infty}^{\infty} dk \int_C d\omega e^{i(kx - \omega t)} U(k, \omega) \quad (3.6)$$

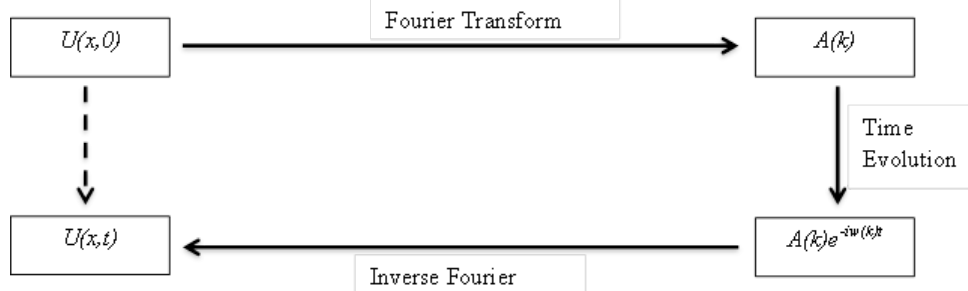


Figure 3.1: Logic map of using a Fourier transform to solve a linear PDE analytically. Typically, it is desired to obtain the full solution to a differential equation, $U(x, t)$, through knowledge of the initial condition $U(x, 0)$. Instead of solving the differential equation in space and time, it is much simpler to Fourier-Laplace transform into wave-number and frequency space, (k, ω) , solve the algebraic equation, and then invert the transform.

where the contour \mathcal{C} is in the complex ω plane and lies above any singularities of $U(k, \omega)$, i.e., \mathcal{C} is in the upper half of the complex plane. Since the intended goal is to apply the transformation to the linearized equation, Eq. (3.2), we need to note that under the Laplace transformation the treatment of the partial derivative with respect to time is

$$\begin{aligned} \int_0^\infty dt e^{i\omega t} \frac{\partial U}{\partial t} &= \int_0^\infty dt \left(\frac{\partial}{\partial t} [e^{i\omega t} U] - i\omega e^{i\omega t} U \right) \\ &= e^{i\omega t} U(x, t)|_0^\infty - i\omega U(x, \omega) \\ &= -U(x, t = 0) - i\omega U(x, \omega). \end{aligned}$$

and the Fourier transform replaces the $\partial/\partial x$ operator with ik . Note that the term involving $\lim_{t \rightarrow \infty} e^{i\omega t} U(x, t) = 0$ because $\text{Im}(\omega) > 0$. Applying this transformation to Eq. (3.2) gives us

$$-i\omega U(k, \omega) - U(k, t = 0) + (ik)^2 U(k, \omega) = 0 \quad (3.8)$$

or

$$[-i\omega + (ik)^3] U(k, \omega) = U(k, t = 0), \quad (3.9)$$

so we can easily solve for $U(k, \omega)$,

$$U(k, \omega) = \frac{iU(k, t=0)}{\omega + k^3}, \quad (3.10)$$

and setting the denominator equal to zero results in the dispersion relation for (3.2).

Now applying the inverse Laplace transform yields the desired solution

$$U(x, t) = \int_{\mathcal{C}} \frac{d\omega}{2\pi} U(k, \omega) e^{-i\omega t} \quad (3.11)$$

where \mathcal{C} lies above the singularities of $U(k, \omega)$. Only one singularity occurs at $\omega = -k^3$, and it lies on the real axis. We can apply Cauchy's residue theorem and deform it analytically to \mathcal{C}' , which is a contour that lies below any singularities,

$$U(k, t) = \int_{\mathcal{C}'} \frac{d\omega}{2\pi} U(k, \omega) e^{-i\omega t} - 2\pi i \frac{1}{2\pi} iU(k, t=0) e^{ik^3 t}. \quad (3.12)$$

As \mathcal{C}' moves further down the imaginary axis the first term in Eq. (3.12) vanishes, so

$$U(k, t) = -i^2 U(k, t=0) e^{ik^3 t} \quad (3.13)$$

or

$$U(x, t) = \frac{1}{2\pi} \int_{-\infty}^{\infty} dk U(k, t=0) e^{ik^3 t}, \quad (3.14)$$

by application of the inverse Fourier transform.

This procedure is well known for producing solutions to linear partial differential equations. We now turn to a procedure for solving nonlinear PDEs. In the nonlinear case, the IST provides analogous information to $U(k, \omega)$ and k , which correspond to the scattering data and the eigenvalues, respectively. The next section will provide details on the process of obtaining such information, along with the importance in regard to the IST.

3.2 Sturm-Liouville Theory

There is a deep connection between eigenvalue equations of Sturm-Liouville theory and partial differential equations. It turns out that when the eigenvalues of a particular Sturm-Liouville problem are independent of time, then the corresponding potential is also a solution to a specific PDE. Therefore, the nonlinear PDE can be reduced to solving the linear eigenvalue equation.

Here we address a typical Sturm-Liouville problem, in the context of quantum mechanics and the 1D time independent Schrödinger equation. The following section will develop the relationship between the KdV equation and the Sturm-Liouville problem. Later on, the procedure for the DNLS equation will be quoted without proof.

3.2.1 The Sturm-Liouville problem

Differential equations of the type similar to the Sturm Liouville equation,

$$\psi_{xx} + (\lambda - U(x))\psi = 0 \quad (3.15)$$

subject to boundary conditions at (a, b) , where $a \leq x \leq b$, appear in a multitude of applications in mathematics and physics. They have been thoroughly studied in quantum mechanics under the alias of the Schrödinger equation. Another application of Eq. (3.15) is wave propagation in inhomogeneous media (in the classical regime).

When the eigenfunction, $\psi(x)$, is subject to a potential, $U(x)$, and boundary conditions are imposed, there can only be a non trivial solution for specific values of λ (or a finite number of eigenvalues λ_n if the domain of x is not infinite). Determining the impact of the eigenvalues λ_n on the solution of the eigenfunction $\psi(x)$ and the effect of the boundary conditions on the eigenvalues is known as the *Sturm-Liouville Problem* [15].

For an example of a Sturm-Liouville problem and its physical meaning, we can

look at the quantum mechanical energy eigenvalue equation

$$H\psi = E\psi \quad (3.16)$$

where H is the Hamiltonian and represents the total energy of the system. Looking at only one spatial dimension, we have

$$H\psi = \left(-\frac{\hbar^2}{2m} \frac{d^2}{dx^2} + V(x) \right) \psi = E\psi \quad (3.17)$$

Further, if we define

$$\tilde{U}(x) \equiv \frac{2mV(x)}{\hbar^2} \quad (3.18)$$

and

$$\tilde{\lambda} \equiv \frac{2mE}{\hbar^2} \quad (3.19)$$

leaving us with

$$\psi_{xx} + (\tilde{\lambda} - \tilde{U}(x))\psi = 0. \quad (3.20)$$

It is useful to scale the independent variable x to $\bar{x} = x/x_0$ so that the differential equation is dimensionless; this results in

$$\frac{d^2\psi}{dx^2} = \frac{1}{x_0^2} \frac{d^2\psi}{d\bar{x}^2}. \quad (3.21)$$

We now have the Sturm-Liouville equation in dimensionless coordinates

$$\psi_{\bar{x}\bar{x}} + (\lambda - U)\psi = 0, \quad (3.22)$$

where

$$\lambda = x_0^2 \tilde{\lambda} = \frac{2mx_0^2}{\hbar^2} E \quad (3.23)$$

$$U = x_0^2 \tilde{U}(x) = \frac{2mx_0^2}{\hbar^2} V(\bar{x}). \quad (3.24)$$

Now let's suppose we are interest in a potential of the form

$$V(x) = -\frac{\hbar^2}{mx_0^2} \operatorname{sech}^2\left(\frac{x}{x_0}\right) \quad (3.25)$$

i.e.,

$$U = \frac{2mx_0^2}{\hbar^2} V(\bar{x}) = -2 \operatorname{sech}^2(\bar{x}) \quad (3.26)$$

then it can be shown that a solution to (3.22) with the potential (3.26) is

$$\psi_1 = A \operatorname{sech}(\bar{x}) \quad (3.27)$$

with an eigenvalue of $\lambda_1 = -1$. Reverting to physical units, the energy of this “bound state” is

$$E_1 = \frac{-\hbar^2}{2mx_0^2}. \quad (3.28)$$

The significance of these bound states in regards to soliton theory will emerge in a later section. Note, however, that the function U in (3.26) is nothing but the one-soliton solution to the KdV equation that we saw in Chapter 1. There are also an infinite number of scattering solutions when the energy E is positive,

$$\psi_{\pm} = A e^{\pm i \frac{\sqrt{2mE}}{\hbar} x} \left[i \frac{\sqrt{2mE}}{\hbar} x_0 \mp \tanh(\bar{x}) \right]. \quad (3.29)$$

With the scaling

$$\frac{\sqrt{2mE}}{\hbar} = \frac{\sqrt{\lambda}}{x_0} \quad (3.30)$$

we can rewrite Eq. (3.29) as

$$\psi_{\pm} = A e^{\pm i \sqrt{\lambda} x} \left[i \sqrt{\lambda} \mp \tanh(x) \right]. \quad (3.31)$$

All of the states that satisfy Eq. (3.31) are considered “reflectionless” since the coefficient of reflection is zero. It is easy to see that this is true, by looking at the right going wave ($+x$) or the left going wave ($-x$) individually. The next section will go into more detail of the implication of a potential that has reflection in the solution of

the eigenfunction with respect to soliton theory.

3.3 Sturm-Liouville operator in Soliton theory

In the realm of soliton theory, the Sturm-Liouville operator is applied with a much different method than in quantum mechanics, but shares an eerie resemblance. Quantum mechanics has shown that the 1D time independent Schrödinger equation can describe the wave-like behavior of a particle that is free or bound to a potential, $V(x)$. The eigenvalues correspond to the bound states of the particle.

When looking at how the Sturm-Liouville operator is used in nonlinear wave theory, the potential is considered to be the wave form of the nonlinear wave (later on, it can be seen that this potential can be the initial wave profile, or a wave profile that is changing with time). In most cases, the potential $U(x)$ in the equation

$$\psi_{xx} + (\lambda - U(x))\psi = 0 \quad (3.32)$$

is considered as the initial wave profile of the nonlinear wave. The response of the eigenfunction, ψ , reveals significant information about the nonlinear wave, such as the possible eigenvalues and the scattering coefficients, i.e., the scattering data. The presence of eigenvalues (which lead to bound solutions of ψ) for the nonlinear wave $U(x)$ indicate that the solution is a soliton or is composed of solitons. If there is a nonzero “reflection” coefficient, then the solution also contains dispersive waves (and it will be shown later that potentials with no reflection have solutions that only contain solitons). Therefore, the initial configuration of the wave $U(x, t = 0)$ determines the amount and type of soliton constituents.

Figure 3.2 traces the steps in acquiring soliton solutions from nonlinear partial differential equations. The first step was just discussed, where a wave profile $U(x)$ is mapped onto the Sturm-Liouville problem in the form of the potential, which is also known as the direct scattering transformation. Application of this transform leads to spatial information about the nonlinear wave, such as if the function $U(x)$ is comprised of solitons or dispersive waves. This is analogous to the Fourier transform,

since the Fourier transform uses spatial information to provide all of the different frequencies of waves that are superimposed on top of each other.

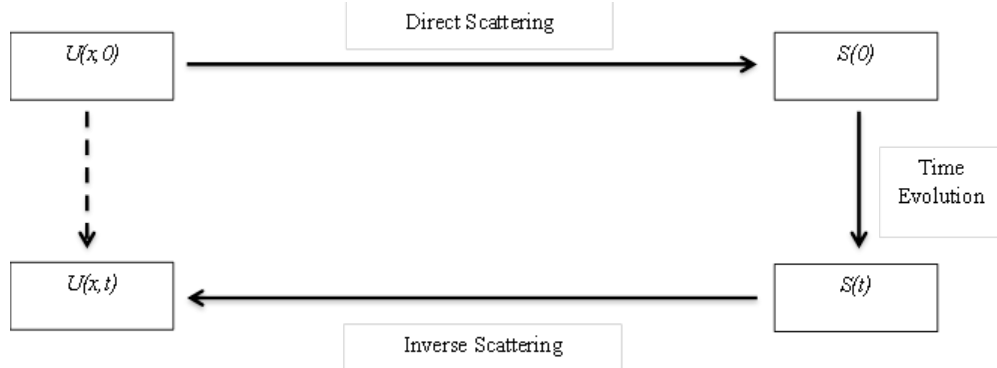


Figure 3.2: Logic map of using the direct and inverse scattering transform to solve a nonlinear evolution equation. The direct scattering transformation leads to the eigenfunction's response to the initial wave profile, which is known as the *scattering data*, $S(0)$. This information contains the transmission and reflection coefficients, which are dependent on the eigenvalues. Analytically, this leads to all the possible eigenvalues, or solitons, that arise from the initial condition. The time evolution of the scattering data is dependent on the nonlinear PDE, and acquiring this relation usually implies that the nonlinear PDE is integrable. Inversion of the scattering transform is accomplished by the use of the time dependence of the scattering data.

Inversion of the scattering transform uses the time evolution of the scattering data to produce a complete solution of $U(x, t)$. Producing the time evolution of the scattering information is the most difficult part of the process, because it varies for each nonlinear equation. With respect to this thesis, the mathematical theory behind the inverse transform is not important, but what is important is that a reflectionless potential yields a “simple” analytical solution for $U(x, t)$ containing only solitons. Potentials with reflection lead to dispersive waves, and are generally much more complicated to treat analytically.

3.3.1 Importance of the Eigenvalues

In soliton theory, the Sturm-Liouville equation is used in the direct scattering transformation, which leads to finding the scattering data and the eigenvalues for the specified

potential $U(x)$, i.e., the initial wave configuration. What is needed to complete this picture of the direct scattering transform is to understand how the eigenvalues behave with respect to time. It is necessary for the inverse transform that if the potential has some time dependence $U(x, t)$, then the eigenvalues must be invariant with time.

To demonstrate the concept of the eigenvalues being invariant, or constant, with respect to time, we can use a method developed by Peter Lax in 1968 (the proof that follows can be found in Lamb [15]). It will allow us to see that the solution to the KdV equation

$$U_t + 6UU_x + U_{xxx} = 0 \quad (3.33)$$

is a potential in the Sturm-Liouville equation such that the eigenvalues do not vary in time. To start the process it is convenient to write the Sturm-Liouville equation in operator form

$$\mathcal{L}\psi = \lambda\psi \quad (3.34)$$

where

$$\mathcal{L} = D^2 - u(x, t) \quad (3.35)$$

and $D = d/dx$. Calculating the derivative with respect to time gives us

$$(\mathcal{L}\psi)_t = \mathcal{L}\psi_t + \mathcal{L}_t\psi = \lambda\psi_t + \lambda_t\psi. \quad (3.36)$$

The time derivative operating on $(\mathcal{L}\psi)$ using (3.35) is just

$$(\mathcal{L}\psi)_t = \psi_{xxt} - u\psi_t - u_t\psi = \mathcal{L}\psi_t - u_t\psi. \quad (3.37)$$

Therefore, along with Eq. (3.36), it can be deduced that $\mathcal{L}_t = -u_t$. The primary goal is to allow the function $u(x, t)$ to vary in time, but requiring that the eigenvalues are constant in time $\lambda_t = 0$. Therefore, we can introduce some linear differential operator K , where the temporal derivative of ψ can be expressed as $\psi_t = K\psi$, which can be considered a “guess” for all intents and purposes. This would allow us to rewrite Eq. (3.36) as

$$([\mathcal{L}, K] - u_t)\psi = \lambda_t\psi \quad (3.38)$$

where

$$[\mathcal{L}, K] \equiv \mathcal{L}K - K\mathcal{L}. \quad (3.39)$$

Since we are requiring λ be constant, the linear differential operator K must satisfy the relation, $[\mathcal{L}, K] - u_t = 0$, which is an operator equation.

We can start with a simple differential operator $K_1 = aD$, and also restrict a to be dependent only on the function u and its spatial derivatives. In this case, expansion of the Sturm-Liouville operator and K_1 gives us

$$\begin{aligned} [\mathcal{L}, K_1] \psi &= (\mathcal{L}K_1 - K_1\mathcal{L})\psi \\ &= (D^2 - u)(a\psi_x) - aD(\psi_{xx} - u\psi) \\ &= 2a_x D^2\psi + a_{xx} D\psi + au_x \psi \end{aligned} \quad (3.40)$$

With one last assumption, i.e., that the coefficient a is actually constant (that is $a_x = 0$), the first two terms vanish, and (3.38) becomes

$$(u_t - au_x)\psi = -\lambda_t\psi. \quad (3.41)$$

The term in the parenthesis is not a differential operator, so that if $\lambda_t = 0$ then $u(x, t)$ must satisfy

$$u_t - au_x = 0. \quad (3.42)$$

That is, the solution to this PDE, $u(x, t)$, when used as the potential in (3.34) results in constant eigenvalues. Since the solutions to this linear PDE require that u not be a function of x and t separately, but that $u(x + at)$, it is easy to see that the potential translates such that $u(x + at)$, leaving the eigenvalues unaltered as time progresses. Of course, this is just the well known linear advection equation. To obtain a nonlinear PDE with this method, a more complicated differential operator K is needed.

The next logical step would be to use a second derivative, $K_2 = aD^2 + fD + g$, but it can be shown that it also leads to the advection equation. Let us consider the

linear operator $K_3 = aD^3 + fD + g$, which gives

$$\begin{aligned} [\mathcal{L}, K_3] \psi &= (2f_x + 3au_x)D^2\psi + (f_{xx} + 2g_x + 3au_{xx})D\psi \\ &\quad + (g_{xx} + au_{xxx} + fu_x)\psi. \end{aligned} \quad (3.43)$$

As was done in the case involving K_1 , we require that the coefficients of the $D^2\psi$ and $D\psi$ terms vanish, so that we can obtain a differential equation for u only. Integrating the coefficients with respect to x , we get the differential relations

$$f = -\frac{3}{2}au + c_1 \quad (3.44)$$

and

$$g = -\frac{3}{4}au_x + c_2 \quad (3.45)$$

where c_1 and c_2 are constants of integration (that could possibly be functions of time).

We are left with

$$[\mathcal{L}, K_3] \psi = (g_{xx} + au_{xxx} + fu_x)\psi \quad (3.46)$$

and using our knowledge of f and g , Eqs. (3.44) and (3.45), we arrive at the relation

$$[\mathcal{L}, K_3] \psi = \left[\frac{1}{4}a(u_{xxx} - 6uu_x) + c_1u_x \right] \psi. \quad (3.47)$$

We can set $a = -4$ to simplify the coefficients, and we can also set the function $c_1(t)$ to zero, because it can easily be scaled away by transforming the independent variables $dx' = dx + c_1(t)dt$ and $dt' = dt$. This results in a new equation for $u(x, t)$, which is the standard KdV equation

$$u_t - 6uu_x + u_{xxx} = 0. \quad (3.48)$$

Note that (3.33) can be obtained with $u \rightarrow -U$. If $u(x, t)$ behaves according to Eq. (3.48), then

$$[\mathcal{L}, K_3] - u_t = 0 \quad (3.49)$$

is satisfied, resulting in $\lambda_t = 0$. This is very significant result, because this tells

us that if a potential that varies temporally in the Sturm-Liouville equation, is also a solution to the KdV equation then its eigenvalues λ remain unchanged in time. Basically, if $U(x, t)$ retains its shape but translates in time, then the bound states for that potential function have the same energy.

Using this method one could obtain an infinite number of higher order nonlinear equations characterized by odd linear operators $K_3, K_5, K_7\dots$ [9]. However, none except the KdV equation have been shown to be physically significant.

3.3.2 Non-reflectionless Potentials

To demonstrate the significance of the reflection coefficient, a simple example using the KdV equation, Eq. (3.48), will be used. A well known solution to the KdV equation is

$$u(x, t) = -U_0 \operatorname{sech}^2(x - ct), \quad (3.50)$$

where U_0 and c must satisfy a specific relationship (see Eq. (1.1)). For the purposes of the scattering problem, the solution is inspected at $t = 0$. It turns out, that the KdV equation can produce many solitons depending on the amplitude of the initial wave profile. This is can be seen when Eq. (3.50) is mapped onto the Sturm-Liouville problem,

$$\psi_{xx} + (\lambda + U_0 \operatorname{sech}^2 x) \psi = 0, \quad (3.51)$$

where Eq. (3.50) is used as the potential. Then a simple variable transformation $T = \tanh(x)$ can be used to change the independent variables, which results in

$$\frac{d}{dx} \equiv \operatorname{sech}^2 x \frac{d}{dT} = (1 - T^2) \frac{d}{dT}. \quad (3.52)$$

Equation (3.51) is then transformed into

$$\frac{d}{dT} \left[(1 - T^2) \frac{d\psi}{dT} \right] + \left(U_0 + \frac{\lambda}{(1 - T^2)} \right) \psi = 0, \quad (3.53)$$

which is the *associated Legendre equation*. If $U_0 = N(N + 1)$ then an analytical solution can easily be obtained with the Legendre polynomials. From the perspective

of solitons and scattering theory, the value of N corresponds to the number of solitons; therefore when the relation $U_0 = N(N+1)$ is satisfied, the potential can be considered reflectionless.

For a value of $N = 1$, $U_0 = 2$, which makes (3.50) equivalent to (3.26) and the solution is that of a single soliton. Furthermore, when $N = 2$ we have $U_0 = 6$, which leads to the conclusion that an initial wave profile with any amplitude other than $U_0 = 2, 6, 12\dots$ is not a reflectionless potential for the Sturm-Liouville equation. The positive energy reflectionless solution for $U_0 = 2$ was shown in Eq. (3.31).

Figure 3.3 shows the evolution of an initial wave profile where $U_0 = 4$ which is not a “simple” soliton solution because it contains other wave forms. It is comprised of two solitons that are moving to the right (the smaller amplitude soliton moves slowly) and another wave form that is traveling to the left. It is also important to note that the amplitude of the wave traveling to the left is small. Therefore, it approximately satisfies the linear approximation of the KdV equation,

$$u_t + u_{xxx} = 0 \quad (3.54)$$

which deems it a dispersive wave.

3.4 2x2 eigenvalue problem for the DNLS

This section will aid in development of the treatment of the DNLS equation with respect to the direct scattering (DST) and inverse scattering transform (IST). A generalization of the IST known as the “AKNS scheme” allows it to be applicable to other problems, namely the DNLS equation. This scheme uses a 2x2 eigenvalue problem as a generalization of the Sturm-Liouville equation in the form of coupled linear first order differential equations [8]. As shown by Kawata and Inoue [13], IST maps the DNLS equation into the following eigenvalue problem,

$$\Phi_x = D \cdot \Phi \quad (3.55)$$

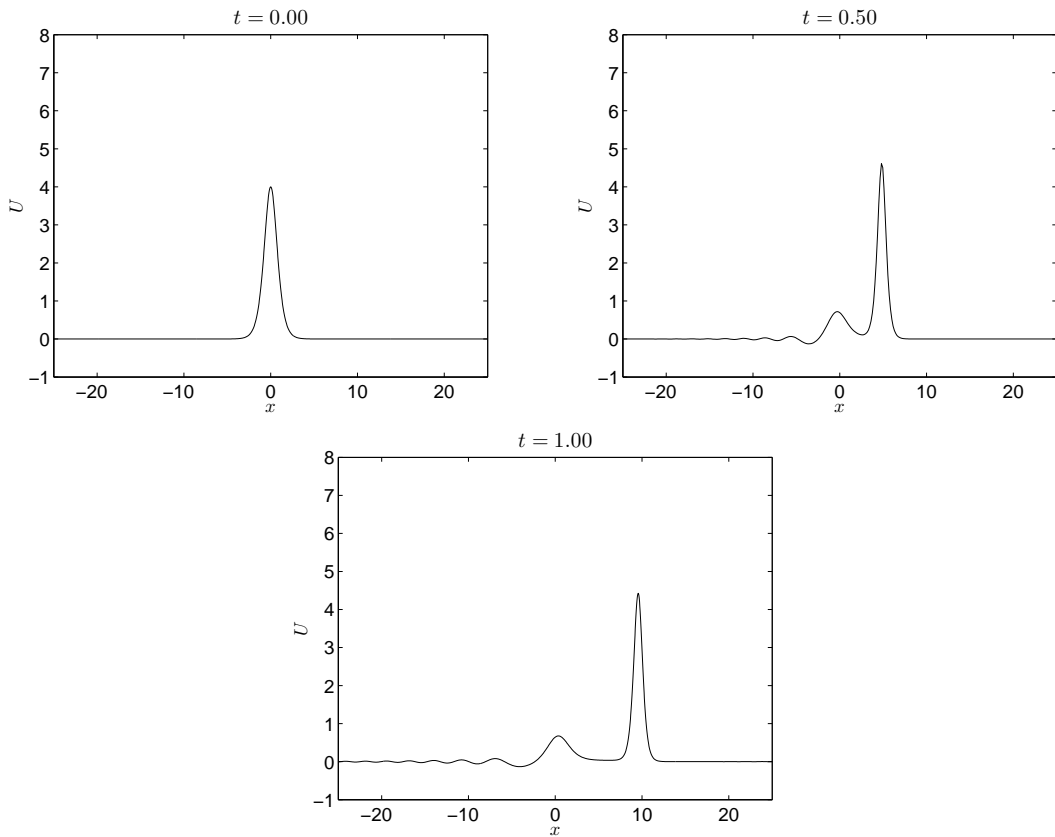


Figure 3.3: Time evolution of an initial wave profile for the KdV equation with $U_0 = 4$, which generates two solitons and a dispersive wave that is traveling in the opposite direction from the two solitons. This is a result of a numerical solution through integration of the KdV equation using a combination of a one step Lax-Wendroff and a backward time centered space scheme. Details on how this solution was calculated numerically will follow in Chapter 4.

where

$$\Phi(x, t; \lambda) = \begin{pmatrix} \phi_{11} & \phi_{12} \\ \phi_{21} & \phi_{22} \end{pmatrix} \quad (3.56)$$

and

$$D = \lambda \begin{pmatrix} -i\lambda & b(x, t) \\ \bar{b}(x, t) & i\lambda \end{pmatrix}, \quad (3.57)$$

which is a system of four coupled first-order differential equations, two of which are redundant, where $b(x, t)$ is the wave profile of the magnetic field (\bar{b} denotes complex conjugate of b). The magnetic field, $b(x, t)$, has the form

$$b(x, t) = b_y(x, t) + ib_z(x, t). \quad (3.58)$$

The time dependence of Φ is given by the relation

$$\Phi_t = F \cdot \Phi \quad (3.59)$$

where

$$F = \begin{pmatrix} A & B \\ C & -A \end{pmatrix}. \quad (3.60)$$

The forms of A , B and C must be chosen so that $\Phi_{xt} = \Phi_{tx}$ reduces to the DNLS equation [11]. This means that

$$\begin{aligned} A &= 2i\lambda^4 + i(|b|^2 - b_0^2)\lambda^4 \\ B &= -2b\lambda^3 - [b(|b|^2 - b_0^2) + ib_x]\lambda \\ C &= -2\bar{b}\lambda^3 + [-\bar{b}(|b|^2 - b_0^2) + i\bar{b}_x]\lambda. \end{aligned} \quad (3.61)$$

The focus of this section is not on the time dependence of the scattering information that is associated with the inverse scattering transform, but looking into the scattering information for the direct transform.

For the eigenvalue problem presented by the DNLS being mapped by the IST, the asymptotic boundary conditions are needed. For the perpendicularly and obliquely

propagating wave, the nonvanishing boundary conditions are

$$\Phi^\pm(x, t; \lambda, \zeta) \rightarrow T(\lambda, \zeta) J(\Lambda x) \text{ when } x \rightarrow \pm\infty \quad (3.62)$$

while $\Phi(x, t; \lambda, \zeta)$ has the same form as Eq. (3.56). The forms of the matrices $T(\lambda, \zeta)$ and $J(\Lambda, \zeta)$ are

$$T(\lambda, \zeta) = \begin{pmatrix} -ib_0 & \lambda - \zeta \\ \lambda - \zeta & ib_0 \end{pmatrix}, \quad (3.63)$$

and

$$J(\Lambda, \zeta) = \begin{pmatrix} e^{-i\Lambda x} & 0 \\ 0 & e^{i\Lambda x} \end{pmatrix}, \quad (3.64)$$

where

$$\Lambda = \lambda\zeta \text{ and } \zeta = \sqrt{\lambda^2 - b_0^2} \quad (3.65)$$

which was developed by Kawata and Inoue [13]. The relation between the two asymptotic forms of $\Phi(x, t; \lambda, \zeta)$ involves the scattering matrix $S(t; \lambda, \zeta)$

$$\Phi^-(x, t; \lambda, \zeta) = \Phi^+(x, t; \lambda, \zeta) \cdot S(t; \lambda, \zeta) \quad (3.66)$$

where

$$S(t; \lambda, \zeta) = \begin{pmatrix} s_{11} & s_{12} \\ s_{21} & s_{22} \end{pmatrix}. \quad (3.67)$$

For nearly parallel waves, the eigenvalues are complex which gives rise to two parameter solutions. For the oblique or perpendicular case, on the other hand, the eigenvalues are either complex or completely real [11]. The left column of Eq. (3.66) is

$$\begin{pmatrix} \phi_{11}^- \\ \phi_{21}^- \end{pmatrix} = \begin{pmatrix} \phi_{11}^+ & \phi_{12}^+ \\ \phi_{21}^+ & \phi_{22}^+ \end{pmatrix} \begin{pmatrix} s_{11} \\ s_{21} \end{pmatrix}. \quad (3.68)$$

Since the functional forms of Φ^+ are known from Eq. (3.62), the scattering coefficients s_{11} and s_{21} can be calculated if the eigenfunction Φ is known as $x \rightarrow \infty$. This results

in the ability to numerically calculate the eigenvalues for an arbitrary potential $b(x, t)$ where the zeros of $S(\lambda, \zeta; t)$ are the location of the eigenvalues, λ .

Numerical calculation of the eigenvalues requires the ability to solve the 2x2 eigenvalue problem as an initial value problem (more details of this method will be discussed in Chapter 5) for any given eigenvalue. Using a fourth order Runge-Kutta method could be used to solve for $\Phi(x)$, which is demonstrated in Figure 3.4. It shows the solution to the 2x2 eigenvalue problem, for $\lambda = 0.4$, where the two different one parameter soliton solutions (bright and dark) where used as the potential. Since the two different functions are solitons, the solutions are bounded.

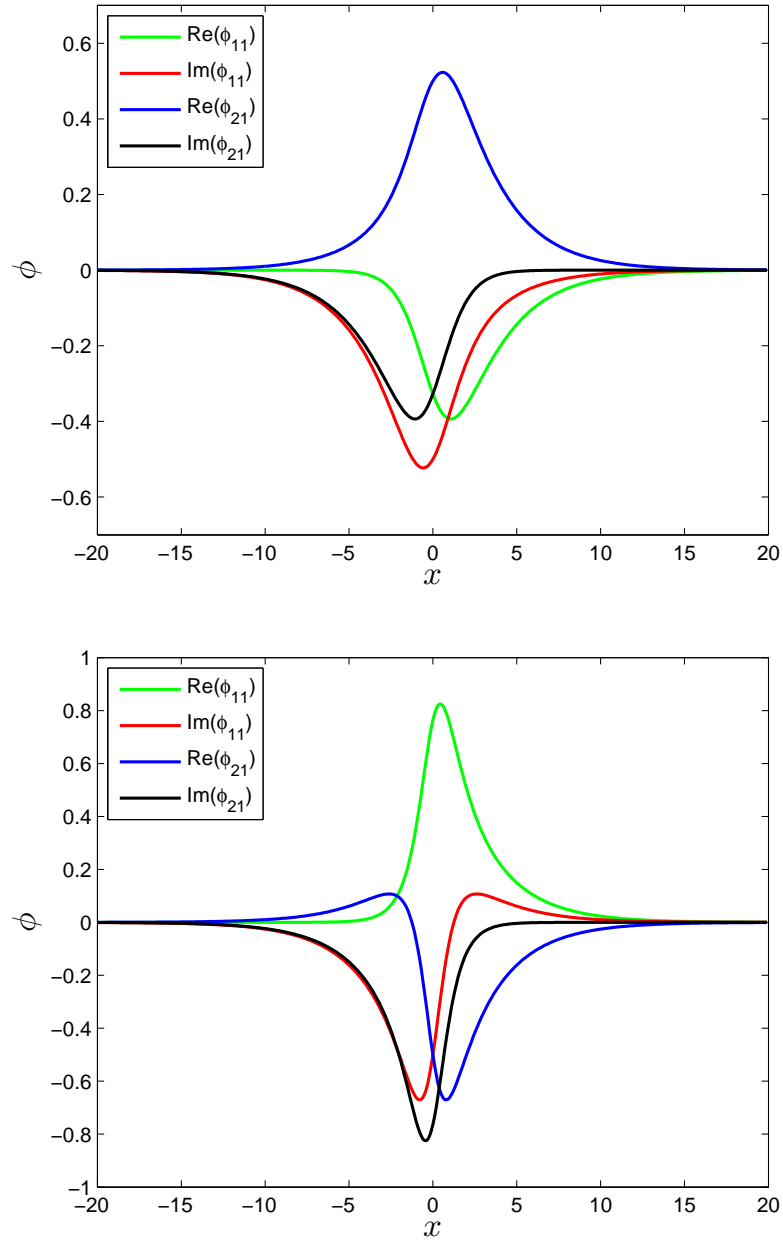


Figure 3.4: Left components of the eigenfunction $\Phi(x)$, ϕ_{11} and ϕ_{21} for two different potential functions $b(x, t)$, where the potential functions used were a one parameter dark soliton a) and bright b) soliton with both eigenvalues of $\lambda = 0.4$. Calculation of the eigenfunction utilized a fourth-order Runge-Kutta scheme by integrating from left to right. The problem was treated as an initial value problem by solving Eq. (3.55) with initial conditions set as the boundary conditions presented in Eq. (3.62).

Chapter 4

Numerical Solutions of Nonlinear Partial Differential Equations

Since the recent development of reliable computing power and speeds has dramatically increased over the past decade, there has been a closely related increase in fitting numerically produced results with theory. In the case of differential equations, this is done through estimating derivatives as finite differences. Ordinary differential equations are estimated by creating a one-dimensional mesh, which acts as the domain of the differential equation. The derivative terms in the differential equation can then be estimated utilizing Taylor series expansions and choosing the number of grid points used to estimate these derivative terms.

4.1 Convection Equation

When attempting to produce numerical methods to solve complicated equations, it's convenient to study the basic well solved equations that have physical resemblance to their more complicated counterparts. For example, when trying to develop a method to solve a nonlinear convection equation it would be wise to understand the linear convection problem and which numerical methods are effective. In later sections, nonlinear and convective type equations will be treated numerically, therefore it is useful to provide a detailed description of which numerical method will be employed.

A very popular and effective method for handling the linear convection equation is the Lax-Wendroff one-step method, which was proposed by Lax and Wendroff in 1960 [10]. The method is $\mathcal{O}(\Delta t^2) + \mathcal{O}(\Delta x^2)$ accurate and is produced by a forward time series Taylor expansion, where the time derivatives can be expressed in terms of spatial derivatives. For example, if we expand the function $y(x)$ about the point x_i , we have

$$y_{i+1} = y(x_{i+1}) = y(x_i + \Delta x) \quad (4.1)$$

and then applying the Taylor expansion we get

$$y(x_n + \Delta x) \approx y(x_n) + \Delta x \frac{dy}{dx}|_{x_n} + \mathcal{O}(\Delta x^2) \quad (4.2)$$

$$= y_n + \Delta x y'_n + \mathcal{O}(\Delta x^2). \quad (4.3)$$

The $\mathcal{O}(\Delta x^2)$ term is denotes higher order and represents the error.

The one dimensional convection equation is

$$\frac{\partial f}{\partial t} = -u \frac{\partial f}{\partial x} \quad (4.4)$$

for some function $f(x, t)$. It can be solved exactly by any function $f(x - ut)$ which describes a waveform that is traveling to the right with speed u . As mentioned earlier, the first process in the Lax-Wendroff type method is a forward Taylor expansion in time, retaining terms to second order in Δt

$$f_i^{n+1} = f_i^n + \Delta t f_t|_i^n + \frac{\Delta t^2}{2} f_{tt}|_i^n + \mathcal{O}(\Delta t^3), \quad (4.5)$$

where

$$f_i^n = f(x_i, t_n) \quad (4.6)$$

and

$$x_{i+1} = x_i + \Delta x \quad (4.7)$$

$$t_{n+1} = t_n + \Delta t \quad (4.8)$$

Notice that the indices denote the spatial iterative steps, i , and the temporal iterative steps, n , respectively. The first and second derivatives in time can be replaced by $-uf_x$ (from the PDE, Eq. (4.4)) and the second derivative can be replaced with

$$f_{tt} = (f_t)_t = (-uf_x)_t = (-uf_t)_x = (u^2 f_x)_x = u^2 f_{xx}, \quad (4.9)$$

so Eq. (4.5) becomes

$$f_i^{n+1} = f_i^n - \Delta t u f_x|_i^n + \frac{\Delta t^2}{2} u^2 f_{xx}|_i^n + \mathcal{O}(\Delta t^3). \quad (4.10)$$

Now the spatial derivatives can be approximated by second order center difference equations. The first derivative can be approximated as

$$f_x|_i^n = \frac{f_{i+1}^n - f_{i-1}^n}{2\Delta x} + \mathcal{O}(\Delta x^2), \quad (4.11)$$

and the second derivative can be approximated as

$$f_{xx}|_i^n = \frac{f_{i+1}^n - 2f_i^n + f_{i-1}^n}{\Delta x^2} + \mathcal{O}(\Delta x^2). \quad (4.12)$$

Finally, Eq. (4.10) can be rewritten as

$$f_i^{n+1} = f_i^n - \Delta t u \left(\frac{f_{i+1}^n - f_{i-1}^n}{2\Delta x} \right) + \frac{\Delta t^2}{2} u^2 \left(\frac{f_{i+1}^n - 2f_i^n + f_{i-1}^n}{\Delta x^2} \right). \quad (4.13)$$

The constant $c = u\Delta t/\Delta x$ can be introduced as the *convection constant*, so the final Lax-Wendroff one step approximation of the linear convection equation is

$$f_i^{n+1} = f_i^n - \frac{c}{2} (f_{i+1}^n - f_{i-1}^n) + \frac{c^2}{2} (f_{i+1}^n - 2f_i^n + f_{i-1}^n). \quad (4.14)$$

Figure 4.1 depicts the estimation of the $n+1$ th time step graphically. After the arrival of Eq. (4.14), which is also known as a *finite difference equation*, it is important to determine what values of c are required for the estimated solution to be stable. This is accomplished by performing a von Neumann stability analysis.

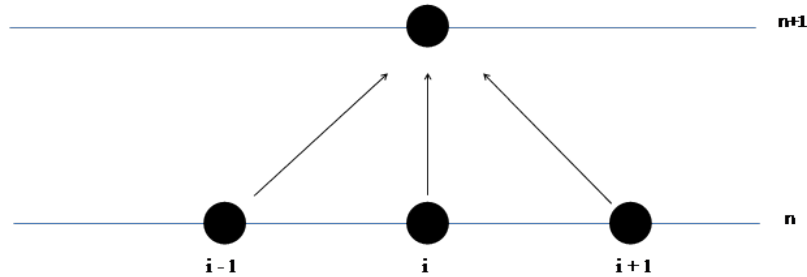


Figure 4.1: Graphical representation of the dependence on the grid points.

4.1.1 Von Neumann Stability Analysis

When modeling PDE's, it is important consider the general behavior of the solution as well as the stability of the numerical approximation developed. There are four general requirements needed for a proper numerical solution to be generated, and they are

1. Consistency
2. Stability
3. Order
4. Convergence

A numerical method is considered *consistent* when the difference between the original PDE or ODE and the finite difference equation (i.e., the truncated higher order terms left over from Taylor expansions) vanishes as the grid spacings approach zero. *Order* is used to categorize the behavior of the global error, which should be decreasing as the grid spacing goes to zero. *Stability* is one of the most important requirements for a proper numerical scheme, and must be analyzed for every finite difference approximation. For a PDE or ODE that is stable, the FDE must produce a bounded solution if the method is to be considered stable. Similarly, if the PDE/ODE that is being approximated is unstable, then the numerical solution must also be unstable. Convergence of an FDE is ensured when the requirements of stability and consistency are both satisfied.

Von Neumann's method for stability analysis is useful for linear PDE's because it is based on Fourier decomposition of the numerical error [10]. This method is powerful, because numerical schemes are generally hindered by numerical error. Finite difference schemes are stable when the error produced at one time step does not increase significantly compared to the previous time step. If the errors grow with increasing temporal steps, then the numerical method is unstable. An expression for the exact solution in a single time step can be written as

$$f_i^{n+1} = G f_i^n , \quad (4.15)$$

where G is called the amplification factor. For the solution of $f(x, t)$ to be bounded, which is a constraint produced by using Fourier series decomposition, the solution of Eq. (4.14) at $T = T_{max}$ or $T = N\Delta t$ must be

$$f_i^N = G^N f_i^0 \quad (4.16)$$

where N is the maximum temporal iteration. This condition needs to be met because the Fourier decomposition assumes that the solution is periodic. This leads to the requirement of $|G| \leq 1$ for the numerical solution to be bounded, this will allow us to produce a convergence criteria.

From the earlier analysis, it can be observed that each progressing time step is not only dependent on f_i^n but it also depends on f_{i+1}^n and f_{i-1}^n . To develop an expression for G , f_{i+1}^n and f_{i-1}^n need to be written in terms of f_i^n , which is accomplished by expressing the spatial information for a single time step in a complex Fourier series. All the components of the Fourier series in one time step are propagated forward in time independent of each other. Therefore, the solution is just the sum of all the Fourier components at that time step. The complex Fourier series for $f(x, t^n)$ is represented as

$$f(x, t_n) = F(x) = \sum_{m=-\infty}^{\infty} A_m e^{Ik_m x} , \quad (4.17)$$

where the $I = \sqrt{-1}$ and k_m , the wavenumber, is defined as

$$k_m = \frac{2m\pi}{2L} , \quad (4.18)$$

where L is the length of the domain. With these definitions for Eqs. (4.17) and (4.18), f_i^n can be rewritten, looking at only one Fourier component,

$$f_i^n = f(x_i, t_n) = A_m e^{Ik_m x_i} = A_m e^{Ik_m(i\Delta x)} = A_m e^{Ii(k_m \Delta x)} . \quad (4.19)$$

Now a relation between f_i^n and $f_{i\pm 1}^n$ can be developed, where $f_{i\pm 1}^n$ can be expressed as

$$\begin{aligned} f_{i\pm 1}^n &= f(x_{i\pm 1}, t_n) = A_m e^{Ik_m(x_i \pm \Delta x)} \\ &= A_m e^{Ik_m(i\pm 1)(\Delta x)} = A_m e^{Ik_m(\Delta x)} e^{\pm Ik_m(\Delta x)} = f_i^n e^{\pm Ik_m(\Delta x)} . \end{aligned} \quad (4.20)$$

This representation of $f_{i\pm 1}^n$ will allow for simple substitution into Eq. (4.14), the finite difference approximation to the linear convection equation. These relations are applicable only when the m th components of the complex Fourier series are kept. This means that all components of (4.17) and all values of Δx must be considered to ensure stability.

The exponential terms in Eq. (4.20) are periodic with a period of 2π ; therefore, it is only required to analyze G over the domain $0 \leq k_m \Delta x \leq 2\pi$. Since $k_m \Delta x$ is effectively an angle, we can let $\theta = k_m \Delta x$, and Eq. (4.20) can be written as

$$f_{i\pm 1}^n = f_i^n e^{\pm I\theta} \quad (4.21)$$

These relations can be substituted into (4.14) to produce

$$f_i^{n+1} = f_i^n - \frac{c}{2} (f_i^n e^{I\theta} - f_i^n e^{-I\theta}) + \frac{c^2}{2} (f_i^n e^{I\theta} - 2f_i^n + f_i^n e^{-I\theta}) . \quad (4.22)$$

Factoring out f_i^n from the right hand side, and employing Euler's relation $e^{\pm I\theta} = \cos\theta + I\sin\theta$ the amplification factor can be written as

$$G = 1 - Ic\sin\theta + c^2(\cos\theta - 1) = [c^2\cos\theta + (1 - c^2)] - Ic\sin\theta. \quad (4.23)$$

Since there is a requirement on the value of the amplification factor, $|G| \leq 1$, we can develop constraints on the values of θ and c . Equation (4.23) describes an ellipse in the complex plane, where the center of the ellipse is located at $1 - c^2$, and the axes are dependent on c and c^2 .

In Figure 4.2, it is shown that ellipses within the unit circle, representing $|G| \leq 1$, are stable because they satisfy the amplification factor constraint. This means that for a stable solution, the primary constraint is on the value of c , because it determines the size of the ellipse, therefore

$$c = \frac{u\Delta t}{\Delta x} \leq 1 \quad (4.24)$$

is the condition that needs to be satisfied for a stable numerical solution, which is also referred to as convergence criteria.

4.2 Diffusion Equation

Since the purpose of this paper is to explore numerically the behavior of nonlinear dispersive waves, it would be beneficial to explain how a dispersive equation is numerically solved. This is due to the fact that solitons exhibit diffusive properties that cancel out the nonlinear steepening effect. The steepening effect of these nonlinear PDE's act similar to the convection equation that was discussed in §4.1.

This section will develop a suitable method for solving the diffusion equation

$$\frac{\partial f}{\partial t} = \alpha \frac{\partial^2 f}{\partial x^2}, \quad (4.25)$$

which is a parabolic PDE (see appendix for details on PDE classifications). A suitable method for solving the diffusion equation is the *backward-time centered-space* (BTCS) method, which is a “fully implicit method.” It will become clear later why

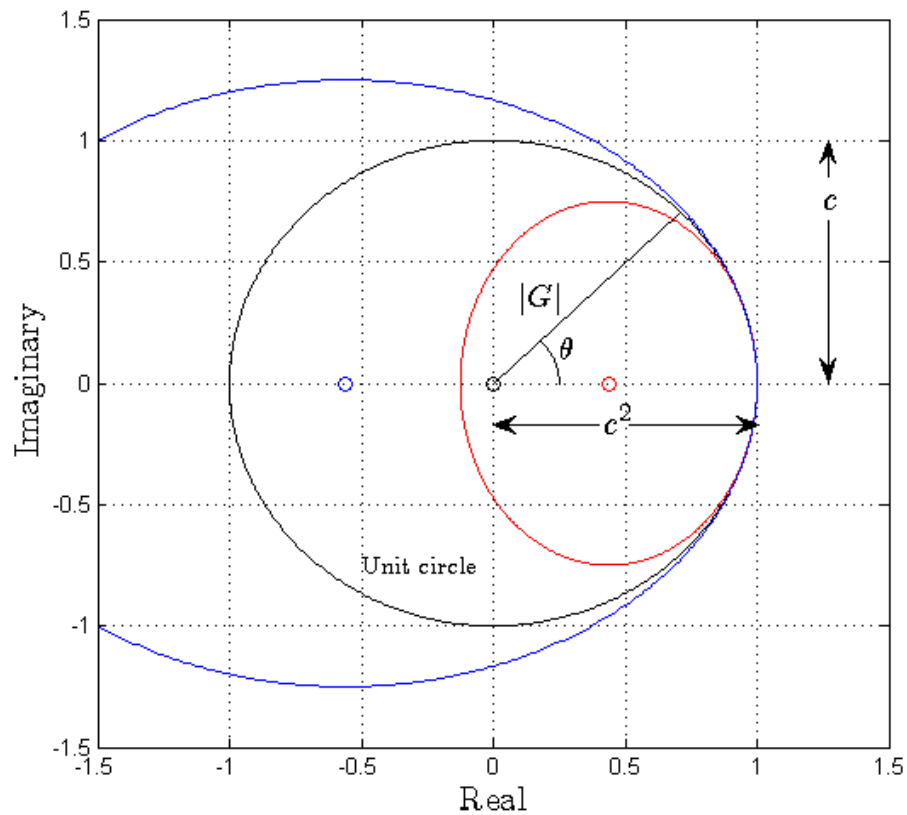


Figure 4.2: Locus plot of the amplification factor G . Two ellipses are displayed with values $c = 0.75$ and $c = 1.25$, along with a unit circle, $c = 1$, centered at the origin.

this method is considered implicit, but the most important property of this method is its unconditional stability. Von Neumann stability analysis allows for a simple proof of the scheme's stability.

The first step in finding a numerical approximation for the diffusion equation is to acquire an approximation for the time derivative. This is done exactly the same way as in §4.1, which begins with a Taylor series expansion of f_i^n around a single time step Δt .

$$f_i^n = f|_i^{n+1} + (-\Delta t)f_t|_i^{n+1} + \frac{(-\Delta t)^2}{2}f_{tt}|_i^{n+1} + \mathcal{O}(\Delta t^3) \quad (4.26)$$

This is where the name “backward” emerges. Rather than Taylor expanding around the current time (n th time step), we are expanding around a future time ($n+1$)th time step, see Eq. (4.5). An expression for the time derivative evaluated at the next time step ($n+1$) is required because two points are needed to acquire an estimation of a derivative, so solving for $f_t|_i^{n+1}$ and grouping the f_{tt} term with the higher order terms produces

$$f_t|_i^{n+1} = \frac{f_i^{n+1} - f_i^n}{\Delta t} + \left[\frac{(\Delta t)}{2}f_{tt}|_i^{n+1} + \mathcal{O}(\Delta t^2) \right]. \quad (4.27)$$

The last term can be eliminated because it is not required for the backward-time centered-space numerical scheme. The final approximation

$$f_t|_i^{n+1} = \frac{f_i^{n+1} - f_i^n}{\Delta t} + \mathcal{O}(\Delta t), \quad (4.28)$$

is therefore only first order accurate in time. Now Eq. (4.28) can be substituted into the diffusion equation along with a second order centered space approximation (evaluated at the future time step t_{n+1}) for the second derivative. These substitutions allow for the complete finite difference approximation equation for the diffusion equation with an accuracy of $\mathcal{O}(\Delta t)$ and $\mathcal{O}(\Delta x^2)$,

$$\frac{f_i^{n+1} - f_i^n}{\Delta t} = \alpha \frac{f_{i+1}^{n+1} - 2f_i^{n+1} + f_{i-1}^{n+1}}{\Delta x^2}. \quad (4.29)$$

On the right hand side of Eq. (4.29), it can be observed that all of the functional

evaluations are at t_{n+1} as opposed to t_n . That is, this scheme is *backward* in time, which approximates all spatial information in the $(n+1)$ th time step from the values obtained in the n th time step. A *forward* time finite difference method would use the spatial information in the n th time step to approximate the $(n+1)$ th step.

The goal is to solve for $f(t_{n+1})$, and those terms can be collected on the right hand side. Also the diffusion number, $d = \alpha\Delta t/\Delta x^2$, can be introduced into Eq. (4.29) and provide less clustered form. The final product is

$$-df_{i-1}^{n+1} + (1 + 2d)f_i^{n+1} - df_{i+1}^{n+1} = f_i^n, \quad (4.30)$$

which is an implicit method for solving for the $(n+1)$ th value in terms of the n th value because f_i^{n+1} can not be solved for explicitly. There are two unknown values that neighbor f_i^{n+1} , which are f_{i+1}^{n+1} and f_{i-1}^{n+1} . With appropriate boundary conditions, Eq. (4.30) can be solved as a system of equations for f_i^{n+1} using a matrix method, $0 \leq i \leq N$, where N is the number of spatial points. It is simple because the matrix is tri-diagonal.

For every numerical scheme, it is necessary to investigate the stability to validate the usefulness of the numerical method. The Von Neumann stability analysis discussed in §4.1.1 is suitable for developing an analytical expression for the stability of the diffusion equation approximation, Eq. (4.30), because of the approximation's linearity. Substitution of the Fourier series representations of f_{i+1}^{n+1} and f_{i-1}^{n+1} yields

$$-df_i^{n+1}e^{-I\theta} + (1 + 2d)f_i^{n+1} - df_i^{n+1}e^{I\theta} = f_i^n, \quad (4.31)$$

and then solving for f_i^{n+1} gives

$$f_i^{n+1}(1 + 2d - 2d\cos\theta) = f_i^n. \quad (4.32)$$

After substitution of the amplification factor G and solving for it, the stability condition is

$$G = \frac{1}{1 + 2d(1 - \cos\theta)} \leq 1. \quad (4.33)$$

To achieve a stable numerical solution, $|G| \leq 1$ is always satisfied by Eq. (4.33) for any value of θ and d ; therefore, the BTCS method for solving the diffusion equation is “unconditionally stable”.

4.3 Korteweg-de Vries Equation

The Korteweg-de Vries equation is a nonlinear partial differential equation that describes the behavior of waves in shallow water. It was one of the first nonlinear PDE's that produced exactly solvable and soliton solutions. The KdV equation contains a nonlinear term and a dispersive term which allows the solitary wave phenomena to occur. The KdV equation has the form

$$\frac{\partial U}{\partial t} + \underbrace{\alpha U \frac{\partial U}{\partial x}}_{\text{nonlinear term}} + \underbrace{\beta \frac{\partial^3 U}{\partial x^3}}_{\text{dispersive term}} = 0 . \quad (4.34)$$

where α and β are free parameters, and one standard selection is $\alpha = 6$ and $\beta = 1$ (see Appendix A.1 for details of scaling).

When trying to numerically solve nonlinear PDE's, it is helpful to split the equation's spatial derivatives and solve them separately with different numerical schemes that have been proven to accurately calculate the term under question, which is known as *operator splitting* [7]. For instance, the term with the most complications is the nonlinear term, and it will be solved first. The numerically approximated solution of

$$\frac{\partial U}{\partial t} = -\alpha U \frac{\partial U}{\partial x} \quad (4.35)$$

will serve as an intial guess, and then will be corrected by using it as the initial condition for

$$\frac{\partial U}{\partial t} = -\beta \frac{\partial^3 U}{\partial x^3} . \quad (4.36)$$

A suitable scheme to employ for solving the nonlinear equation would be the Lax-Wendroff one-step method, because it works very well with the linear convection equation, although some complications arise because of the nonlinearity.

As previously explained in §4.1, the Lax-Wendroff one-step method starts with expanding $U(x, t)$ in a Taylor series in time, as done in Eq. (4.5),

$$U_i^{n+1} = U_i^n + \Delta t U_t|_i^n + \frac{\Delta t^2}{2} U_{tt}|_i^n + \mathcal{O}(\Delta t^3) . \quad (4.37)$$

Since the KdV equation only contains a first order time derivative, the second term in Eq. (4.37) can be replaced with

$$U_t = -\alpha U U_x . \quad (4.38)$$

It is now appropriate to derive what should replace the U_{tt} term in Eq. (4.37). To do this, we can start with Eq. (4.38) and differentiate it with respect to time, which produces

$$U_{tt} = (U_t)_t = (-\alpha U U_x)_t = -\alpha(U_t U_x + U(U_x)_t) . \quad (4.39)$$

With simple substitution of Eq. (4.38) along with the commutative properties of $\partial/\partial t$ and $\partial/\partial x$, Eq. (4.39) can be rewritten as

$$U_{tt} = -\alpha(-\alpha U U_x^2 + U(U_t)_x) = \alpha^2(U U_x^2 + U(U U_x)_x) \quad (4.40)$$

or,

$$U_{tt} = \alpha^2(U U_x^2 + U U_x^2 + U^2 U_{xx}) = \alpha^2 U(2U_x^2 + U U_{xx}) \quad (4.41)$$

Now Eqs. (4.38) and (4.41) can be placed into Eq. (4.37) so the Taylor series expansion in time for the nonlinear term is only dependent on spatial derivatives

$$U_i^{n+1} = U_i^n - \alpha \Delta t (U U_x)|_i^n + \frac{\Delta t^2}{2} \alpha^2 U(2U_x^2 + U U_{xx})|_i^n + \mathcal{O}(\Delta t^3) . \quad (4.42)$$

This allows for the estimation of the entire nonlinear term by replacing the spatial derivative terms with finite difference approximation equations. Therefore, the U_x and U_{xx} terms can be approximated with

$$U_x|_i^n = \frac{U_{i+1}^n - U_{i-1}^n}{2\Delta x} \quad (4.43)$$

and

$$U_{xx}|_i^n = \frac{U_{i+1}^n - 2U_i^n + U_{i-1}^n}{\Delta x^2}. \quad (4.44)$$

Equations (4.43) and (4.44) are centered-space finite difference approximations, so making the proper substitutions into Eq. (4.42), the final finite difference approximation equation using a Lax-Wendroff one-step scheme is

$$\begin{aligned} U_i^{n+1} = U_i^n - \alpha \Delta t U_i^n & \left(\frac{U_{i+1}^n - U_{i-1}^n}{2 \Delta x} \right) + \\ & \frac{\alpha^2 \Delta t^2}{2} U_i^n \left[2 \left(\frac{U_{i+1}^n - U_{i-1}^n}{2 \Delta x} \right)^2 + U_i^n \left(\frac{U_{i+1}^n - 2U_i^n + U_{i-1}^n}{\Delta x^2} \right) \right]. \end{aligned} \quad (4.45)$$

Since Eq. (4.45) is only approximating the nonlinear term, the result of this calculation is going to be an estimation which will be used in the calculation of the dispersive term, which is the third order derivative in the KdV equation. Since the equation

$$U_t = -\beta U_{xxx} \quad (4.46)$$

does not have a clear PDE classification, but with insight of how physical phenomena governed by the KdV behave, it can be inferred that this term acts as similar to the diffusion equation. With this insight, we can attempt to develop a treatment to solve this PDE similar to ones proposed to solve the diffusion equation.

Fully implicit methods are very powerful when it comes to solving parabolic, or diffusion-type, equations because they are generally unconditionally stable. Explicit methods are generally conditionally stable, which leads to adjusting the spatial and temporal steps. Sometimes the temporal step Δt becomes extremely small in turn leading to large computation times. Reduction in computation time is a direct result of the implicit numerical scheme's unconditional stability, but using this type of method is numerically intensive because all the spatial information is calculated each time step (i.e., solving a system of equations each time step). This is easily remedied by using an LU decomposition matrix method for inverting matrices, where the decomposition is only required once for the entire process. The backward-time centered-space method is desirable for solving Eq. (4.46) because of its unconditional

stability and simplicity of deriving the finite difference approximation.

To arrive at a BTCS method, we must derive the necessary finite difference approximation that produces an equation to represent backward time stepping. First, U_i^n is expanded in time around the $(i, n+1)$ point using a Taylor series expansion,

$$U_i^n = U_i^{n+1} + U_t|_i^{n+1}(-\Delta t) + \frac{1}{2}U_{tt}|_i^{n+1}(-\Delta t)^2 + \mathcal{O}(\Delta t^3). \quad (4.47)$$

Since the desired quantity is the first time derivative approximation for the *next* time step, it is ideal to solve Eq. (4.47) for $U_t|_i^{n+1}$, which gives

$$U_t|_i^{n+1} = \frac{U_i^{n+1} - U_i^n}{\Delta t} + \mathcal{O}(\Delta t). \quad (4.48)$$

Using a second order centered-space finite difference approximation for the third spatial derivative in Eq. (4.46), the BTCS approximation can be written as

$$\frac{U_i^{n+1} - U_i^n}{\Delta t} = -\beta \frac{U_{i+2}^{n+1} - 2U_{i+1}^{n+1} + 2U_{i-1}^{n+1} - U_{i-2}^{n+1}}{2\Delta x^3}, \quad (4.49)$$

which is the same as (4.29) except that a third derivative appears on the right hand side as opposed to a second derivative. Equation (4.49) can be rearranged as

$$-dU_{i+2}^{n+1} + 2dU_{i+1}^{n+1} + U_i^{n+1} - 2dU_{i-1}^{n+1} + dU_{i-2}^{n+1} = U_i^n \quad (4.50)$$

where $d = -\beta\Delta t/2\Delta x^3$. It is difficult to solve for U_i^{n+1} because there are five unknowns, i.e., the matrix has four off-diagonals that are nonzero, in contrast to the tri-diagonal matrix that is consistent with Eq. (4.31). This is also known as a “band matrix.” Therefore a system of equations must be written to solve for each spatial point at once for each time step. For example, if we start at the 6th spatial point

(i.e., $i = 6$) and create two more equations for $i = 7$ and $i = 8$, we have

$$-dU_8^{n+1} + 2dU_7^{n+1} + U_6^{n+1} - 2dU_5^{n+1} + dU_4^{n+1} = U_6^n \quad (4.51)$$

$$-dU_9^{n+1} + 2dU_8^{n+1} + U_7^{n+1} - 2dU_6^{n+1} + dU_5^{n+1} = U_7^n \quad (4.52)$$

$$-dU_{10}^{n+1} + 2dU_9^{n+1} + U_8^{n+1} - 2dU_7^{n+1} + dU_6^{n+1} = U_8^n \quad (4.53)$$

which can be written as a band matrix for all spatial grid points i as

$$\mathbf{A}U^{n+1} = \mathbf{b} . \quad (4.54)$$

A simple matrix solver, using the LU decomposed matrices, can be employed to solve Eq. (4.54) for the next time step, where the current time step information is stored in \mathbf{b} . The current time step information is the estimated U^{n+1} from solving the nonlinear term Eq. (4.45)

4.4 Periodic Boundary Conditions

For these numerical methods to work properly near the boundary of the spatial grid, it is necessary to impose boundary conditions on the end points of the grid which can be seen in Figure 4.3. Looking at the finite difference equation for the Lax-Wendroff one step method, boundary conditions need to be imposed on the grid points $i = 0$ and N where N is the maximum spatial grid point.

Since the solutions will be localized, a large domain and periodic boundary conditions will produce the effect of an infinite domain; therefore the boundary conditions $U \rightarrow 0$ as $x \rightarrow \pm\infty$ will essentially be satisfied. What is meant by periodic boundary conditions is at the N th grid spacing ($i = N$), the $(i+1)$ th term will be replaced with the first grid spacing, and the opposite happens at the first grid spacing. Essentially for Eq. (4.45), we will have the following points equal to each other.

$$U_{-1}^n = U_N^{n+1} \quad (4.55)$$

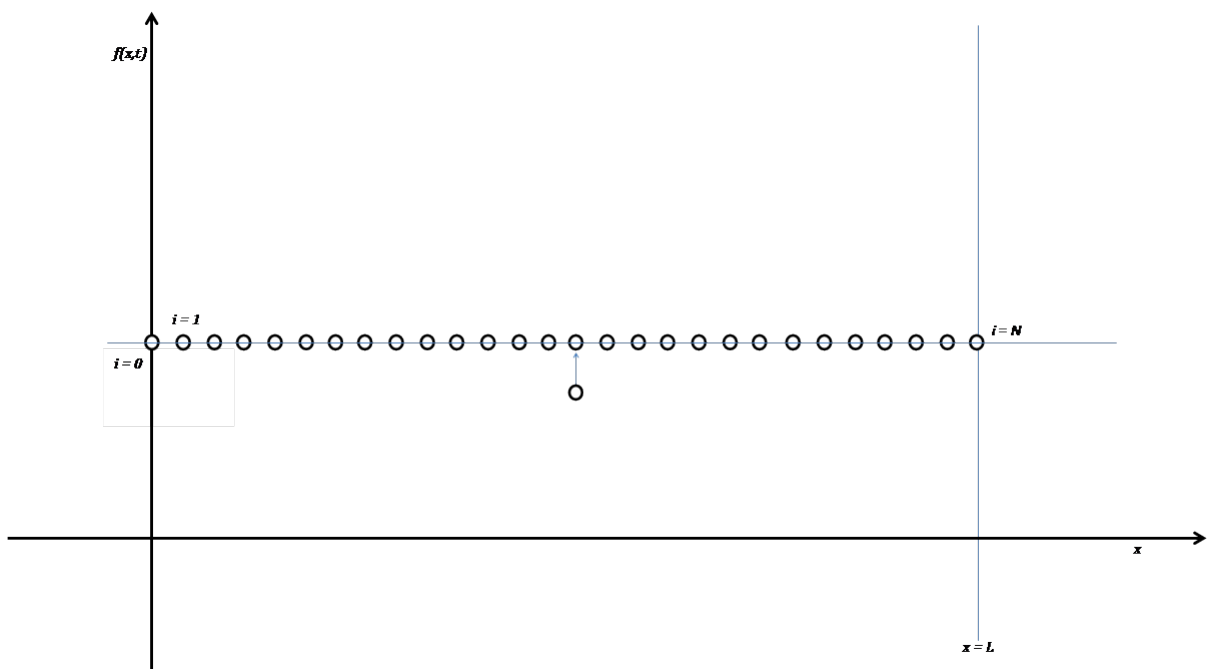


Figure 4.3: This figure displays a general outline of the grid spacing at time step n with boundaries at $x = 0$ and $x = L$.

and

$$U_{N+1}^n = U_0^{n+1} \quad (4.56)$$

Applying these boundary conditions to the diffusive term, Eq. (4.50) is a bit more complicated, because terms in the banded matrix, \mathbf{A} , need to be adjusted. If we look at the grid point $i = 0$, according to the finite difference equation, the $i - 1$ and $i - 2$ terms are outside the domain. These terms need to be replaced with two terms at the other end of the domain, so

$$\text{when } i = 0 \rightarrow U_{i-2}^{n+1} = U_{N-1}^{n+1} \text{ and } U_{i-1}^{n+1} = U_N^{n+1} \quad (4.57)$$

and

$$\text{when } i = 1 \rightarrow U_{i-2}^{n+1} = U_N^{n+1}. \quad (4.58)$$

The same goes for the end spatial point. Therefore the matrix \mathbf{A} becomes

$$\mathbf{A} = \begin{pmatrix} 1 & 2d & -d & 0 & \cdots & d & -2d \\ -2d & 1 & 2d & -d & 0 & \cdots & d \\ d & -2d & 1 & 2d & -d & 0 & \vdots \\ 0 & \ddots & \ddots & \ddots & \ddots & \ddots & 0 \\ \vdots & 0 & d & -2d & 1 & 2d & -d \\ -d & \cdots & 0 & d & -2d & 1 & 2d \\ 2d & -d & \cdots & 0 & d & -2d & 1 \end{pmatrix}.$$

This means that the matrix is no longer banded because it has nonzero “corners”, which complicates the inversion process somewhat. However, since most of the off-diagonal elements are still zero, the matrix can still be factorized using the LU decomposition method.

4.5 Derivative Nonlinear Schrödinger Equation

After an in depth analysis of how to treat convection, diffusion, and the KdV equation, a numerical solution for the Derivative Nonlinear Schrödinger Equation (DNLS) will

be developed in this section. Producing simulations of the nonlinear waves that are governed by the DNLS equation can provide information of the processes that enable these soliton solutions. As mentioned earlier, the DNLS equation can be derived from the magnetohydrodynamic equations that describe the behavior of plasmas. Using the reductive perturbation technique with the appropriate assumptions, the DNLS equation can be derived for the magnetic field strength.

For low plasma β , the DNLS can describe waves propagating perpendicular to the background magnetic field, or waves that propagate parallel to the background magnetic field. This section will focus on the parallel propagation case,

$$\frac{\partial b}{\partial t} + \alpha \frac{\partial}{\partial x} (|b|^2 b) + i\mu \frac{\partial^2 b}{\partial x^2} = 0 , \quad (4.59)$$

where

$$b(x, t) = B_y + iB_z , \quad (4.60)$$

and $b(x, t) \rightarrow b_0 \neq 0$ as $x \rightarrow \pm\infty$. The coefficients α and μ depend on the type of plasma under inspection. For example, for a cold plasma ($\beta < 1$) we have

$$\alpha = \frac{1}{4} \frac{v_A}{B_0^2}, \quad \mu = \frac{1}{2} \frac{v_A^2}{\Omega_i} \quad (4.61)$$

where v_A is the Alfvén velocity, B_0 is the background magnetic field, and Ω_i is the ion gyrofrequency. For a warm plasma, the coefficients are

$$\alpha = \frac{1}{4} \frac{v_A}{B_0^2} \frac{1}{1 - \beta}, \quad \beta = \frac{c_s^2}{v_A^2} . \quad (4.62)$$

The coefficients are not in dimensionless form, therefore we can introduce dimensionless variables and transform the DNLS equation to dimensionless variables, which is done in Appendix A.2.

As explained in §4.3, it is profitable to split complicated nonlinear PDE's into two different PDE's when trying to produce a numerical approximation of the equation, because it reduces the complexity of the finite difference equation. For the DNLS equation, the nonlinear term is the most complicated to solve and a suitable numerical

method for the diffusive term was investigated in Section 4.2. The main goal is to develop a method using

$$\frac{\partial b^*}{\partial t} = -\alpha \frac{\partial}{\partial x} (|b^*|^2 b^*) \quad (4.63)$$

where $b^*(x, t)$ is the first estimate of $b(x, t)$. This estimate, b^* , will be used to solve the diffusive term,

$$\frac{\partial b}{\partial t} = -i\mu \frac{\partial^2 b}{\partial x^2}, \quad (4.64)$$

which will produce the solution $b(x, t)$ for the same time step used to solve Eq. (4.63).

Lax-Wendroff type numerical schemes to solve PDE's are useful for convective type processes which in the case of the DNLS the nonlinear term acts similarly because it produces a nonlinear steepening effect. The one step method was used earlier to produce sufficient numerical solvers for the linear convection equation and the nonlinear term in the KdV equation, which is the nonlinear convection equation.

Since the nonlinear term in the KdV equation was weakly nonlinear, it was trivial to produce the necessary derivatives in time for the Taylor series expansion. With the DNLS equation, this freedom is not present and it can be difficult producing a one step Lax-Wendroff scheme. A two step Lax-Wendroff scheme is available and is powerful for solving nonlinear equations, because it uses calculations at half time steps to make an approximation which provide second order accuracy in time and space ($\mathcal{O}(\Delta t^2) + \mathcal{O}(\Delta x^2)$).

Essentially the scheme has a prediction equation and then a correction equation, which is evaluated over one full time step. The first step of the Lax-Wendroff scheme calculates values for $b(x, t)$ at a half time step, and half spatial grid points, for example at $n+1/2$ and $i\pm 1/2$. This scheme is explicitly solved, so for simplicity the nonlinear product inside the derivative operator is calculated before the solution is estimated. This allows for a simpler expression of Eq. (4.63) to be written as

$$\frac{\partial b}{\partial t} = -\alpha \frac{\partial g(b(x, t))}{\partial x}, \quad (4.65)$$

which is in flux conservative form, where

$$g(b(x, t)) = b(x, t)|b(x, t)|^2 \quad (4.66)$$

The Lax-Wendroff first step finite difference approximation for Eq. (4.65) for the $(i + 1/2)$ th step is

$$\frac{b_{i+1/2}^{n+1/2} - (b_i^n + b_{i+1}^n)/2}{(\Delta t)/2} = -\alpha \frac{g_{i+1}^n - g_i^n}{\Delta x}. \quad (4.67)$$

Note that b^n is known for all i . For the second Lax-Wendroff step, the $i - 1/2$ spatial iteration is required. Using the same form as Eq. (4.67), the backward space finite difference approximation for the $(n + 1/2)$ th time step is

$$\frac{b_{i-1/2}^{n+1/2} - (b_i^n + b_{i-1}^n)/2}{(\Delta t)/2} = -\alpha \frac{g_i^n - g_{i-1}^n}{\Delta x}. \quad (4.68)$$

Solving for the $b_{i\pm 1/2}^{n+1/2}$ terms yields

$$b_{i+1/2}^{n+1/2} = \frac{b_i^n + b_{i+1}^n}{2} - \frac{\alpha \Delta t}{2 \Delta x} (g_{i+1}^n - g_i^n) \quad (4.69)$$

and

$$b_{i-1/2}^{n+1/2} = \frac{b_i^n + b_{i-1}^n}{2} - \frac{\alpha \Delta t}{2 \Delta x} (g_i^n - g_{i-1}^n). \quad (4.70)$$

Using Eqs. (4.69) and (4.70), the second step in is calculated with

$$\frac{b_i^{n+1} - b_i^n}{\Delta t} = -\alpha \frac{g_{i+1/2}^{n+1/2} - g_{i-1/2}^{n+1/2}}{\Delta x}, \quad (4.71)$$

which uses a first center ordered difference in space for the half time step. Solving for b_i^{n+1} produces

$$b_i^{n+1} = b_i^n - \frac{\alpha \Delta t}{\Delta x} \left(g_{i+1/2}^{n+1/2} - g_{i-1/2}^{n+1/2} \right). \quad (4.72)$$

where

$$g_{i\pm 1/2}^{n+1/2} = g \left(b_{i\pm 1/2}^{n+1/2} \right) \quad (4.73)$$

and $b_{i\pm 1/2}^{n+1/2}$ was obtained from Eqs. (4.69) and (4.70). The solution to Eq. (4.72) is the solution to the nonlinear portion of the DNLS equation. As previously stated, this value for b_i^{n+1} is an estimate of the DNLS numerical solution which in turn will be “updated” by using these values for b_i^{n+1} as the initial conditions for the diffusive term.

A numerical method was developed in §4.2 for the diffusion equation that was implicit as well as unconditionally stable. There will be a slight difference here because the nature of the diffusive term in the DNLS is complex. Starting with the diffusion term

$$\frac{\partial b}{\partial t} = -i\mu \frac{\partial^2 b}{\partial x^2}, \quad (4.74)$$

and substituting BTCS finite difference approximations yields

$$\frac{b_i^{n+1} - b_i^n}{\Delta t} = -i\mu \left(\frac{b_{i+1}^{n+1} - 2b_i^{n+1} + b_{i-1}^{n+1}}{\Delta x^2} \right). \quad (4.75)$$

Introducing the variable $D = i\mu\Delta t/\Delta x^2$ and moving the b^{n+1} terms on the right hand side to the left gives

$$Db_{i-1}^{n+1} + (1 - 2D)b_i^{n+1} + Db_{i+1}^{n+1} = b_i^n, \quad (4.76)$$

which implicitly contains the solution of b_i^{n+1} for all given i that the values of b_i^n are provided from the solution of the nonlinear approximation, Eq. (4.72). Again, this results in a banded matrix, where the system of equations can be solved using LU factorization method.

4.5.1 Stability Analysis of the Lax-Wendroff Two-Step/BTCS scheme

As mentioned earlier, the nonlinear term and the dispersive term were solved separately for numerical and analytical convenience. This allows for stability analysis of each term individually or the overall stability. As done in §4.2, we can apply the von Neumann stability analysis to the dispersive term. Recalling that the FDE for this

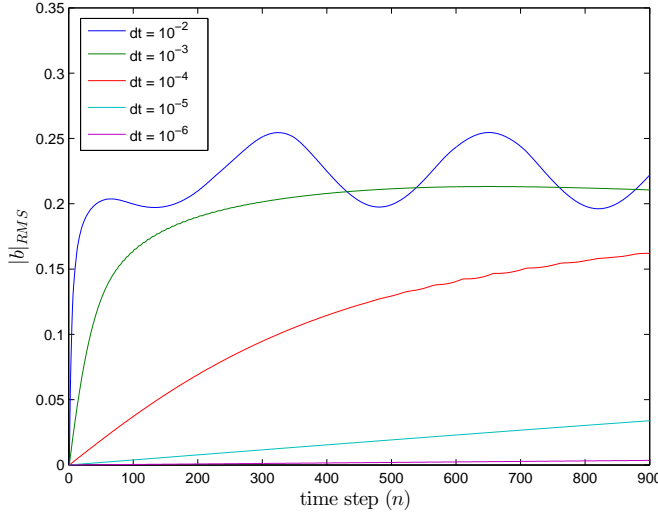


Figure 4.4: Stability analysis of several selections for Δt (dt). The root mean square error drops significantly with decreasing Δt . The initial profile used was a two parameter soliton with an eigenvalue $\lambda = 0.5 + 0.5i$. It can be seen that the largest time step was unstable due to the oscillations of the root mean square error.

term was

$$Db_{i-1}^{n+1} + (1 - 2D)b_i^{n+1} + Db_{i+1}^{n+1} = b_i^n, \quad (4.77)$$

we can replace the $b_{i\pm 1}^{n+1}$ terms with $b^{n+1}e^{\pm I\theta}$, resulting in

$$Db^{n+1}e^{-I\theta} + (1 - 2D)b_i^{n+1} + Db^{n+1}e^{+I\theta} = b_i^n. \quad (4.78)$$

Now Euler's formula can be used to simplify Eq. (4.78), and then substitution of the amplification factor G yields

$$D\cos\theta + (1 - 2D) = \frac{1}{G}, \quad (4.79)$$

or

$$G = \frac{1}{(1 - 2D) + D\cos\theta}, \quad (4.80)$$

which is the same as for the diffusion equation. By inspection, the condition $|G| \leq 1$ is always satisfied even though D is complex. It was relatively trivial producing

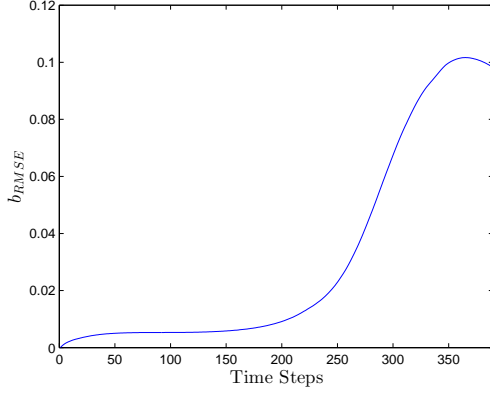


Figure 4.5: Plot of the root mean square error between the numerical and analytical solutions of the DNLS equation. The value of the time step used was $dt = 10^{-4}$, therefore smaller time steps should reduce the RMS.

a relation for the dispersive term because of its linearity. However, analyzing the stability of the nonlinear term is non-trivial. Von Neumann stability analysis cannot be applied for this term because linearity is a strict requirement for producing stability relations similar to Eq. (4.80).

Although the nonlinearity prevents the ability to use the von Neumann stability analysis, we can use the stability condition acquired from the linear convection FDE as a guide for the values of Δx and Δt . This is possible because of the flux conservative nature of the Lax-Wendroff method. A rough estimate for the stability condition for the nonlinear term is

$$1 \geq \frac{\alpha \Delta t}{\Delta x} \quad (4.81)$$

which restricts Δt to be smaller than Δx if $\alpha = 1$. Another useful technique to investigate stability of the overall Lax-Wendroff/BTCS method would be to vary the time step, Δt , and determine its influence over a large number of time steps. This can be done by evaluating the root mean square error between a numerical solution and a known analytical solution.

Figure 4.4 demonstrates the effect of decreasing the temporal step value, Δt , on the root mean squared error between the numerical solution and the analytical solution. Ideally the smaller the time step, the more accurate the solution becomes, but has the

converse effect on computational time. Another reinforcement of the scheme's ability to numerically integrate the DNLS equation accurately is a comparison with a known analytical solution along with calculating the root mean square error between the numerical and analytical solutions. Figure 4.6 demonstrates a test of the numerical scheme derived earlier using a two parameter soliton solution with an eigenvalue of $\lambda = 0.5 + 0.5i$. The waveform does hold its shape and does not disperse, but more concrete evidence of its stability comes from Figure 4.5, which displays the root mean square (RMS) error between the analytical and numerical solutions, where the time step used was $dt = 10^{-4}$. Decreasing the time step will lead to a decrease in the numerical error, which will decrease the RMS.

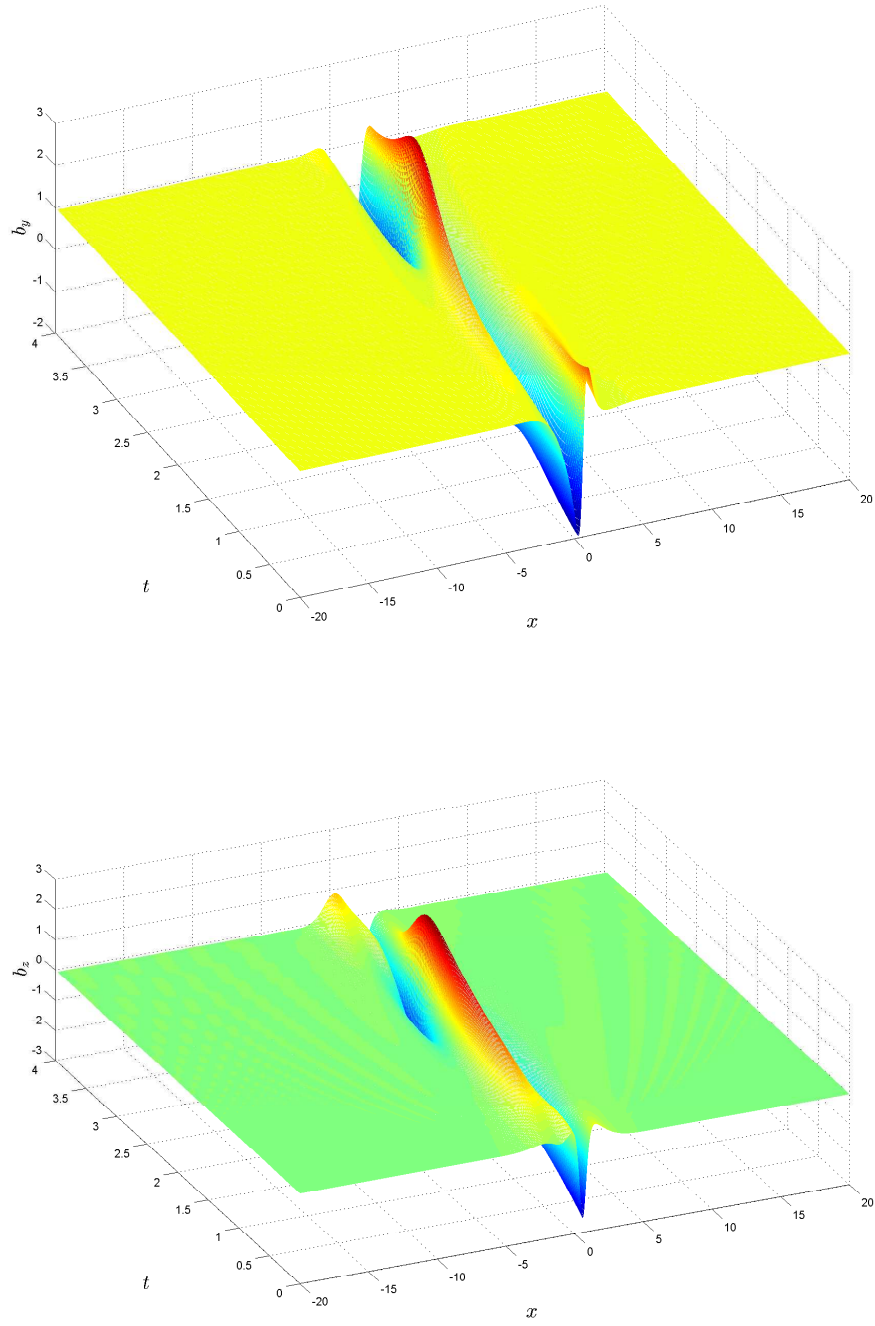


Figure 4.6: Numerical solution of the DNLS with a two parameter soliton solution with an eigenvalue of $\lambda = 0.5 + 0.5i$. The time step used in this numerical integration was $dt = 10^{-4}$.

Chapter 5

Preliminary Analysis of Ulysses data

The main goal of this thesis is to provide preliminary evaluation of an event observed by the Ulysses spacecraft that has characteristics familiar with a soliton that is governed by the DNLS equation. It has been reported [21, 27] that the Ulysses spacecraft has made observations of small scale solitary structures in the interplanetary magnetic field (IMF), which is the magnetic field generated by the Sun's internal processes and encompasses most of the solar system. The IMF is the field that permeates the space between planetary magnetospheres and the Sun.

The primary mission of the Ulysses spacecraft was to produce a characterization of the heliosphere as a function of solar latitude. Points of interest for the mission were when the spacecraft made passes at or over 70 degrees solar latitude at both of the Sun's poles. Ulysses reached 70 degrees South on June 26th, 1994 and started a 4 month observation of the high latitudes taking measurements of the Sun's corona. There were two magnetometers on board the spacecraft, a vector helium magnetometer and a flux gate magnetometer. The magnetic field data was collected with a time resolution of 2 vectors per second and a sensitivity of 10 pT [2]. In addition, the plasma measurements were made by SWOOPS (solar wind observations over the poles of the sun), which used electrostatic analyzers to measure the electron and ion energies that are present in the solar wind [3].

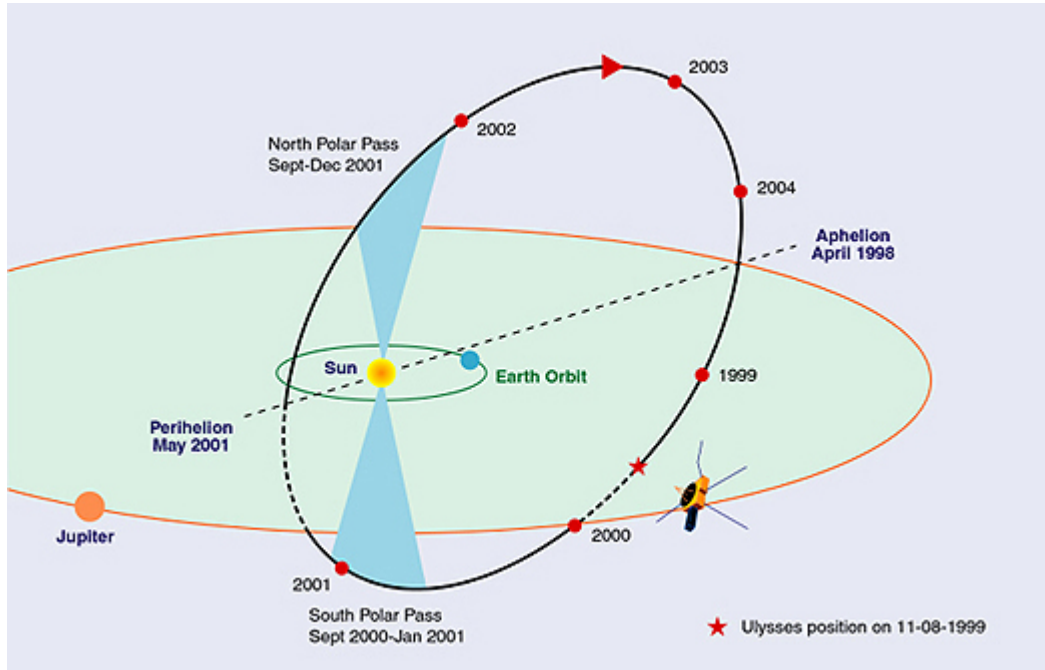


Figure 5.1: Pictorial representation of Ulysses trajectory, from [1].

The following sections will provide an analysis of the plasma characteristics during the event, which was identified by Rees et al. [21] as a possible soliton candidate. Figure 5.2 displays the the list of magnetic pulses that were identified in the Ulysses magnetometer data, and the event that will be analyzed is highlighted. A rotation of the coordinate system of that specific magnetic bump will be performed with a minimum variance transformation. Minimum variance analysis uses spatial averages of the magnetic field vectors to produce a magnetic variance matrix. Eigenvalues that are associated with this magnetic variance matrix determine the rotation made from the current coordinate system (RTN coordinates, which will be explained later), where the smallest eigenvalue is associated with the minimum variance direction. Eigenvectors that are connected with the eigenvalues provide the directions for the coordinate system rotation. The main purpose of this transformation is to rotated into a coordinate system where the minimum variance direction is going to be considered as the direction of propagation of this magnetic pulse.

After the minimum variance transformation of the magnetic bump observed on

Table 5.1: Ulysses Orbital Elements on Feb. 21st 2001

Parameter	Variable	Value
Radial Distance from Sun	r	1.685 AU
Semi-Major Axis	a	3.37 AU
Eccentricity	e	0.602
Radial distance at Aphelion	r_a	5.4 AU
Radial distance at Perihelion	r_p	1.34 AU
Specific Angular Momentum	h	$6.531 \times 10^9 \text{ km}^2/\text{s}$
Specific Energy	ϵ	$-83.92 \text{ km}^2/\text{s}^2$

February 21st, 2001, analytical solutions provided by the DNLS equation will be used as an analogue of the data for analysis. This is done by selecting a suitable type of soliton (two parameter, in this case), and comparing the transverse components of b with the intermediate and maximum variance coordinates along with the hodogram, determined from the minimum variance rotation. It turns out, that the two parameter soliton's form corresponded the best with the minimum variance transformed magnetometer data. Reasoning for this step in the analysis lies behind the fact that the types of mathematical techniques used to interpret the data has a strict requirement of the wave profile being smooth and continuous. There is inherent noise in the data itself, therefore these small variations might lead to false results. An appropriate soliton is found, where the morphology does correspond well with the minimum variance transformed magnetic pulse, but the amplitudes are different. Therefore the profile that is used as the analogue will be a scaled version of the analytical soliton solution.

With the selected soliton profile that mimics the data, a 2x2 eigenvalue shooting method solve was performed on that two parameter soliton that was scaled. The 2x2 eigenvalue shooting method consisted of a fourth order Runge-Kutta initial value problem solver, which solved for the eigenfunction Φ from left to right. Then a root finding method, Muller's method, was used to determine where the function $\phi_{11}(\lambda) = 0$. So the RK4 method solved for the from left to right, and Muller's method produced a guess for the eigenvalue, this guess was inserted back into RK4 and solved again from left to right. This process was iterated until the shooting

Year	Day of Year	Time, hours: minutes	Sun-Spacecraft Range, AU	Heliolatitude, deg
1991	004	12:52	1.62	-1.0
1991	004	13:13	1.62	-1.0
1991	004	13:45	1.62	-1.0
1991	005	04:34	1.63	-1.0
1991	021	11:06	1.81	-1.9
1991	090	08:32	2.57	-3.9
1991	091	04:57	2.58	-3.9
1991	091	05:43	2.58	-3.9
1991	091	09:20	2.58	-3.9
1991	183	21:10	3.51	-5.0
1992	014	19:56	5.19	-5.9
1994	067	09:48	3.49	-55.2
1994	071	11:32	3.46	-55.7
1995	068	20:44	1.34	3.9
1995	076	11:43	1.34	9.9
1998	163	08:06	5.40	-8.7
2000	093	11:30	3.73	-50.3
2000	093	13:27	3.73	-50.3
2000	171	12:12	3.31	-59.0
2001	039	02:46	1.77	-61.3
2001	052	03:35	1.68	-55.3
2001	052	05:57	1.68	-55.3
2001	052	06:13	1.68	-55.3
2001	052	09:23	1.68	-55.2
2001	052	09:28	1.68	-55.2
2001	117	21:34	1.37	-14.1
2001	135	17:09	1.34	-0.2
2001	136	09:06	1.34	0.3
2001	140	18:30	1.34	3.8
2001	140	22:01	1.34	3.9
2001	231	10:35	1.66	65.1
2002	198	08:14	3.75	38.0
2003	012	08:40	4.50	23.1

Figure 5.2: List of the events identified by Rees et al. [21], that were classified as small scale solitary magnetic pulses. The event that will be analyzed is highlighted.

method converged on an eigenvalue where the solution of ϕ_{11} at the right end of the domain was zero. In a later section, a demonstration of this method converging on a known soliton solution is provided. Also, the shooting method is performed on the smooth scaled two parameter soliton that was considered as an analogue of the magnetic pulse. The method converged on an eigenvalue that turned out to be on the real axis in the complex eigenvalue λ plane.

The last section will implement the DNLS numerical integration method, which was developed in Chapter 4, as a way of determining if the magnetic field data contains a soliton component, dispersive waves, or both. This is done because due to the fact that the way the shooting method is set up, it only determines if an eigenvalue is present in a specific potential (i.e., initial wave profile), which one was found for the scaled two parameter soliton. It does not determine if the potential is reflectionless or what parameter (one or two) soliton solution corresponds with the

converged eigenvalue. As a first case, the Ulysses magnetometer data, which was transformed under the minimum variance analysis, was used as the initial condition, and only dispersive waves form without any solitons. The next situation will use the two parameter wave profile that best matched the data along with a small oscillation in the background of b_y , which results in the two parameter soliton's dissipation. Finally, the last case uses a "scaled" soliton that was used as an analogue of the data, as the initial wave profile for the integration scheme. As was revealed with the 2x2 eigenvalue shooting method, a one parameter dark soliton does form, and the eigenvalue is close to the eigenvalue that was found by the shooting method.

5.1 Magnetic bump observed on February 21st, 2001

Measurements that the magnetometer made are displayed in Radial-Tangential-Normal coordinates (RTN), where R is the spacecraft-Sun radial distance, T is the vector produced by

$$\hat{T} = \hat{\omega} \times \hat{R} \quad (5.1)$$

where $\hat{\omega}$ is the Sun's spin axis, and the N is

$$\hat{N} = \hat{R} \times \hat{T}. \quad (5.2)$$

Figure 5.3 displays the configuration of the RTN coordinate system. Figure 5.4 displays the magnetometer data observed by the Ulysses spacecraft of the structure that will be investigated. It can be seen that the structure is localized. The plasma characteristics are important when providing an analysis of spacecraft data because they provide information on the state of the plasma during the observation. Since we will interpret the magnetic field structure as a soliton that behaves according to the DNLS equation, it is important to calculate the plasma β along with the angle of propagation with respect to the background magnetic field to determine what type of nonlinear wave this structure might be.

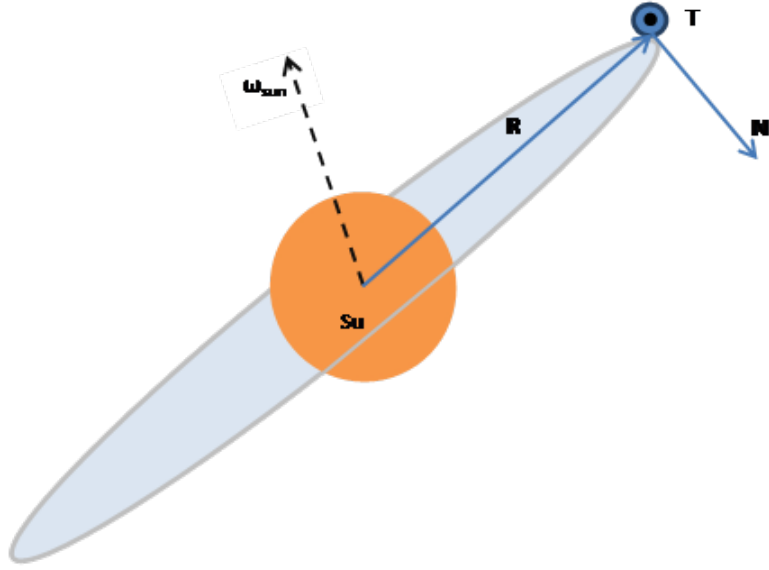


Figure 5.3: Radial-Tangential-Normal Coordinates. The radial component, \mathbf{R} is the vector from the center of the Sun to the spacecraft. The tangential component, \mathbf{T} , is the cross product of the Sun's spin axis, $\hat{\omega}$, with the radial direction, and the normal direction completes the right handed coordinate system by crossing \mathbf{R} with \mathbf{T} .

5.1.1 Plasma Characteristics

Using the ion temperature and density measurements made by SWOOPS, the ion temperature observed was $T_i \approx 4 \times 10^4$ K and the proton density was $n_i \approx 0.4 \text{ cm}^{-3}$. From these values, the pressure can be calculated

$$p_o = n_i k T_i = 2.76 \times 10^{-13} \text{ J/m}^3, \quad (5.3)$$

where k is Boltzmann's constant. The background magnetic field strength was about $B_0 \approx 1 \text{ nT}$, therefore the Alfvén speed was

$$v_A = \frac{B_0}{\sqrt{\mu_0 m_i n_i}} = 34.5 \text{ km/s}, \quad (5.4)$$

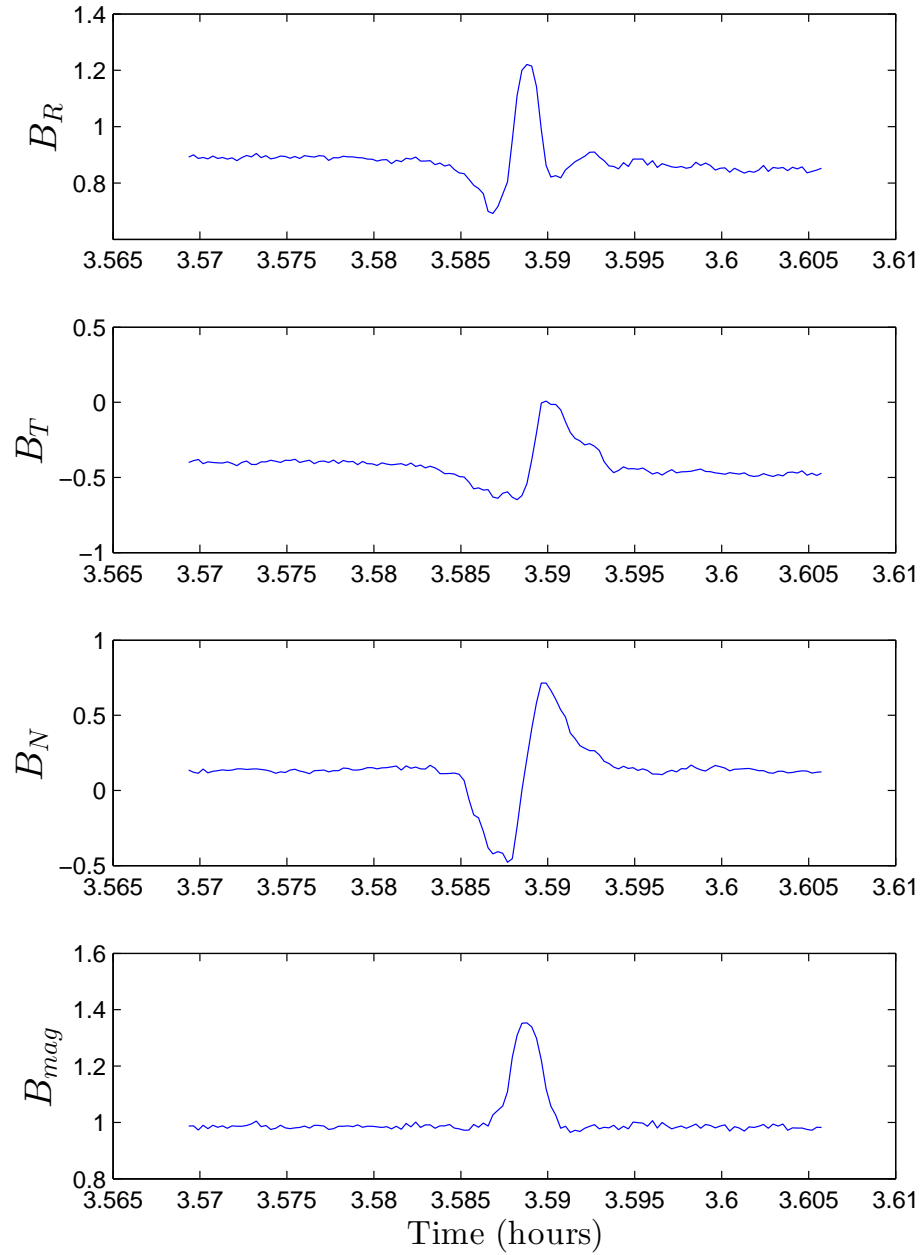


Figure 5.4: Magnetic field components (and magnitude) measured by the VGM/FGM magnetometers on the Ulysses spacecraft on February 21st, 2001. The components are in RTN coordinates (see text for explanation).

where μ_0 is the permeability of free space, and m_i is the proton mass. Finally, the plasma β was

$$\beta = \frac{p_0}{\frac{B_0^2}{2\mu_0}} = 0.69. \quad (5.5)$$

Lengths in the DNLS equation are scaled to the ion inertial length (c/ω_{pi}), and the ion plasma frequency was calculated to be

$$\omega_{pi} = \sqrt{\frac{n_i e^2}{\epsilon_0 m_i}} \approx 830 \text{ Hz}, \quad (5.6)$$

so the ion inertial length was calculated to be

$$\frac{c}{\omega_{pi}} = 360 \text{ km}. \quad (5.7)$$

The orbital elements of Ulysses are needed to understand the length scale of the measured structure, which are presented in Table 5.1. Using these elements and the energy equation,

$$\frac{v^2}{2} - \frac{\mu}{r} = \epsilon = -\frac{\mu^2}{2h^2}(1 - e^2), \quad (5.8)$$

the velocity of the spacecraft was calculated to be

$$v = \sqrt{2 \left(\epsilon + \frac{\mu}{r} \right)} = 29.75 \text{ km/s}. \quad (5.9)$$

Since the spacecraft is moving at about 30 km/s, the dimensionless spacing in between each magnetic field measurement is

$$\frac{\Delta x}{c/\omega_{pi}} \approx 0.1 \quad (5.10)$$

because the measurements are made with a 1 second resolution.

5.2 Minimum Variance Analysis of Observed Solitary Structure

Minimum variance analysis is a powerful technique used to produce an estimation of the direction of a one-dimensional current layer, wavefront or some other time of transitional layer in a plasma [24]. Applying a minimum variance transformation to the event that is displayed in Figure (5.4), would minimize one of the three magnetic field components which would effectively serve as the direction of propagation (or in context of the DNLS equation, the x direction). The other two components would be the intermediate and maximum variations, i.e., B_y and B_z , respectively.

To perform the transformation, the magnetic variance matrix needs to be calculated from the raw data measurements, which is done using

$$M_{\mu\nu} = \langle B_\mu B_\nu \rangle - \langle B_\mu \rangle \langle B_\nu \rangle \quad (5.11)$$

where the subscripts μ and ν denote the Cartesian components (i.e., 1,2,3 is X, Y, Z) and the brackets $\langle \rangle$ denote a spatial average (refer to Ref [24] for more details). The corresponding eigenvalues of the magnetic variance matrix $M_{\mu\nu}$ determine the minimum, intermediate and maximum variances, where the minimum eigenvalue is the estimated variance along the normal of the boundary or current layer, and its eigenvector is the minimum variance direction. Therefore, the intermediate eigenvalue will lead to the intermediate variance direction, and the maximum eigenvalue will lead to the maximum variance direction.

It can be seen from Eq. (5.11) that the size of the interval of the measured data will affect the structure of the magnetic variance matrix, altering its eigenvalues and corresponding eigenvectors. Therefore, it is necessary to pick an optimal interval size for performing the minimum variance transformation. This optimum size is when the minimum variance coordinate is smallest. This was done by calculating the root mean square error for all of the data points in the minimum variation coordinate, b_{min} , for different interval sizes. Figure 5.5 shows the dependence of the root mean square error of b_{min} on the number of data points used in the minimum variance transformation

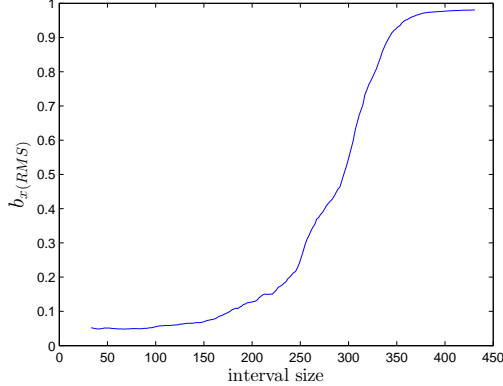


Figure 5.5: Root mean square error of b_{min} as a function of the interval size added to number of data points encapsulating just the event (expressed as the amount of data points used for the minimum variance analysis).

around the observed solitary wave structure. The proper interval was determined to be anywhere from 50-100 data points in addition to the number of data points of the just the isolated event (which was 32 points, or 32 seconds of magnetometer data).

Figure 5.6a displays the observed wave structure after the rotation from the RTN coordinate system to the minimum variation coordinate system, with an optimal amount of time series data which minimized the minimum variance. For comparison for with soliton solutions provided by the DNLS equation, the minimum variance direction is going to be considered as the direction of propagation or x . Transverse components of the wave, b_{inter} and b_{max} , will be compared to the transverse components of the DNLS solution, b_y and b_z , respectively. The polarization of the waveform, which can be seen in Figure 5.6b, has a resemblance to that of a banana. The angle of propagation with respect to the background magnetic field (or the angle between the minimum variance eigenvector and the background magnetic field vector of the raw data) can be calculated using

$$\theta = \cos^{-1} \left(\frac{\hat{\mathbf{x}} \cdot \mathbf{B}_0}{|\hat{\mathbf{x}}| \cdot |\mathbf{B}_0|} \right) \approx 88.6^\circ \quad (5.12)$$

where $\hat{\mathbf{x}}$ is the minimum variation direction eigenvector and \mathbf{B}_0 is the background magnetic field vector. The angle of propagation relative to the background magnetic

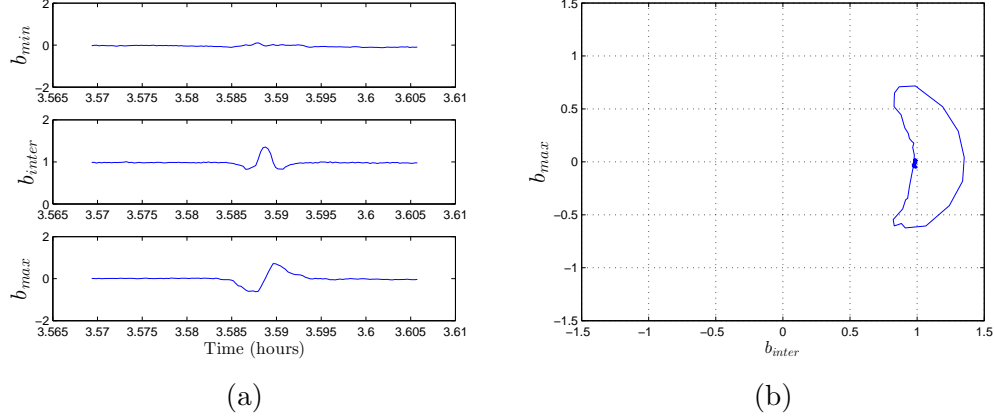


Figure 5.6: (a) The three components of the magnetic field after the minimum variance transformation. (b) The hodogram of the minimum variance transformed data is also displayed. The soliton can be considered as a “banana polarized” soliton because of the distinct form of its hodogram.

field is close to perpendicular, therefore it can be considered as an oblique Alfvén wave.

5.3 Comparison of observed event with solitons solutions of the DNLS

The observed bump in the magnetic field presented in the previous section was found and analyzed previously by Rees et al. [21], in which a comparison with a one parameter bright soliton was made. The next section will provide the comparison and conclusions made about the observed bump. Following Rees et al.’s [21] analysis, a comparison between the event and a two parameter soliton will be made, showing more morphological agreement than the comparison of the one parameter soliton.

5.3.1 Previous comparison to one parameter bright soliton

This particular event was analyzed by Rees et al. [21], but they were not able to provide complete correspondence between a theoretical soliton solution provided by

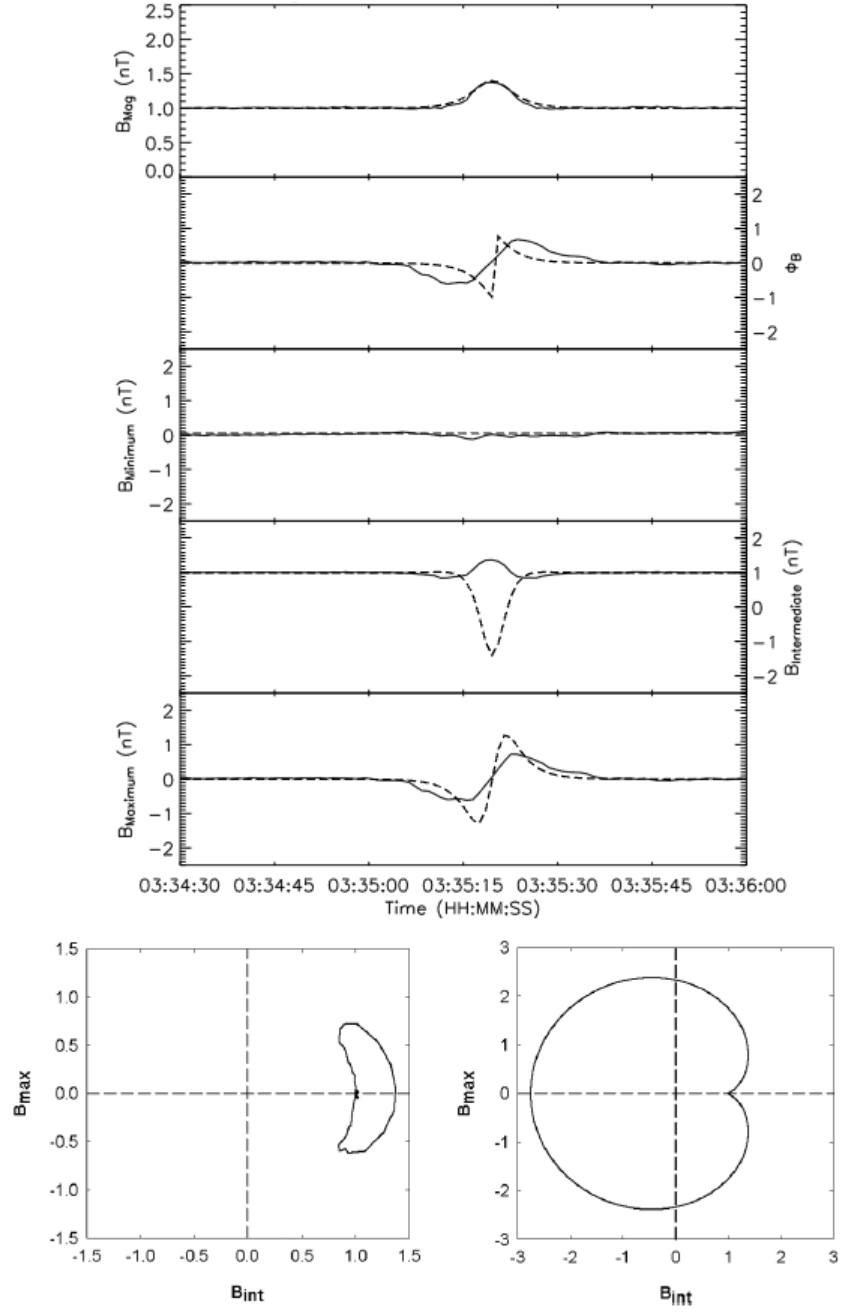


Figure 5.7: Comparison of observed solitary structure with a one parameter bright soliton made by Rees et al. [21]. The comparison was made using a solution to the DNLS provided by Baumgärtel [5]. There is a strong agreement between the minimum variance transformed data and the magnitude and B_{minimum} , with slight correlation for B_{maximum} . However, the hodogram and $B_{\text{intermediate}}$ component are very different.

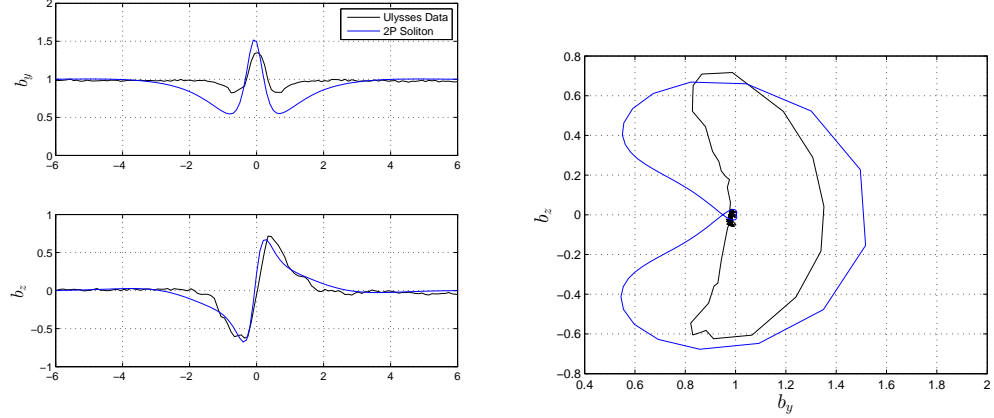


Figure 5.8: Comparison of observed solitary structure with a two parameter soliton with an eigenvalue of $\lambda = 0.4 + 0.5i$. The wave amplitudes did not match, so the analytical solution provided in Chapter 2 was scaled to attain the best agreement possible, where $t = 3.7$.

the DNLS equation and the solitary wave structure that was measured by Ulysses. Some features seem to have a correlation with a bright, one-parameter soliton, but the exact morphology did not agree definitively, which can be seen in Figure 5.7. However, it was shown by Sauer et al. [25] that there is a sensitive dependence on the plasma conditions, such as β , temperature anisotropy, etc., between the different classes of solitons that could exist. While we know the value of β , the temperature anisotropy was not measured, and without knowledge of these conditions, it is difficult to make quantitative comparisons between observed solitary wave structures and solutions to the DNLS equation.

The observed event does show strikingly familiar features to soliton solutions of the DNLS equation, but the features resemble those of a two parameter soliton as opposed to a one parameter soliton. However, the shape of the two parameter soliton is not static (see Figure 2.5). With only spatial information about the observed wave structure, and no temporal information, it is difficult to make a strong comparison.

5.3.2 Two parameter soliton comparison

Strong resemblance between the two parameter soliton and the data can be seen in Figure 5.8 which displays a scaled two parameter soliton with $\lambda = 0.4 + 0.5i$ superimposed the minimum variance transformed data, shows a higher level of agreement than the comparison made by Rees et al. [21]. The values of the real and imaginary parts of λ have different effects on the waveform and periodicity of the two parameter soliton, which was taken into account when selecting an eigenvalue. Since the solution $b(x, t)$ is a rational function of ϕ (refer back to §2.3.2), we can rewrite ϕ to look like

$$\phi = \exp[-\kappa(x - c_g t)] \exp[i k(x - c_{ph} t)] \quad (5.13)$$

where

$$\kappa = 2\Lambda_i, \quad c_g = \Omega_i/\Lambda_i \quad (5.14a)$$

$$k = 2\Lambda_r, \quad c_{ph} = \Omega_r/\Lambda_r \quad (5.14b)$$

where $\Omega = \Omega_r + i\Omega_i$ and $\Lambda = \Lambda_r + i\Lambda_i$ ($\Lambda_{r,i}$ and $\Omega_{r,i}$ are real valued) and is analogous to its “phase velocity” and “group velocity” [18]. It can be seen that if κ becomes large, the soliton’s overall width should shrink, and if k becomes large then the peak in the middle of the packet becomes thin as well. If $\text{Im}(\lambda)$ becomes much larger than $\text{Re}(\lambda)$, the soliton takes on the form of a wave packet (as $\text{Re}(\lambda) \rightarrow 0$) and as long as $\text{Im}(\lambda) > \text{Re}(\lambda)$, the polarization has a banana or crescent shape. If $\text{Re}(\lambda)$ becomes much larger than $\text{Im}(\lambda)$, the width of the soliton grows, and the splitting between a dark and bright soliton occurs when $\text{Im}(\lambda) \rightarrow 0$. The choice of $\lambda = 0.4 + 0.5i$ permitted the closest polarization and forms of b_y and b_z .

5.4 Application of the Direct scattering transform

A detailed explanation of the 2x2 eigenvalue problem for nonvanishing boundary conditions in the DST/IST perspective for the DNLS equation was provided in §3.4. The following analysis will apply the direct scattering transformation numerically to

calculate the scattering data and eigenvalues, if any occur, associated with the two parameter soliton that was compared to the scaled minimum variance transformed magnetometer data.

5.4.1 Calculation of Eigenvalues through the Numerical DST

As mentioned earlier, the direct scattering transform uses the waveform as the potential function on the scattering problem

$$\Phi_x = D \cdot \Phi. \quad (5.15)$$

It can be seen that ϕ_{11} and ϕ_{21} are coupled and the equations for ϕ_{11} and ϕ_{21} are just the complex conjugates of ϕ_{11} and ϕ_{21} . If we investigate the asymptotic forms of Φ for various potentials and they turn out to be bounded for $x \rightarrow \pm\infty$ we can consider the potential to contain a soliton. The scattering matrix contains the information on how the asymptotic forms of Φ^+ and Φ^- relate to each other. Ideally, only two components of the scattering matrix is necessary (the left or the right) in numerically solving the ODE, Eq. (5.15). Looking at the components of the scattering matrix, Eq. (3.68) can be expanded to

$$\begin{pmatrix} \phi_{11}^- & \phi_{12}^- \\ \phi_{21}^- & \phi_{22}^- \end{pmatrix} = \begin{pmatrix} \phi_{11}^+ & \phi_{12}^+ \\ \phi_{21}^+ & \phi_{22}^+ \end{pmatrix} \begin{pmatrix} s_{11} & s_{12} \\ s_{21} & s_{22} \end{pmatrix}. \quad (5.16)$$

The boundary conditions for the first column of Φ^- are

$$\begin{pmatrix} \phi_{11}^- \\ \phi_{21}^- \end{pmatrix} = \begin{pmatrix} -ib_0 e^{-i\Lambda x} \\ (\lambda - \zeta) e^{-i\Lambda x} \end{pmatrix} \rightarrow \begin{pmatrix} 0 \\ 0 \end{pmatrix} \quad (5.17)$$

as $x \rightarrow -\infty$ if $\text{Im}(\Lambda) > 0$. If we insert the BC's for Φ^+ on the right hand side of Eq. (5.17) we have

$$\begin{pmatrix} \phi_{11}^- \\ \phi_{21}^- \end{pmatrix} = \begin{pmatrix} -ib_0 s_{11} e^{-i\Lambda x} + (\lambda - \zeta) s_{12} e^{+i\Lambda x} \\ (\lambda - \zeta) s_{11} e^{-i\Lambda x} + ib_0 s_{21} e^{+i\Lambda x} \end{pmatrix}. \quad (5.18)$$

It can be seen that the solution to Φ is bounded when $s_{11}(\lambda) = 0$ for $x \rightarrow +\infty$ and $\text{Im}(\Lambda) > 0$. Therefore, an eigenvalue occurs when $s_{11} = 0$, but s_{21} does not have to be zero for an eigenvalue to be present. A value of zero for s_{21} results in a reflectionless potential, because the reflection coefficient is given by $\rho(\lambda) = s_{21}/s_{11}$.

With this insight, a shooting method numerical solver was created to determine eigenvalues for specific potentials. To determine the scattering data with the shooting method, the BC's for ϕ_{11}^- and ϕ_{21}^- were used as initial conditions and a fourth order Runge-Kutta ODE solver was used to solve for ϕ_{11}^+ and ϕ_{21}^+ with a chosen potential and three guesses for the value of λ . Since Φ^+ is dependent on λ , Muller's root finding method was used to search for when $\phi_{11}^+(\lambda) = 0$ by updating the Runge-Kutta solver with each new successive iteration. Muller's method is based on the secant method, and it constructs a parabola using three guesses, allowing it to produce roots that are complex valued [10], even if the first three guesses are real valued.

The two parameter soliton solution that was compared to the transformed data in the previous section is a solution to the DNLS equation that was acquired from the IST; therefore, the shooting method should find the correct eigenvalue. Figure 5.9 shows the final iteration of the shooting method 2x2 eigenvalue problem solver, demonstrating the concept that the eigenvalue of a specific soliton solution can be found numerically. The next step was to use the numerical 2x2 eigenvalue solver with the minimum variance transformed magnetometer data. Unfortunately, an eigenvalue was not able to be found which could be a result of the amount of noise present in the data. However, an eigenvalue was found using the scaled two parameter soliton in Figure 5.8, which can be seen in Figure 5.10

The eigenvalue that led to the bound state in Figure 5.10, was on the real axis with a value of $\lambda = 0.807$. Real valued eigenvalues are one parameter solitons, therefore if the scaled two parameter soliton is used as an initial condition for the DNLS equation, a one parameter bright or dark soliton should appear. Also, since the profile that was selected does not resemble a one parameter soliton, it can be concluded that the numerical solution will not only contain a soliton, but there will be a dispersive wave component as well (from the concepts of solitons presented in Chapter 1).

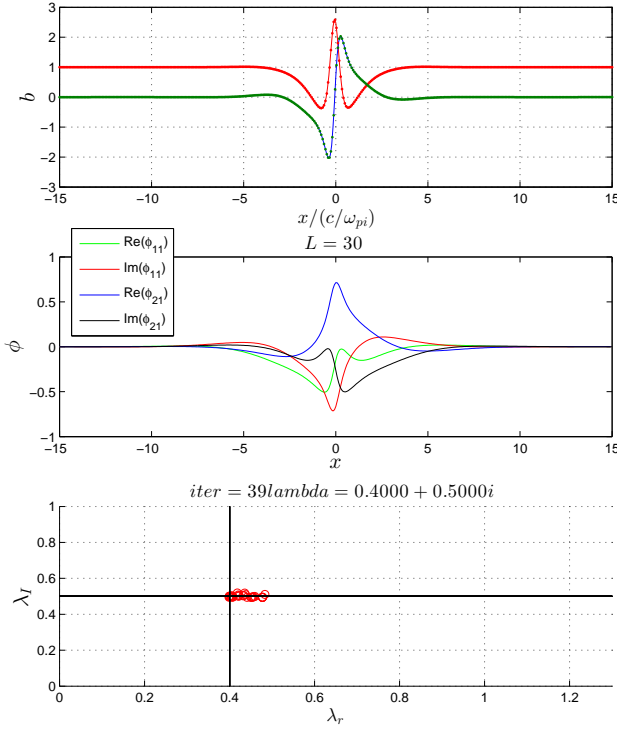


Figure 5.9: The final iteration of the shooting method eigenvalue solver with the 2×2 eigenvalue problem and the two parameter soliton with an eigenvalue of $\lambda = 0.4 + 0.5i$ as its potential. The solver was able to find the correct eigenvalue, as a demonstration of the method’s effectiveness.

5.5 Numerical Integration of the DNLS equation

A method for solving the DNLS equation was derived and presented in §4.5, and the next two sections will build on what was identified in the previous sections of this chapter. First, a two parameter soliton with an eigenvalue of $\lambda = 0.4 + 0.5i$ will be chosen as the initial condition for numerically integrating the DNLS along with another case where there is a small oscillatory perturbation in the background that would represent a coherent noise.

Following that, the minimum variance transformed data will be studied with

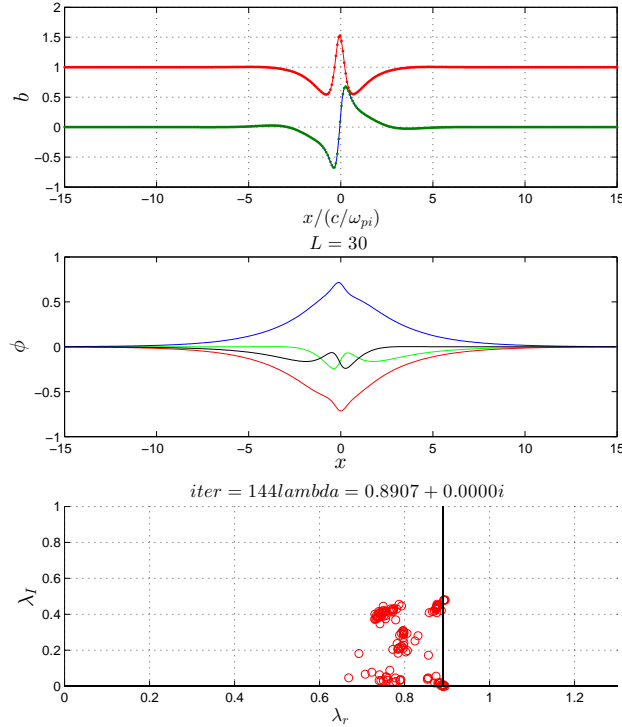


Figure 5.10: (a) The scaled waveform of the two parameter soliton used to mimic the magnetic field data. (b) Bound solution to the 2x2 eigenvalue problem. (c) Eigenvalue guesses, with the final guess on the real axis in the complex plane of λ , with a value of 0.8907.

the DNLS numerical solver although the RK shooting method eigenvalue searching method was unable to find an eigenvalue. From the inconclusive results for the shooting method performed on the data, one can make a reasonable conclusion that only dispersive waves will form. Since the magnetic field data has incoherent background noise, the scaled version of the two parameter soliton that was found to have a correlation with the data will be numerically integrated as well. As a result from the previous section, an eigenvalue of $\lambda = 0.8907$ was found with the RK shooting method eigenvalue solver, therefore a one parameter soliton with that associated eigenvalue should form.

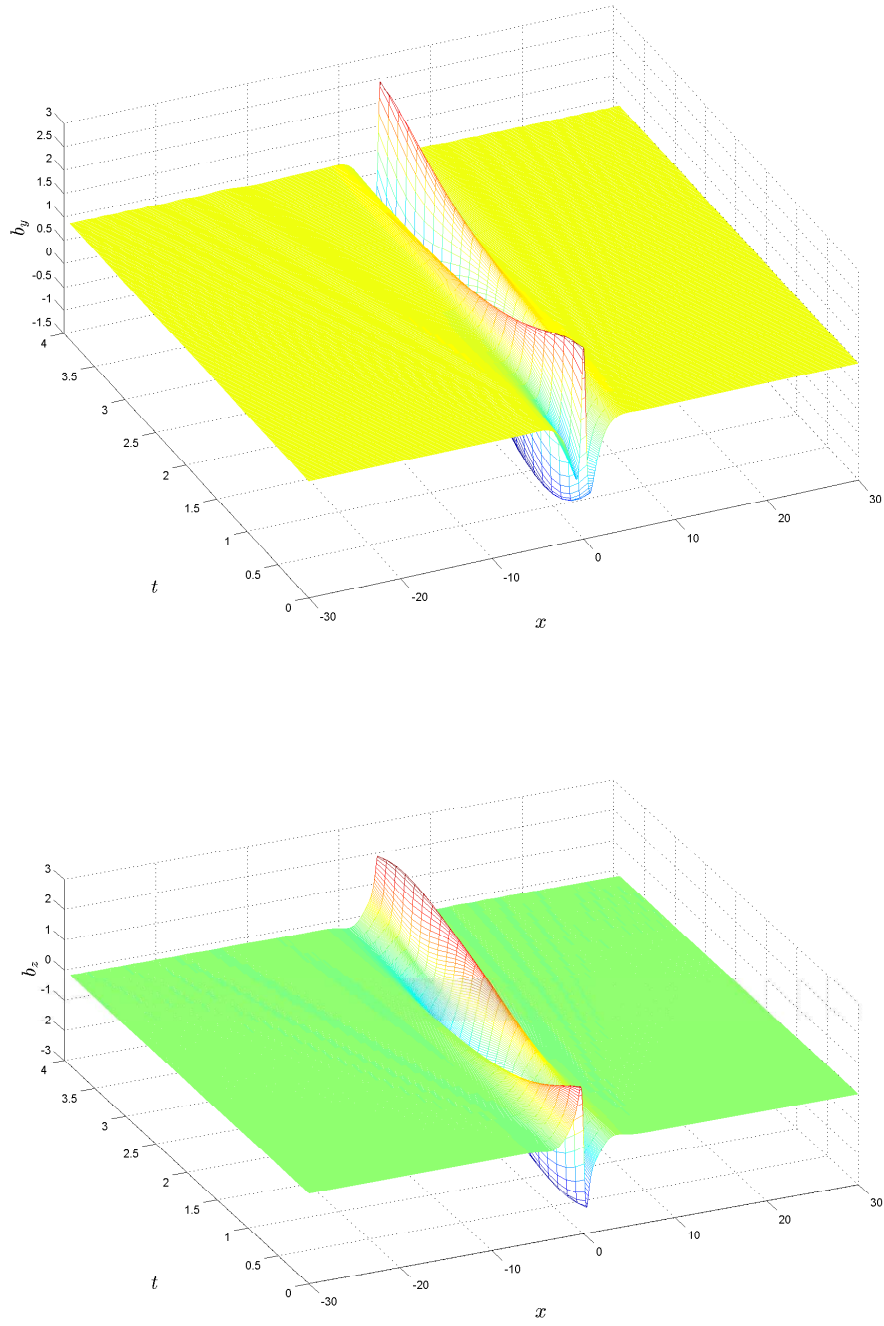


Figure 5.11: The initial wave form of the used as the initial condition for numerically integrating the DNLS for the figures above was a two parameter soliton with $\lambda = 0.4 + 0.5i$. As agreement with theory, the numerical solution only contains a soliton and no dispersive wave component.

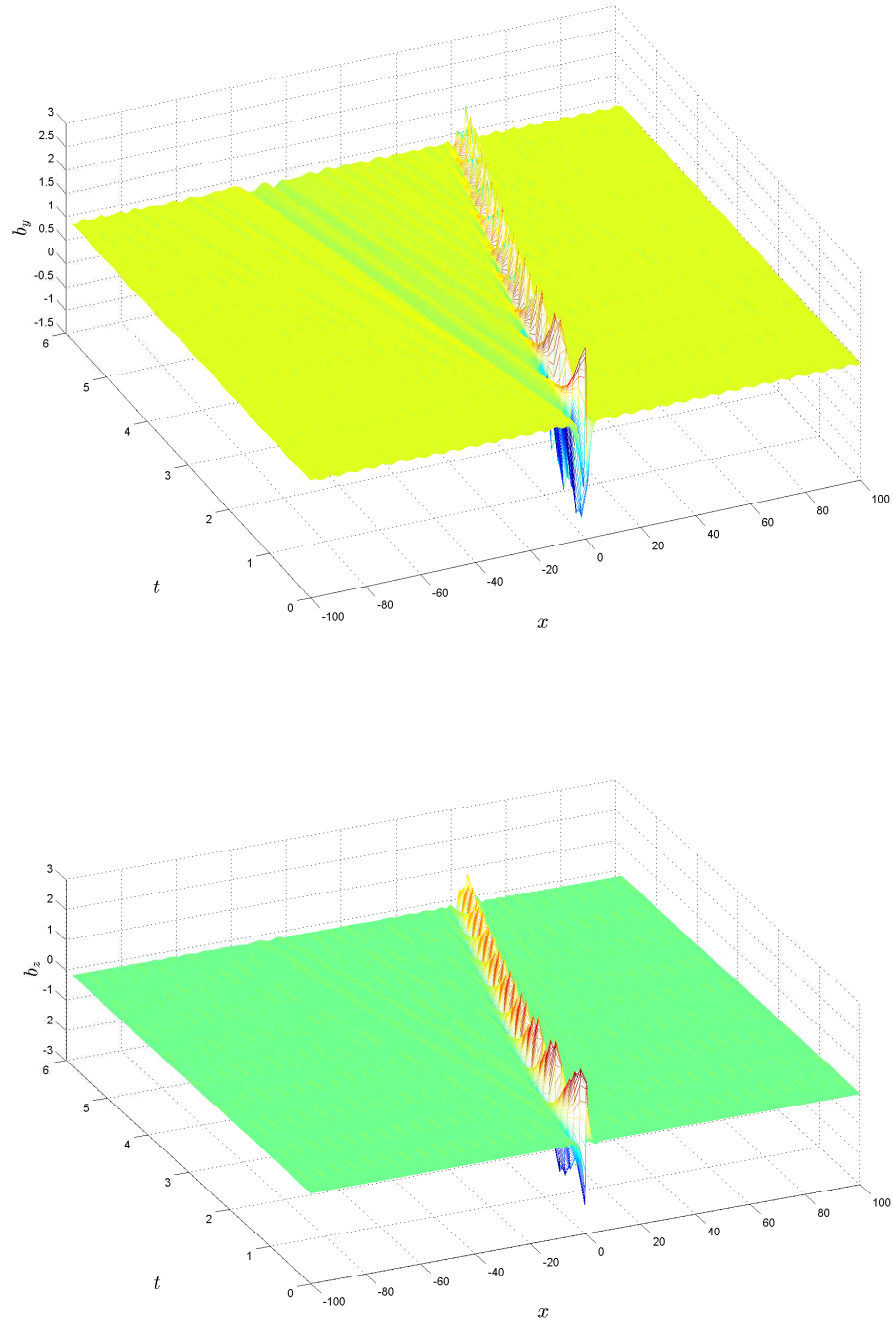


Figure 5.12: The effect of the background small amplitude oscillations on the two parameter soliton with $\lambda = 0.4 + 0.5i$. It can be seen that the soliton's amplitude diminishes, but it does seem to hold its local waveform.

5.5.1 Analytical two parameter soliton as initial profile

This section will demonstrate the time evolution of the two parameter soliton with $\lambda = 0.4 + 0.5i$ that was used to match the morphology of the magnetic pulse observed by the Ulysses spacecraft. Solitons are nondispersing, meaning they retain their shape, therefore when used as an initial condition for solving the DNLS equation, the nonlinear structure should not dampen or disperse. This first figure demonstrates this property of solitons (Figure 5.11).

An interesting case would be to introduce a background small amplitude oscillatory wave, and study how these oscillations would affect the two parameter soliton's form and periodicity. These small oscillations could be considered as coherent background noise. Figure 5.12 demonstrates how the background small amplitude sinusoidal wave can affect the consistency of the soliton. It does disperse, resulting in two dark solitons propagating in the opposite direction of the main wave profile. The soliton does seem to hold its localization, but its wave form becomes dramatically altered, this can be a result of the eigenvalue shifting and losing its ability to remain constant as time progresses.

5.5.2 Ulysses magnetometer data as initial profile

Earlier, it was mentioned that the shooting method for the 2x2 eigenvalue problem did not find an eigenvalue. This means that no soliton should show up, and only dispersive waves will form if the data is used as the initial wave profile for the DNLS integration scheme. Figure 5.13 shows the time evolution of the minimum variance transformed data. It can be seen that no solitons form, just dispersive waves propagate in both directions away from the initial wave configuration. This could be a result of the noise associated with the magnetometer data.

An argument can be made that the dispersive waves formed primarily from the inherent noise of the magnetometer data. Therefore, a scaled two parameter soliton will be used as a smooth analogue of the observed event. It was identified earlier that the RK shooting method was able to find an eigenvalue for this specific wave profile, which was on the real axis in the complex λ plane. This means a one parameter

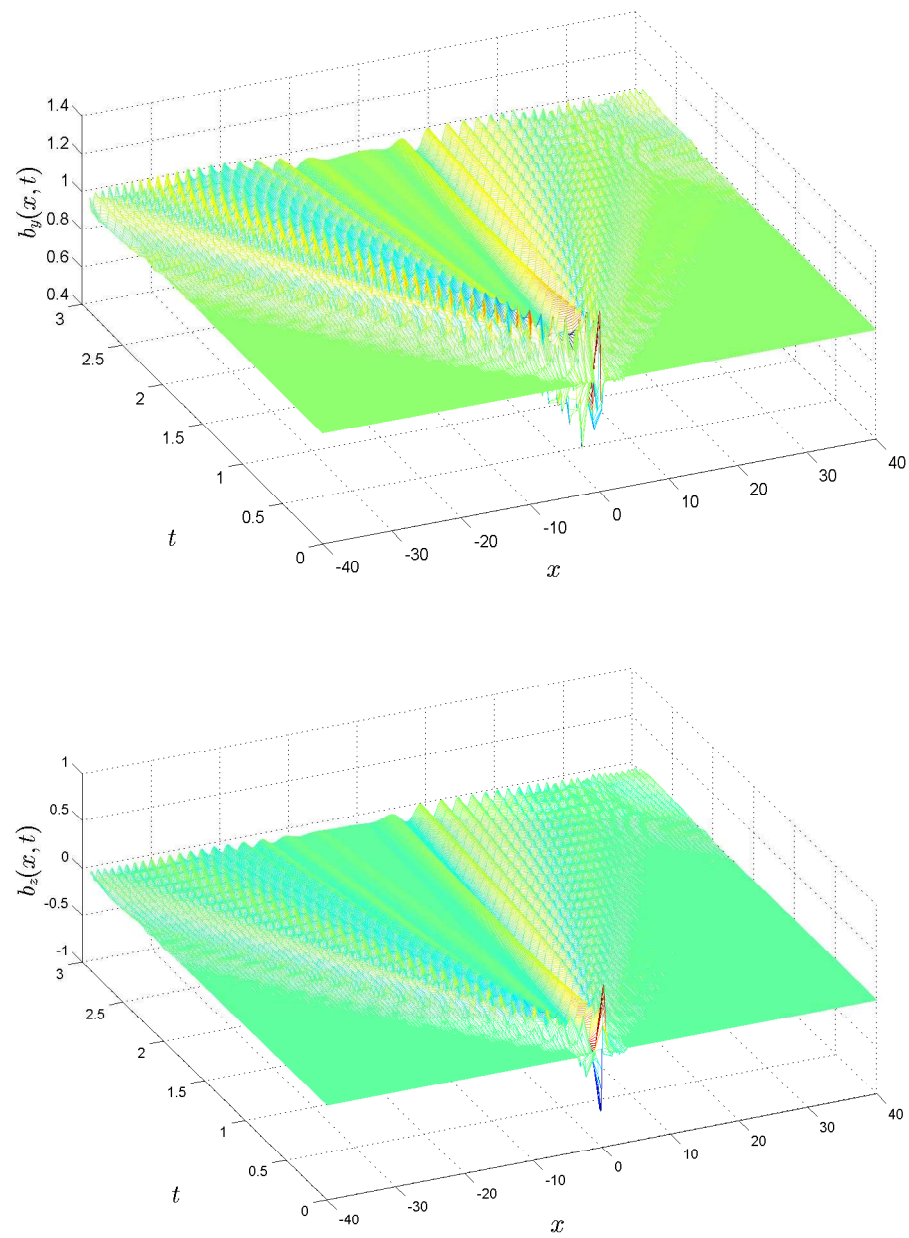


Figure 5.13: The wave form of the data without scaling was used as the initial condition. No eigenvalue was found for this initial wave profile, therefore no soliton forms and only dispersive waves form.

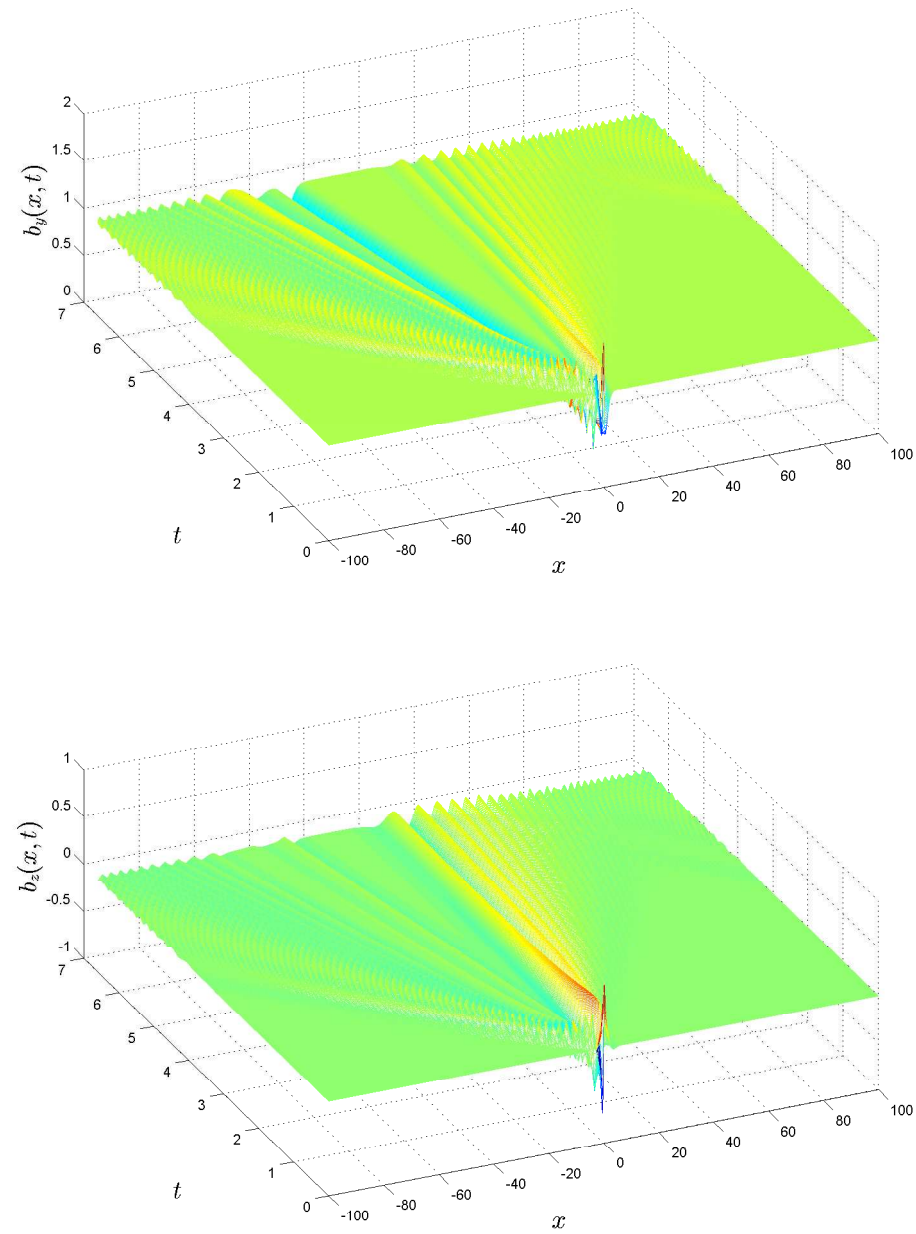


Figure 5.14: Numerical solution of the DNLS with the scaled two parameter soliton ($\lambda = 0.4 + 0.5i$) used as the initial wave profile. It can be seen that a dark soliton does form moving in the $-x$ -direction in the plot of b_y , along with dispersive waves.

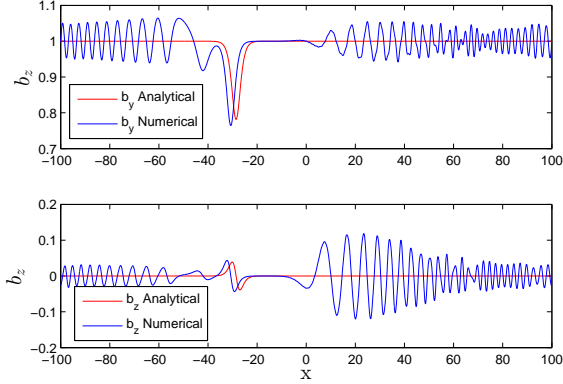


Figure 5.15: The last time step with of the DNLS numerical integration scheme with a dark one parameter soliton with $\lambda = 0.8907$ superimposed. The shapes of the two plots correlate, and the amplitudes are relatively close to each other.

soliton should form from the scaled two parameter configuration, however it should be noted that the waveform of ϕ_{11} and ϕ_{21} did not provide any insight to which type of one parameter soliton should form (bright or dark).

Looking at Figure 5.14, it is clear that a one parameter dark soliton does form along with small amplitude dispersive waves. When making a comparison between the numerical solution of the data and the scaled two parameter solution, it can be seen that the dispersive waves produced in the solution with the magnetometer data are slightly larger in amplitude. This could be a product of the noise in the data itself, or the padding required to extend the domain of the magnetometer data for proper use in the DNLS numerical integration scheme. The key point of these last two solutions is that the smooth data led to generation of a one parameter soliton, while the noisy data did not.

Another important argument to make is that the dark one parameter soliton that was generated by the scaled two parameter soliton, see Figure 5.14, from the numerical integration of the DNLS equation is that its corresponding eigenvalue is $\lambda = 0.8907$. This value was predicted by the RK shooting method eigenvalue solver, therefore the validity of the DNLS integration method will be reinforced by the 2x2 eigenvalue shooting method. This was done easily by graphical superimposition of an analytical one parameter soliton on the last time step of the DNLS numerical solution, which

demonstrated in Figure 5.15.

It can be seen easily that the soliton that was generated by the DNLS integration scheme by using the scaled two parameter soliton, which was used to mimic the event observed by the Ulysses VGM/FGM data, as the initial wave configuration is indeed a dark soliton. The eigenvalue that was predicted by the RK shooting method is extremely close, the slight difference in amplitudes results from a numerical loss in the RK shooting method. It can be reasonably concluded that the event that was observed on February 21st 2001 does have a soliton component, with the presence of dispersive waves.

Chapter 6

Conclusions and Further study

In this thesis, a detailed preliminary analysis was made of a magnetic bump observed by the Ulysses spacecraft on February 21st, 2001 using the perspective of soliton theory and numerical integration of the DNLS equation. It was shown that the minimum variance transformed data was too noisy by itself to successfully apply the direct scattering transformation (in the form of a 2x2 eigenvalue problem) to determine if an eigenvalue was present in the profile, i.e. a soliton. However, a smooth and continuous profile, which was a scaled two parameter soliton solution of the DNLS equation, that resembled the morphology of the transformed magnetic bump did lead to the determination of an eigenvalue, which was $\lambda = 0.8907$.

When the time evolution of this smooth profile was examined, by directly integrating the DNLS equation with the profile as the initial condition, a dark one parameter soliton formed with approximately the same eigenvalue that was predicted by the 2x2 eigenvalue shooting method, along with the presence of dispersive waves. The occurrence of dispersive waves implied that the smooth profile was not a pure soliton. This leads to the conclusion that there could be a soliton component present in the magnetic bump, but there wasn't any information leading to the time evolution of the observed pulse.

Several directions can be taken to expand on the conclusions that were made in this thesis. The most prevalent one being to apply the analysis developed in Chapter 5 to the other events identified by Rees et al. [21], with the aide of producing a more

effective way of smoothing the minimum variance transformed data. This will allow for a more convincing argument that the profile has a soliton component when the 2x2 eigenvalue shooting method produces an eigenvalue for a specific observed magnetic pulse or bump. Some more branches of possible research could be:

- Looking into the next order nonlinearity when deriving the the DNLS equation and inspecting its effects on the soliton solution's stability.
- Numerical analysis of the effect on soliton propagation into different plasma environments, such as from low β to high β , in the perspective of the DNLS equation solutions.
- The physical mechanisms that have the potential to generate these nonlinear waveforms in the interplanetary magnetic field.

Essentially, there are many paths that lead to rich research possibilities when treating nonlinear Alfvén waves in the view of the DNLS equation.

Appendix A

APPENDIX

A.1 Scaling for KdV equation for Shallow water waves

It was claimed earlier that nonlinear water waves have a higher speed for higher amplitude waves. The following derivation can be found in “Physics of Solitons”, by Dauxois and Peyrad. Three main assumptions about the fluid are necessary: it is non-viscous, incompressible and irrotational. Starting with Euler’s equation for the assumptions gives us

$$\frac{1}{c_0} \frac{\partial \eta}{\partial t} + \frac{\partial \eta}{\partial x} + \frac{3}{2h} \eta \frac{\partial \eta}{\partial x} + \frac{h^2}{6} \frac{\partial^3 \eta}{\partial x^3} = 0 \quad (\text{A.1})$$

where $c_0 = \sqrt{gh}$ is the characteristic linear wave speed, h is the depth of the water, and η is the height of the water surface from equilibrium. With introduction of the spacial and time scalings $X = x - c_0 t$ and $T = t$, we arrive at

$$\frac{\partial}{\partial t} = -c_0 \frac{\partial}{\partial X} + \frac{\partial}{\partial T} \quad (\text{A.2})$$

$$\frac{\partial}{\partial x} = \frac{\partial}{\partial X} . \quad (\text{A.3})$$

Using the transformations (A.2) and (A.3), first two terms in Eq (A.1) become

$$\frac{1}{c_0} \frac{\partial \eta}{\partial t} + \frac{\partial \eta}{\partial x} = \frac{1}{c_0} \left[-c_0 \frac{\partial \eta}{\partial X} + \frac{\partial \eta}{\partial T} \right] + \frac{\partial \eta}{\partial X} \quad (\text{A.4})$$

$$= \frac{1}{c_0} \frac{\partial \eta}{\partial T} \quad (\text{A.5})$$

which leads the Euler's equation for with the reference frame moving at c_0 ,

$$\frac{1}{c_0} \frac{\partial \eta}{\partial T} + \frac{3}{2h} \eta \frac{\partial \eta}{\partial X} + \frac{h^2}{6} \frac{\partial^3 \eta}{\partial X^3} = 0. \quad (\text{A.6})$$

Finally, we to change to dimensionless variables. This is done be introduction the relations

$$\phi = \frac{\eta}{h}, \quad \xi = \frac{X}{X_0}, \quad \tau = \frac{T}{T_0}, \quad (\text{A.7})$$

which changes (A.6) to

$$\frac{\partial \phi}{\partial \tau} + \left(\frac{3}{2} \frac{c_0 T_0}{X_0} \right) \phi \frac{\partial \phi}{\partial \xi} + \left(\frac{h^2}{6} \frac{c_0 T_0}{X_0^3} \right) \frac{\partial^3 \phi}{\partial \xi^3} = 0. \quad (\text{A.8})$$

which implies that there are really only two coefficients that need to be determined. They are

$$\alpha = \left(\frac{3}{2} \frac{c_0 T_0}{X_0} \right) \quad (\text{A.9})$$

and

$$\beta = \left(\frac{h^2}{6} \frac{c_0 T_0}{X_0^3} \right) \quad (\text{A.10})$$

where α and β are any desired numerical values, which will inevitably determine the characteristic length and time scales, X_0 and T_0 . Typically, for the KdV equation $\alpha = 6$ and $\beta = 1$, therefore

$$\frac{X_0}{T_0} \frac{1}{c_0} = \frac{1}{4} \quad \text{or} \quad \frac{X_0}{T_0} = \frac{c_0}{4} \quad (\text{A.11})$$

and

$$\frac{1}{6} \left(\frac{h}{X_0} \right)^2 4 = 1 \quad \text{or} \quad \left(\frac{h}{X_0} \right)^2 = \frac{2}{3} \rightarrow X_0 = \sqrt{\frac{2}{3}} h. \quad (\text{A.12})$$

Without choosing values for α and β , the relations of the coefficients, in general, are

$$\left(\frac{h}{X_0}\right)^2 = \frac{\alpha}{9\beta} \text{ or } X_0 = \sqrt{\frac{\alpha}{9\beta}}h \quad (\text{A.13})$$

and

$$\frac{c_0 T_0}{X_0} = \frac{c_0 T_0}{\sqrt{\frac{\alpha}{9\beta}}h} \text{ or } T_0 = \frac{h}{c_0} \sqrt{\frac{4\alpha^3}{81\beta}}. \quad (\text{A.14})$$

A.2 Scaling for the Derivative Nonlinear Schrödinger Equation

This section will present the scaling of the DNLS equation for oblique wave propagation, which follows in [20]. It starts with the vector DNLS equation (VDNLS)

$$\frac{\partial \tilde{B}}{\partial t} + \alpha \frac{\partial}{\partial x} \left[(|B|^2 + 2B_0 B_x) \tilde{B} \right] - \alpha B_0 \tilde{\nabla} (|B|^2 + 2B_0 B_x) + i\mu \frac{\partial^2 \tilde{B}}{\partial x^2} = 0 \quad (\text{A.15a})$$

$$\frac{\partial B_x}{\partial x} + \nabla_{\perp} \cdot B_{\perp} = 0 \quad (\text{A.15b})$$

where the magnetic field, \mathbf{B} , has the form

$$\mathbf{B} = (B_0 + \epsilon B_x, \epsilon^{1/2} B_y, \epsilon^{1/2} B_z), \quad (\text{A.16})$$

where $\epsilon = \omega/\Omega_i \ll 1$, which is an assumption made in the derivation of the VDNLS where ω is the frequency of the wave and Ω_i is the ion gyrofrequency. The VDNLS, is most commonly rewritten in complex form, as opposed to vector notation, therefore

$$\tilde{B} = B_y + iB_z \quad (\text{A.17})$$

or

$$\mathbf{B}_{\perp} = (B_y, B_z) \quad (\text{A.18})$$

where the coordinates are

$$x \rightarrow \epsilon(x - v_A t) \quad (\text{A.19a})$$

$$\begin{pmatrix} x \\ y \end{pmatrix} \rightarrow \epsilon^{3/2} \begin{pmatrix} x \\ y \end{pmatrix} \quad (\text{A.19b})$$

$$t \rightarrow \epsilon^2 t \quad (\text{A.19c})$$

which are transformations from the MHD equations used to derive the VDNLS to the Alfvén reference frame. and the transverse differentiation representation of ∇ is

$$\tilde{\nabla} = \frac{\partial}{\partial y} + i \frac{\partial}{\partial z} \quad (\text{A.20a})$$

$$\nabla_{\perp} = \left(\frac{\partial}{\partial y}, \frac{\partial}{\partial z} \right). \quad (\text{A.20b})$$

It can be shown that the coefficients, for arbitrary β , are

$$\alpha = \frac{1}{4} \frac{v_A}{B_0^2} \frac{1}{1 - \beta} \quad (\text{A.21a})$$

$$\mu = \frac{1}{2} \frac{v_A^2}{\Omega_i} \quad (\text{A.21b})$$

where c is the speed of light, and Ω_i is the ion gyrofrequency. The VDNLS equation was derived with the assumption of parallel propagation, i.e. $\tilde{B} \rightarrow 0$ as $x \rightarrow +\infty$. A one dimensional equation for oblique propagation is needed, therefore we can change coordinates to the system (x', y', z') where x' makes an angle θ with x and y' lies in the xy -plane, and $z = z'$. If we let $\epsilon = 1$, then decomposition of B yeilds

$$\begin{aligned} B_x &= B_x' \cos \theta - B_{y'} \sin \theta - B_0 \\ B_y &= B_x' \sin \theta + B_{y'} \cos \theta \\ B_z &= B_{z'} \end{aligned} \quad (\text{A.22a})$$

If we make an assumption, that the solution to the VNDLS only varies in the x' direction, then we have

$$\begin{aligned}\frac{\partial}{\partial x} &= \cos\theta \frac{\partial}{\partial x'} \\ \frac{\partial}{\partial y} &= \sin\theta \frac{\partial}{\partial x'} \\ \frac{\partial}{\partial z} &= 0.\end{aligned}\tag{A.23a}$$

It can easily be seen that this immediately gives us

$$B_{x'} = B_0 \cos\theta\tag{A.24}$$

from Eq (A.15b). Substitution of Eqns (A.22a) and (A.23a) into (A.15a), along with treating $\sin^2\theta$ as $\mathcal{O}(\epsilon)$ and neglecting terms with order ϵ we arrive at

$$\frac{\partial \tilde{\mathbf{B}}'}{\partial t} + \alpha \frac{\partial}{\partial x'} \left[\left(|\tilde{\mathbf{B}}'|^2 - \mathbf{B}_{y0}^2 \right) \tilde{\mathbf{B}}' \right] + i\mu \frac{\partial^2 \tilde{\mathbf{B}}'}{\partial x'^2} = 0\tag{A.25}$$

where $\tilde{\mathbf{B}}' = \mathbf{B}_{y'} + i\mathbf{B}_{z'}$ and $\mathbf{B}_{y0} = B_0 \sin\theta$. For oblique propagation, it is convenient for the reference frame to move perpendicular to the background magnetic field B_0 and since the wave frame is already moving at the Alfvén velocity, the only reduction is $\sin\theta \rightarrow 1$ so $B_{y0} \rightarrow B_0$.

As similarly done with the KdV equation, it is important to transform the equation into dimensionless coordinates, so we can introduce the dimensionless variables

$$b = \frac{\tilde{\mathbf{B}}'}{B_0}, \xi = \frac{x'}{x_0}, \tau = \frac{t'}{t_0}\tag{A.26}$$

and substitution into (A.25) gives us

$$\frac{\partial b}{\partial \tau} + \alpha \frac{t_0 B_0^2}{x_0} \frac{\partial}{\partial \xi} \left[\left(|b|^2 - b_0^2 \right) b \right] + i \frac{\mu}{x_0^2} \frac{\partial^2 b}{\partial \xi^2} = 0\tag{A.27}$$

which is the DNLS equation in dimensionless form.

Bibliography

- [1] Angrum, A. and Sedlacko, Daniel. “Ulysses.” *Jet Propulsion Laboratory*. California Institute of Technology. <http://ulysses.jpl.nasa.gov/science/index.html>.
- [2] Balogh, A., Beek, T. J., Forsyth, R. J., Hedgecock, P. C., Marquedant, R. J., and Smith, E. J., “The magnetic field investigation on the ULYSSES mission - Instrumentation and preliminary scientific results,” *Astron. Astrophys. Suppl. Ser.*, **92**, no. 2, 221-236, 1992.
- [3] Bame, S. J., D. J. McComas, B. L. Barraclough, J. L. Phillips, K. J. Sofaly, and J. C. Chavez, “The Ulysses solar wind experiment,” *Astron. Astrophys. Suppl. Ser.*, **92**, 237-265, 1992.
- [4] Boussinesq, J., *Essai sur la theorie des eaux courantes*, Memoires presentes par divers savants à l'Acad. des Sci. Inst. Nat. France, XXIII, pp. 1680, 1877.
- [5] Baumgärtel, K., “Soliton approach to magnetic holes,” *J. Geophys. Res.*, **104**, 28,295-28,308, 1999.
- [6] Darrigol, O., *Worlds of Flow: A History of Hydrodynamics from the Bernoullis to Prandtl*, Oxford University Press, 2005.
- [7] Duran, D.R., *Numerical Methods for Fluids Dynamics with applications to Geophysics*, “Physically insignificant fast waves,” Springer, Second Edition, 417, 2010.
- [8] Drazin, P.G., and R.S. Johnson, *Solitons: An Introduction*, Cambridge University Press, 1989.

- [9] Gardner, C.S. Greene, J.M., Kruskal, M.D., and Miura, R.M., "Korteweg-deVries equation and generalization," *Commun. Pure Appl. Math.*, **27**, 97-133, 1974.
- [10] Hoffman, Joe. *Numerical Methods for Engineers and Scientists*. Second Edition. CRC Press. 2001.
- [11] Hamilton, R. L., D. A. Peterson, and S. M. Libby, "Magnetic hole formation from the perspective of inverse scattering theory," *J. Geophys. Res.*, **114**, A03104, 2009.
- [12] Kaup, D. J. and A.C. Newell, "An exact solution for a derivative nonlinear Schrödinger equation," *J. Math. Phys.*, **19**, 798-901, 1978.
- [13] Kawata, T. and H. Inoue, "Exact solution of the derivative nonlinear Schrodinger equation under the nonvanishing conditions," *J. Phys. Soc. Jpn.*, **44**, 1978.
- [14] Kennel C. F., B. Buti and T. Hada, "Nonlinear, dispersive, elliptically polarized Alfvn waves," *Phys. Fluids*, **31**, 1949-1961, 1988.
- [15] Lamb, G.L. Jr, *Elements of Soliton Theory*. Wiley, 1980.
- [16] Lax, P., "Integrals of nonlinear equations and solitary waves," *Commun. Pure Appl. Math.*, **21**, 467-490, 1968.
- [17] Ludu, A., *Nonlinear Waves and Solitons on Contours and Closed Surfaces*, Springer-Verlag, 2012.
- [18] Mjølhus, E. and T. Hada, "Soliton theory of quasi-parallel MHD waves", 121 169, Ch.4 in *Nonlinear Waves and Chaos in Space Plasmas*, eds. T. Hada and H. Matsumoto, Terra Sci., 1997.
- [19] Mjølhus, E., and J. Wyller, "Nonlinear Alfvén wave in a finite-beta plasma," *J. Plasma Physics*, **40**, 299-318, 1988.
- [20] Mjølhus, E., "Nonlinear Alfvén waves and the DNLS Equation: Oblique Aspects," *Physica Scripta*, **40**, 227-237, 1989.

- [21] Rees, A., A. Balogh, and T. S. Horbury, “Small-scale solitary wave pulses observed by the Ulysses magnetic field experiment,” *J. Geophys. Res.*, **111**, A10106, 2006.
- [22] Rogister, A., “Parallel Propagation of Nonlinear Low-Frequency Waves in High- β Plasma,” *Phys. of Fluids*, **14**, 2733-2739, 1971.
- [23] Ruderman M.S., “DNLS equation for large-amplitude solitons propagating in an arbitrary direction in a high- β Hall plasma,” *J. Plasma Physics*, **67**, 271-276, 2002.
- [24] Sonnerup, B.U., and M. Scheible, “Minimum and Maximum Variance Analysis,” 185-220, Ch.8 in *Analysis Methods for Multi-Spacecraft Data*, eds. Paschmann, G., and Daly, P. , Inter. Space Science Inst., 2000.
- [25] Sauer, K., E. Mjølhus , E. Dubinin and K. Baumgärtel, “Banana-polarized solitons in anisotropic plasmas related to Ulysses observations,” *Geophys. Res. Letters*, **34**, L11109, 2007.
- [26] Scott Russell, J., “Report on waves,” *Fourteenth meeting of the British Association for the Advancement of Science*, 1844.
- [27] Stasiewicz, K., “Theory and Observations of Slow-Mode Solitons in Space Plasmas,” *Phys. Rev. Letters*, **93**, 2004.